Technische Universität München, Physik Department, T30d
Max-Planck-Institut für Physik (Werner-Heisenberg-Institut)

Full Boltzmann equations for leptogenesis

FLORIAN HAHN-WOERNLE

Abstract

In leptogenesis the evolution of a cosmological baryon asymmetry is usually studied by means of momentum integrated Boltzmann equations. To investigate the validity of this approach, we solve the full Boltzmann equations, without the assumption of kinetic equilibrium and including all quantum statistical factors. Beginning with the full mode equations, we derive the usual kinetic equations for the right-handed neutrino number density and integrated lepton asymmetry, and show explicitly the impact of each assumption on these quantities. We investigate also the effects of scattering of the right-handed neutrino with the top quark to leading order in the Yukawa couplings by means of the full Boltzmann equations. On a later stage we extend our studies to an alternative scenario in which the asymmetry is generated via decays of the next-to-lightest right-handed neutrino. Here we provide a restriction on the valid parameter space.

Zusammenfassung

Die Entwicklung einer kosmologischen Baryonenasymmetrie wird in der Leptogenese üblicherweise mittels impulsintegrierter Boltzmanngleichungen untersucht. Zur Überprüfung dieser Vorgehensweise lösen wir die vollen Boltzmanngleichungen, ohne die Annahme kinetischen Gleichgewichts und unter Berücksichtigung aller quantenstatistischen Faktoren. Wir leiten die integrierten kinetischen Gleichungen für rechtshändige Neutrinos und die Leptonenasymmetrie her, und zeigen den Einfluss der für die Integration gemachten Annahmen auf diese Größen. Des Weiteren untersuchen wir die Auswirkungen von Streuprozessen rechtshändiger Neutrinos an Quarks in erster Ordnung der Yukawakopplung mittels der vollen Boltzmanngleichungen. Zuletzt untersuchen wir ein alternatives Szenario, in dem eine Asymmetrie in Zerfällen des zweitleichtesten rechtshändigen Neutrinos erzeugt wird und schränken den gültigen Parameterbereich innerhalb dieses Szenarios ein.

Acknowledgments

First, I would like to express my gratitude towards my research supervisor Michael Plümacher, who suggested this investigation, for his continuous support and the collaboration over the last four years.

Concerning the research presented in this thesis, I am strongly indebted to Yvonne Y. Y. Wong who has always been available for questions and discussions. I benefited a lot from her expertise on the field of numerics and cosmology in general.

I am grateful to Prof. Alejandro Ibarra for being my official supervisor and thus for providing the academic framework for my Ph.D. studies at the Technische Universität München.

For the optimal research possibilities within the framework of the International Max Planck Research School (IMPRS), I would like to thank the Max-Planck-Institute for Physics (MPI) and, in particular, the scientific IMPRS coordinator Frank D. Steffen. I thank Thomas Hahn and Peter Breitenlohner for support in all kinds of computer related issues and the secretary Rosita Jurgeleit for her friendly help in all kinds of bureaucracy related issues.

For many useful advices and his kind availability, I like to express my gratitude towards Georg Raffelt.

Then, I would like to thank all the friends that I had the chance to meet at the MPI during the last years. Special thanks go to my office mates Josef Pradler and Max Huber, my former office mate Felix Rust, Andreas Biffar and Steve Blanchet for the Indian experience, and all the members of the 'astroparticle' group for the enjoyable working atmosphere.

Finally, I am very grateful to my parents for their never-ending support during my studies and Rita Spanu for being part of my life.

Contents

Chapter 1

Introduction

1.1 Matter-antimatter asymmetry

In the last years our knowledge of the history of the early universe has grown considerably, and a cosmological standard picture, the Lambda Cold Dark Matter (ΛCDM) Model has emerged. This model suggests the possibility that shortly after the Big Bang a period of exponential expansion, which is called inflation [1], took place. Immediately after the inflationary phase, the energy content of the universe was dominated by radiation, i.e., all particles species were in chemical equilibrium contributing to the thermal bath of the universe. Thereon the universe expanded and cooled down, entered the phase of matter domination at a temperature of $\sim 10\,\mathrm{eV}$, and finally began a stage of accelerated expansion at a temperature of a few meV [2]. In Figure 1.1 today's energy budget of the universe is shown. Experimentally, the values of the various components are determined by the angular distribution of the temperature fluctuations of the cosmic microwave background (CMB) together with large scale structure and Supernova Type Ia observations. The observation that the expansion of the universe is accelerating today indicates that the dominant contribution to the overall energy budget, about 70%, is provided in the form of a yet unknown un-clustered component, called dark energy [3, 4]. The simplest way to explain dark energy is by adding an Einstein cosmological constant Λ in the Friedman equation. But also dynamical models motivated from particle physics are considered [5, 6]. Another 23% of the energy density consist of a cold, non-baryonic matter component that is called dark matter. Theories beyond the Standard Model of particle physics (SM) provide several candidates: the lightest supersymmetric particle (neutralino, gravitino), axion, sterile neutrino, lightest Kaluza–Klein boson, and many other. Further, a part of 4% of the energy budget is made up by SM baryons and a small fraction of $\sim (0.1 - 2)\%$ is contributed by the (dark) neutrino background. It is remarkable that there is no antimatter contributing to the the total energy budget. In general,
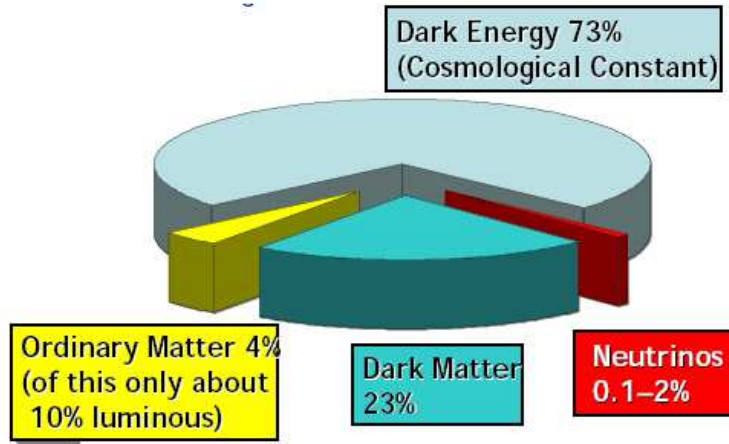
Figure 1.1: The energy budget of the universe.

one could think that the universe in total is matter-antimatter symmetric and that there exist distinct regions that are entirely made of antimatter. Then one would expect matter-antimatter annihilations to occur at the border regions with an emission of high energy photons. The absence of such a photon flux indicates that nearby galaxy clusters consist of matter. Nevertheless, there remains the possibility of a baryon symmetric universe on scales larger than clusters of galaxies (tens of Mpc), which requires a mechanism to explain the segregation on these scales [7, 8].

The observed excess of matter over antimatter in the universe can be conveniently expressed as the net baryon to photon number ratio. The most accurate measurement for this value comes from the CMB by the WMAP satellite [11]:

$$\eta_B^{\mathrm{CMB}} = \frac{n_B - n_{\overline{B}}}{n_\gamma} = \left(6.225 \pm 0.17\right) \times 10^{-10}. \tag{1.1}$$

About 380 000 years after the Big Bang, when the temperature of the universe was $T \sim 0.3 \, \mathrm{eV}$, electrons and protons combined to form neutral hydrogen and, in turn, photons decoupled from the thermal bath forming the nowadays observed CMB. In the angular power spectrum of the CMB the amount of baryons can be seen due to their gravitational interactions with photons: the attractive gravitational force pulls baryons together, but the radiation pressure of the thermal bath, on the other hand, drives them apart. These acoustic oscillations of the photon-baryon fluid at the time of decoupling are observed in the temperature anisotropies of the CMB. In Figure 1.2 we show the de-
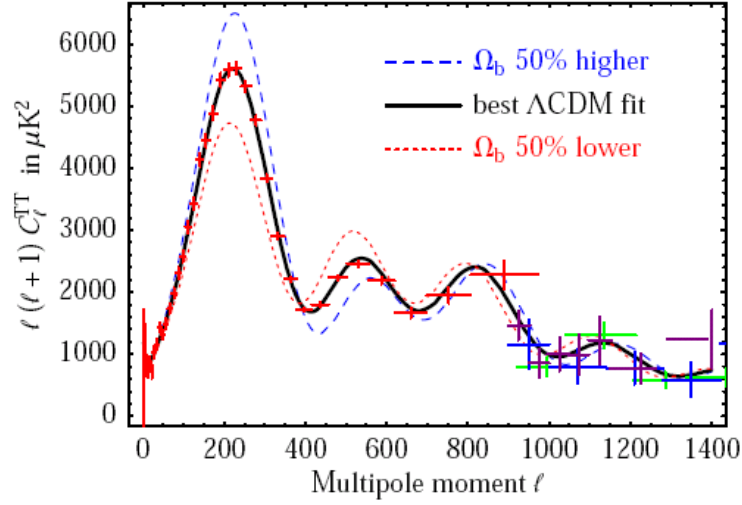
Figure 1.2: Temperature anisotropies of the CMB [9]. The solid black line shows the best fit in the ΛCDM–Model compared to data, whereas variations of the baryonic matter content lead to the dashed blue and pointed red lines.

pendence of the CMB temperature anisotropies on the baryon asymmetry η_B compared to data.

Another powerful test of the standard cosmological picture is the formation of light elements in Big Bang Nucleosynthesis (BBN) [12] taking place at $T \sim 1\,\mathrm{MeV}$ in the first 3 minutes after the Big Bang. The formation and resulting abundances of light elements can be calculated using well-known SM physics and the dependence of the abundances on η_B is shown in Figure 1.3. The consistency of BBN predictions indeed confirms that the thermal bath of the universe has had a temperature $T > \mathrm{MeV}$.

From BBN the following value of the baryon asymmetry can be deduced [13]:

$$4.7 \times 10^{-10} \leq \eta_B^{BBN} \leq 6.5 \times 10^{-10} \quad \text{at} \quad 95\,\%\,\mathrm{CL}. \tag{1.2}$$

Thus, two independent observations taking place at different energy scales point to a baryon asymmetry of the same order of magnitude.

The explanation of this baryon asymmetry is one of the challenging problems of modern cosmology and particle physics and will be the subject of the present thesis. Of course, one could simply impose a baryon asymmetry as an initial condition of the universe. The observed flatness and homogeneity of the universe however, strongly suggest that the earliest epochs were governed by an inflationary period. Thereby, any preexisting asymmetry would have been strongly diluted. As a consequence of this it is nec-
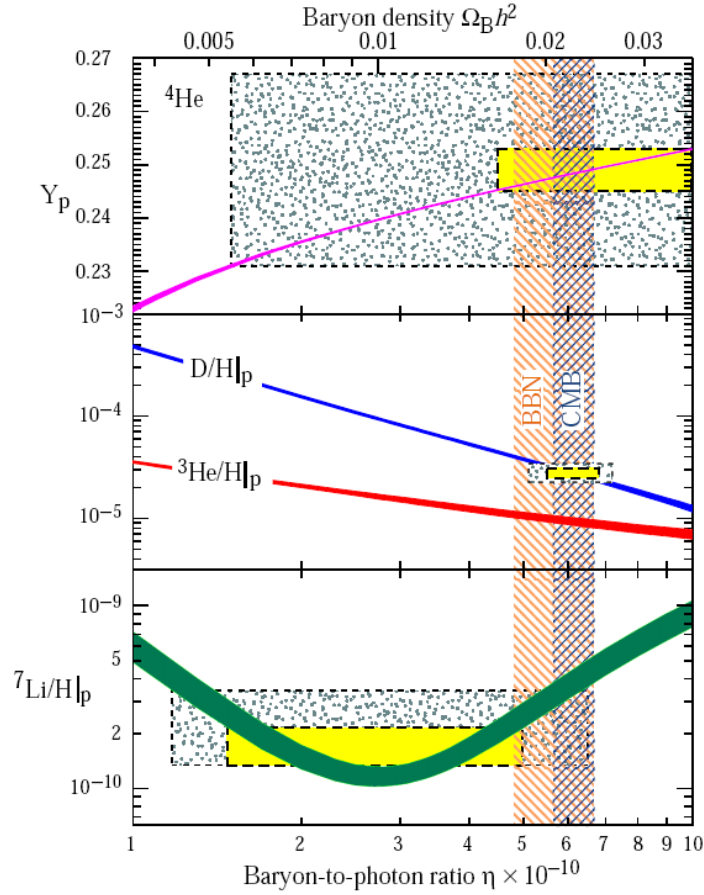
Figure 1.3: Observed abundances of light elements compared to BBN/CMB predictions that depend on the baryonic matter content of the universe [10]. The larger boxes indicate $\pm 2\sigma$ statistical and systematical errors, the smaller yellow boxes 2σ statistical errors.

essary to create the baryon asymmetry dynamically after the reheating process, what is called baryogenesis. In general, any baryogenesis mechanism should start from a matter-antimatter symmetric state and lead to an universe with a net baryon number.

In the SM one could consider the annihilations of baryons and anti-baryons into pions at around $22\,\mathrm{MeV}$. The annihilation rate is given by $\Gamma \simeq n_b^{\mathrm{eq}} \langle \sigma | \mathrm{v} \rangle$, where n_b^{eq} is the equilibrium number density of baryons, v corresponds to the relative velocities of the involved baryons and anti-baryons, and $\langle \sigma | \mathrm{v} \rangle \sim 1/m_\pi^2$, $m_\pi \simeq 135\,\mathrm{MeV}$, is the thermally-averaged annihilation cross-section. After the freeze-out of the annihilation process, the baryon to photon ratio is given by

$$\frac{n_b}{n_\gamma} = \frac{n_{\bar{b}}}{n_\gamma} \simeq 10^{-18},$$

which is far below the measured value. On the other hand, this process does not explain the excess of baryons over anti-baryons since the annihilations freeze-out, leaving the same abundances for baryons and anti-baryons. From this perspective, the standard Big Bang cosmology is unable to explain the baryon asymmetry of the universe and particular baryogenesis models have to be considered in its context. In 1967 Sakharov set up three conditions [14] that have to be satisfied by a baryogenesis model:

1. **Violation of baryon number (B) conservation**
   Beginning at a state with $B = 0$, it is instantaneously clear that in order to end up with a $B \neq 0$ state, B has to be violated.

2. **Violation of charge conjugation (C) and the combined charge and parity symmetries (CP)**
   If $\bar{i}$ denotes the state following a CP transformation of the state i, and $\mathcal{M}\left(i \to b\right)$ is the matrix element for the process $i \to b$, then the principle of detailed balance applies if a theory is invariant under CP and T transformations,

$$\mathcal{M}\left(i \to b\right) = \mathcal{M}\left(\bar{i} \to \bar{b}\right) = \mathcal{M}\left(b \to i\right).$$

   Hence, it is impossible to reach an universe with $B \neq 0$, i.e., $n_b \neq n_{\bar{b}}$, starting with a matter-antimatter symmetric state where $n_i = n_{\bar{i}}$.

3. **Departure from thermal equilibrium**
   The time evolution of a system in thermal equilibrium can be expressed with the help of a density matrix $\rho(t) = e^{-\beta H}$:

$$\langle B(t) \rangle = tr\left(e^{-\beta H} B(t)\right) = tr\left(e^{-\beta H} e^{-i\beta H t} B(0) e^{i\beta H t}\right) = \langle B(0) \rangle,$$

   i.e., an initial state with vanishing B that remains in thermal equilibrium cannot produce any baryon number $B \neq 0$.

1.2 Baryogenesis in the SM

All three Sakharov conditions are fulfilled in the SM of particle physics.

1. Baryon number is violated in anomalous processes. These anomalies are due to the chiral nature of the electroweak theory [15]. There, gauge field configurations exist that represent saddle-point solutions (sphalerons) [16] of the equations of motion. The sphalerons carry topological charges, corresponding to the Chern–Simons numbers. In the SM $SU(2)$ sphalerons lead to an effective 12-fermion

interaction

$$O_{B+L} = \prod_{i=1\cdots 3} (q_{Li}\, q_{Li}\, q_{Li}\, l_{Li}).$$

The sphaleron energy,

$$E_{\text{sph}} = \frac{8\pi}{g} v(T),$$

where $v(T)$ is the temperature dependent vacuum expectation value (vev) of the Higgs field, separates the topologically different vacua of the theory. Transitions from one vacuum to another violate lepton number L and baryon number B, but preserve $B - L$. The tunnelling rate between different vacua is determined by the instanton action S_{inst}, and is highly suppressed at zero temperature [15]: $\Gamma \sim e^{-S_{\text{inst}}} = e^{-\frac{4\pi}{\alpha}} = \mathcal{O}\left(10^{-165}\right)$. This rate is so small that B and L are separately conserved to a very good approximation in accelerator experiments [17]. However, if the system is coupled to a thermal bath, the transitions between different gauge vacua do not happen by tunneling but rather through thermal fluctuations over the energy barrier [18]. For temperatures higher than ~ 100 GeV, the electroweak symmetry is restored, i.e., the Higgs vacuum expectation value vanishes. Hence, the barrier separating different vacua disappears and sphaleron transitions are no longer suppressed. Therefore, in the expanding universe the $B+L$ violating reactions can be in equilibrium and occur with a significant rate. By a combination of analytical and lattice techniques [19], the sphaleron transition rate has been calculated for the symmetric phase of the SM. Here, we will only give the temperature range in which the sphaleron processes are in thermal equilibrium [19–23]:

$$T_{\text{EW}} \sim 100 \text{ GeV} \leq T \leq 10^{12} \text{ GeV}.$$

This seems to imply that for temperatures $T > T_{\text{EW}}$ any existing $B+L$ asymmetry will be washed out. But, since only left-handed fields couple to sphalerons, in the symmetric, high-energy phase a non-zero value of $B + L$ can persist if there is a non-vanishing $B - L$ asymmetry.

2. In the electroweak theory charge conjugation C is violated. Furthermore, in the quark sector of the SM the combined charge and parity conjugation CP is violated in the K and B meson systems. This CP violation is due to a complex phase in the Cabibbo–Kobayashi–Maskawa (CKM) matrix [24, 25], which gives the couplings of the charged currents $W^{\pm}$ to the left-handed up-and down-type quarks. The CKM matrix connects the electroweak eigenstates of down, strange, and bottom quarks with their mass-eigenstates. It is a 3×3 unitary matrix that

can be parametrized by three mixing angles and the CP-violating phase. The CP violation in the $K^0 - \overline{K}^0$-system is measured to be tiny [13],

$$|\varepsilon_{\text{CKM}}| \simeq 2.33 \times 10^{-3}.$$

3. Departure from thermal equilibrium can occur during the electroweak phase transition. For baryogenesis within the SM it is important that this phase transition is strongly first order. First order means that a thermodynamic quantity, the order parameter, changes discontinuously. In the electroweak theory this leads to a condition on the change of the Higgs vev at the critical temperatures T_{c},

$$\frac{\Delta v(T_{\text{c}})}{T_{\text{c}}} > 1.$$

During the transition, two separate thermodynamical phases co-exist in thermodynamical equilibrium. This means that two ground states of the theory exist: a high temperature ground state, described by a vacuum expectation value of the SM Higgs field $v = 0$, and a low temperature state with $v \neq 0$. These states are separated by an energy barrier. At the critical temperature T_{c}, both states are equally favored energetically. But when the temperature drops below T_{c}, the state described by $v \neq 0$ becomes the global vacuum of the theory and quantum tunnelling from the false vacuum ($v = 0$) to the true vacuum ($v \neq 0$) begins. This leads to the nucleation of bubbles of the $v \neq 0$ state in a sea described by the $v = 0$ vacuum. Eventually, these bubbles grow until they fill up all space, completing the phase transition. When the bubble walls pass each point in space, the order parameter v changes rapidly leading to a departure from thermal equilibrium.

Putting all three ingredients together leads to a baryogenesis mechanism dubbed *electroweak baryogenesis* [26, 27]. Here, CP violation occurs in the transitions from the false vacuum to the true vacuum during the bubble nucleation. Since the sphaleron processes are in equilibrium for $T \geq T_{\text{EW}}$, a baryon number B in the false vacuum ($v = 0$) can lead to a net baryon number in the true vacuum ($v \neq 0$) when the phase transition is faster than the sphaleron transition rate. However, it turns out that this mechanism does not work for two reasons. First, the CP violation in the quark sector is not large enough [28] to account for the observed value of the baryon asymmetry. The second reason is that in the SM a Higgs particle mass $m_\Phi \lesssim 45\,\text{GeV}$ [29] is needed in order to have a strong enough first order phase transition. This is clearly not compatible with the lower bound on the Higgs mass $m_\Phi \gtrsim 114\,\text{GeV}$ [13] coming from the LEP II experiment. Therefore, a successful baryogenesis is not possible within the framework of the SM.

1.3   Beyond the SM

In order to achieve successful baryogenesis, a potential extension of the SM must introduce new sources of CP violation and provide a departure from thermal equilibrium during the expansion history of the universe. A possibility is to modify the electroweak phase transition. To achieve this, a two Higgs doublet model [30] can be considered. Here, the Higgs potential has additional parameters, introducing additional sources of CP violation. Another well motivated model is the minimal supersymmetric standard model (MSSM). In the MSSM there exists a supersymmetric partner for each particle of the SM. These superpartners are of bosonic type for SM fermions and of fermionic type for SM bosons. Hence, the field content of the MSSM is doubled compared to the SM. Consequently, this demands a second Higgs doublet with its supersymmetric partner to achieve an anomaly free theory. If one allows for complex parameters, there are, in turn, additional sources of CP violation. A strong first order phase transition is then provided if a light scalar particle couples strongly to the Higgs boson whose mass is constrained $m_\Phi \lesssim 130 \ldots 150\,\text{GeV}$ [31]. In the MSSM the stop, the superpartner of the top quark, couples with the strength of the top Yukawa coupling to the Higgs and provides a strong enough first order phase transition if its mass is not larger than the top mass [32]. Combined with conditions on the Higgs mass and $\tan\beta$, i.e., the ratio of the vacuum expectation values of the two Higgs doublets, this leads to a narrow window in the MSSM parameter space that allows for successful electroweak baryogenesis and might be tested experimentally at the Large Hadron Collider (LHC) soon. However, going beyond the field content of the MSSM, e.g., the next to minimal supersymmetric standard model (nMSSM) with an additional singlet superfield, the parameter space broadens up leaving more possibilities for successful *supersymmetric electroweak baryogenesis* [33–35].

Another baryogenesis model relying on supersymmetry as extension of the SM is *Affleck–Dine baryogenesis* [36, 37]. In unbroken supersymmetry some combinations of scalar slepton, quark, or Higgs fields might not contribute to the scalar potential, describing so-called flat directions of the potential. These fields can develop large vacuum expectation values during inflation. After inflation has come to an end, these fields and their combinations start coherent oscillations around the potential minimum when the expansion rate of the universe H becomes comparable to their masses. If these scalar fields carry baryon or lepton number, a baryon asymmetry can be produced in these oscillations when the fields decay to lighter degrees of freedom.[1]

---

[1]A lepton asymmetry produced by lepton number carrying fields could be transformed to a baryon asymmetry via sphaleron processes, cf. Section 1.2.

A more general class of baryogenesis models relies on grand unified theories (GUTs). These theories provide an elegant way to unify the gauge theories of the electroweak and strong interactions of particle physics at high energies. The gauge group of the SM, $SU(3)_C \times SU(2)_L \times U(1)_Y$, is then incorporated in a higher dimensional gauge group, which, in the minimal case, is of rank 5, i.e., an $SU(5)$. An important prediction of grand unified models is the decay of the proton. The $SU(5)$–GUT models are nearly ruled out because they cannot explain the longevity of the proton, $\tau_{\mathrm{p}} \geq 2.1 \times 10^{29}$ years [38]. To dynamically generate the observed baryon asymmetry in GUTs, the first attempts relied on the (out-of-equilibrium) baryon and lepton number violating decays of heavy colored triplets of Higgs particles [39–41]. These particles have to be heavier than about 10^{12} GeV to explain the long proton lifetime, which makes their production very difficult in the post-inflationary universe [42]. Another problem comes from the $B + L$ violating nature of the simplest GUTs, whereas $B - L$ is conserved. Hence, the SM sphaleron processes would wash-out any produced asymmetry at temperatures below 10^{12} GeV where sphalerons are in equilibrium.

Generally, $SO(10)$ is one of the most promising GUT candidates since it contains, in addition to the 15 Weyl fermions of the SM, right-handed neutrinos that can give rise to the small neutrino masses via the *see-saw* mechanism [43]. They are the main ingredient in the baryogenesis framework based on *leptogenesis* [42], which is the main subject of this investigation. Typically, in those $SO(10)$ models the gauge group is broken at an energy scale of $\sim 10^{16}$ GeV. This finally leads, potentially after several steps of symmetry breaking, to the SM gauge group with an additional $U(1)$ symmetry, whose breaking at a scale of $10^8 - 10^{13}$ GeV gives rise to Majorana masses for the heavy-right-handed neutrinos.

1.4   Neutrinos and the see-saw

We mentioned the see-saw mechanism as the origin of neutrino masses in the context of GUTs at the end of the last section. Since leptogenesis as a mechanism to create the baryon asymmetry in the early universe is a natural consequence of the see-saw mechanism, we will discuss the see-saw mechanism and neutrino masses in more detail.

1.4.1   Experimental results

Neutrino oscillation experiments give clear evidence for neutrino masses. These oscillations stem from the fact that in electroweak processes gauge eigenstates ν_α, $\alpha = e, \mu, \tau$, and not mass eigenstates ν_i, $i = 1, 2, 3$, are involved. A unitary transformation relates

the two eigenstate bases:

$$|\nu_\alpha\rangle = \sum_{i=1}^{3} U_{\alpha_i}^* \, |\nu_i\rangle, \tag{1.3}$$

i.e., each gauge eigenstate is a linear combination of the three mass eigenstates. The unitary lepton mixing matrix U is a 3×3 matrix consisting of three real mixing angles and six phases. It is known as the *Pontecorvo–Maki–Nakagawa–Sakata* (PMNS) matrix. If the neutrinos are Majorana fermions, three of these phases can be rotated away by a redefinition of the fields. The PMNS matrix is usually expressed as the product of three rotation matrices and a diagonal factor,

$$U = \begin{pmatrix} 1 & 0 & 0 \\ 0 & c_{23} & s_{23} \\ 0 & -s_{23} & c_{23} \end{pmatrix} \begin{pmatrix} c_{13} & 0 & s_{13} \, e^{-i\delta} \\ 0 & 1 & 0 \\ -s_{13} \, e^{i\delta} & 0 & c_{13} \end{pmatrix}$$

$$\times \begin{pmatrix} c_{12} & s_{12} & 0 \\ -s_{12} & c_{12} & 0 \\ 0 & 0 & 1 \end{pmatrix} \times \mathrm{diag}\left(\mathrm{e}^{-i\frac{\Phi_1}{2}}, \mathrm{e}^{-i\frac{\Phi_2}{2}}, 1 \right), \tag{1.4}$$

where $s_{ij} = \sin\theta_{ij}$, $c_{ij} = \cos\theta_{ij}$. Here, θ_{ij} are the real mixing angles, δ is the so-called Dirac phase, and $\Phi_{1,2}$ are the Majorana phases that, in contrast to δ, are only different from zero if neutrinos are Majorana fermions. All three phases are sources of CP violation. Thus, one can write for the transition probability of a neutrino travelling a distance L with an energy E from a flavor state α to a flavor state β

$$\begin{aligned} P\left(\nu_\alpha \to \nu_\beta\right) = \delta_{\alpha\beta} &- 4 \sum_{i>j} \mathrm{Re}\left(U_{\alpha i}^* \, U_{\alpha j} \, U_{\beta i} \, U_{\beta j}^* \right) \times \sin^2\left(\frac{\Delta m_{ij}^2 \, L}{4\,E} \right) \\ &+ 2 \sum_{i>j} \mathrm{Im}\left(U_{\alpha i}^* \, U_{\alpha j} \, U_{\beta i} \, U_{\beta j}^* \right) \times \sin^2\left(\frac{\Delta m_{ij}^2 \, L}{4\,E} \right), \end{aligned} \tag{1.5}$$

where $\Delta m_{ij}^2 = m_i^2 - m_j^2$.

The parameters measured by oscillation experiments are summarized in Table 1.1, completed by data received from non-oscillation experiments and cosmology [45]. We will shortly explain these parameters.

Solar anomaly:
In the 1960's R. Davis led the first experiment detecting neutrinos coming from the sun in the Homestake mine in South Dakota [46]. This experiment, which had an energy threshold $E_\nu > 0.814\,\mathrm{MeV}$, was based on a radiochemical technique using Chlorine. In contradiction to the electron neutrino flux predicted by Bahcall [47], the observed

Table 1.1: Summary of present information on neutrino masses and mixings; h accounts for the use of a different nuclear matrix element than the one calculated in [44].

oscillation parameter		central value
solar mass splitting	$\Delta m_{12}^2 =$	$(8.0 \pm 0.3)\,10^{-5}\ \mathrm{eV}^2$
atmospheric mass splitting	$|\Delta m_{23}^2| =$	$(2.5 \pm 0.2)\,10^{-3}\ \mathrm{eV}^2$
solar mixing angle	$\tan^2\theta_{12} =$	0.45 ± 0.05
atmospheric mixing angle	$\sin^2 2\theta_{23} =$	1.02 ± 0.04
'CHOOZ' mixing angle	$\sin^2 2\theta_{13} =$	0 ± 0.05

non-oscillation parameter	probed by	experimental limit
$(m^\dagger m)_{ee}^{1/2}$	β-decay	$m_{\nu_e} < 2.0$ eV
ee-entry of m	$0\nu 2\beta$	$m_{ee} < 0.38\,h$ eV
$\sum\limits_{i=1}^{3} m_i$	cosmology	$m_{\mathrm{cosmo}} < 0.6$ eV

flux was about three times smaller. Later, radiochemical experiments using Gallium, as SAGE [48] (located in Baksan, Russia) and GALLEX/SNO [49, 50] (Gran Sasso, Italy), both having an energy threshold $E_\nu > 0.233\,\mathrm{MeV}$, confirmed this deficit. The water Čerenkov experiments Kamiokande [51, 52] and Super–Kamiokande (Kamioka, Japan) also measured the disappearance of electron neutrinos coming from the sun. In both experiments solar neutrinos are detected via scatterings off electrons, $\nu_{e,\mu,\tau}\,e \rightarrow \nu_{e,\nu,\tau}\,e$, where the kinetic energy T_e and the direction of the scattered electrons are measured; it could be verified that the counted neutrinos come from the sun. Due to background radiation, the energy cut-off is set at $T_e > 5\,\mathrm{MeV}$. In the SNO experiment [53, 54] (Sudbury, Canada), a water Čerenkov detector using heavy water with additional salt, where neutrinos interact via elastic scatterings, charged current, and neutral current interactions, the ν_e and $\nu_{\mu,\tau}$ fluxes were measured separately and the Standard Solar Model was consistently tested. In the Borexino experiment [55] (Gran Sasso, Italy), the real time flux of ^{7}Be neutrinos has been measured in agreement with the Solar Standard Model for the first time. That the disappearance of electron neutrinos is indeed caused by the transitions $\nu_e \rightarrow \nu_{\mu,\tau}$ was shown by the scintillator experiment KamLAND [56, 57], measuring $\overline{\nu}_e$ with an energy threshold $E_\nu > 2.6\,\mathrm{MeV}$ emitted by nuclear reactors. Together with the solar neutrino experiments the best fit parameters, shown in Table 1.1, are derived.

Atmospheric anomaly:

Atmospheric neutrinos are generated in charged pion decays which themselves are produced when primary cosmic rays hit the upper part of the earth's atmosphere. Atmospheric neutrinos gave rise to the first neutrino oscillation evidence in 1998 in the Super–Kamiokande experiment [58] that has originally been designed to measure the proton lifetime. It uses a cylindrical 50 kiloton water detector surrounded by photon multipliers to measure atmospheric neutrinos in charged current scatterings off nucleons. In addition to a deficit in the muon neutrino flux, it measured a zenith angle dependence rendering the $\nu_\mu \rightarrow \nu_\tau$ oscillation with quasi-maximal angle the most convincing explanation. This has been confirmed by the K2K experiment where a pulsed ν_μ beam has been sent from the KEK collider in Japan to the 250 km distant Super–Kamiokande detector. Super–Kamiokande can distinguish between atmospheric neutrinos and neutrinos produced at KEK. Together with water Čerenkov detectors close to the neutrino source at KEK, the neutrino oscillation interpretation, i.e., the transition $\nu_\mu \rightarrow \nu_\tau$, was confirmed [59]. The similarly designed NuMi experiment (Fermilab) measures pulsed ν_μ produced at Fermilab with the Minos detector that is located at a distance of 735 km in the Soudan mine in Minnesota, pointing again to the oscillation explanation [60]. The best-fit parameters of K2K and NuMi are shown in Table 1.1.

'CHOOZ' mixing angle:

The CHOOZ experiment looked at the disappearance of $\overline{\nu}_e$ produced in nuclear reactors in France at a distance of L$\sim$ 1 km from the detector. CHOOZ gives the most stringent upper limit on the angle θ_{13} [61] that, together with atmospheric and K2K data, gives the value shown in Table 1.1.

β-decay:

Since oscillation experiments only measure mass-squared differences, they are insensitive to the absolute neutrino mass scale. On the other hand, β-decay experiments looking at the tail of the energy spectrum in the Kurie-plot give a direct handle on the absolute neutrino mass scale, probing $m_{\nu_e}^2 = \left(m \cdot m^\dagger \right)_{ee} = \sum_i |V_{ei}^2| m_i^2$. The most stringent limits are derived from the tritium β-decay:

$$^3\text{H} \rightarrow {}^3\text{He} + e^- + \overline{\nu}_e \quad \text{with} \quad \text{Q} = 18.6 \,\text{keV}, \tag{1.6}$$

where Q is the total energy released in the β-decay. For this process the most recent results are obtained by the Mainz experiment [62] and the Troitsk experiment [63,

64]:

$$m_{\nu e}^2 = -0.6 \pm 2.2 \pm 2.1 \, \text{eV}^2 \quad \text{MAINZ}$$

$$m_{\nu e}^2 = -2.3 \pm 2.5 \pm 2.0 \, \text{eV}^2 \quad \text{TROITSK}. \tag{1.7}$$

A combination of these constraints leads to the value shown in Table 1.1. The approved upcoming experiment KATRIN [65], having an energy resolution of $1 \, \text{eV}$, is expected to reach a sensitivity down to $m_{\nu e} \simeq 0.35 \, \text{eV}$.

$0\nu 2\beta$-decay:
Double β-decay of ^{76}Ge has been observed with a lifetime of about 10^{21} years. If neutrinos are Majorana particles, the observation of neutrinoless double-β decay ($0\nu 2\beta$-decay) seems feasible. The rate for $0\nu 2\beta$-decay can be expressed as

$$\Gamma_{0\nu 2\beta} = G \cdot |\mathcal{M}_0|^2 \cdot |m_{ee}/h|^2, \tag{1.8}$$

where G is a known phase space factor, $\mathcal{M}_0$ is the nuclear matrix element, see e.g. [44], and $m_{ee} = \sum_i V_{ei}^2 m_i$. The factor $h = \mathcal{M}_0/\mathcal{M}$ accounts for the uncertainty in the calculation of $\mathcal{M}$ and is $\mathcal{O}(\text{few})$. To test the $0\nu 2\beta$-decay rate, in the Heidelberg–Moscow [66] and the IGEX [67, 68] experiment ^{76}Ge has been used. The most stringent bound comes from the CUORICINO experiment, which uses ^{130}Te, giving the value for m_{ee} shown in Table 1.1. In a reanalysis of the Heidelberg–Moscow data parts of the collaboration claim a 4σ discovery signal [69, 70], corresponding to $m_{ee} < 0.19 - 0.68 \, \text{eV}$, with the uncertainty due the nuclear matrix element calculation. Future experiments like GERDA [71], MAJORANA [72], and CUORE [73] will have a sensitivity in the $50 \, \text{meV}$ range.

Cosmology:
The observation of the CMB and the data from large scale structure formation imply a bound on the total energy density Ω_ν contained in neutrinos. Both probes are sensitive to the free-streaming character of relativistic particles. This gives the dominant upper bound on the sum of the neutrino mass. However, this bound varies with the data sets included in the analysis. In Table 1.1 we take the somewhat conservative bound derived in [74].

Conclusion:
Both, direct and indirect measurements indicate a neutrino mass-scale in the sub-eV range, i.e., six orders of magnitude smaller than the electron mass. From a theoretical perspective, it cannot be understood why the Yukawa couplings of neutrinos should be

that small (to get a neutrino mass $m_\nu \approx 0.01\,\text{eV}$ the coupling should be of the order $h \sim 10^{-13}$).

1.5 The see-saw explanation

The see-saw mechanism provides a natural explanation for the smallness of neutrino masses in grand unification theories at high energies [43, 75–78]. As already mentioned in Section 1.3, an $SO(10)$–GUT contains right-handed neutrinos as part of a **16** spinorial representation and is anomaly free. The unification gauge group is then broken down to the SM gauge group at some high scale of order $10^{12} - 10^{16}$ GeV. The right-handed neutrinos obtain Majorana masses since they are not singlets under the $SO(10)$ gauge group and couple to some Higgs representation that develops a vacuum expectation value during this phase transition. Furthermore, as SM gauge singlets their masses are not protected by the SM gauge symmetries, i.e., they can naturally be significantly larger than the SM symmetry breaking scale.

In the minimal (type-I) see-saw model, gauge singlet fermions with Majorana masses M couple to the massless lepton doublet and the Higgs doublet of the SM through Yukawa couplings. These Yukawa couplings then generate a Dirac mass relating the heavy singlets to SM neutrinos upon spontaneous symmetry breaking of the electroweak gauge symmetry. The weakly-interacting neutrinos develop small masses $\sim m_D^2/M$ as we will explain in the following. For the type-I see-saw mechanism the most general gauge invariant renormalizable Lagrangian is given by

$$\mathcal{L} = \mathcal{L}_{SM} + i\overline{\nu}_{Ri}\slashed{\partial}\nu_{Ri} - \overline{l}_{L\alpha}\lambda_{\nu\alpha}\nu_{Ri}\Phi - \frac{1}{2}\overline{\nu_{Ri}^c}M_{M_i}\nu_{Ri} + h.c. \qquad (1.9)$$

Here, we added $i = 1, 2, 3$ right-handed neutrinos ν_{Ri} to the SM with three ($\alpha = e, \mu, \tau$) light generations. The Lagrangian $\mathcal{L}$ contains in addition to the SM Lagrangian the kinetic energy and Majorana mass term for the right-handed neutrinos as well as Yukawa interactions $\lambda_{\nu\alpha}$, between right-handed neutrino singlets ν_{Ri}, left-handed lepton doublets $l_{L\alpha}$, and the Higgs boson scalar doublet $\Phi = (\Phi^0, \Phi^-)$. The covariant derivative in the kinetic energy term for the right-handed neutrinos reduces to $D_\mu = \partial_\mu$ because these are SM singlets. Lepton number violating Majorana mass terms are additionally allowed by the gauge symmetries. The Majorana mass matrix M_{M_i} is a 3×3 complex symmetric matrix and has eigenvalues of $\mathcal{O}(M)$. The charge conjugate of the chiral fermion field, which appears in the Majorana mass term, is defined by $\nu_{Ri}^c \equiv C\overline{\nu_{Ri}}^T$. Furthermore, λ_ν is the 3×3 matrix of neutrino Yukawa couplings. (Note, that one could just put in the Majorana mass term by hand and does not necessarily need a GUT embedding.) After electroweak symmetry breaking the term containing the Yukawa couplings between left- and right-handed neutrino states provides a Dirac mass term for neutrinos, $m_D = \lambda\, v$,

where $v = 174$ GeV is the vacuum expectation value of the Higgs field. The part in the Lagrangian containing Yukawa couplings and the right-handed neutrino Majorana mass term can then be written as

$$L_M = -\frac{1}{2} \left(\overline{\nu}_L, \overline{\nu}_R^c\right) \begin{pmatrix} 0 & m_D \\ m_D^T & M_M \end{pmatrix} \begin{pmatrix} \nu_L^c \\ \nu_R \end{pmatrix}. \tag{1.10}$$

The typical see-saw mechanism assumes that the elements of the Majorana mass matrix are much larger than the Dirac mass matrix entries $M_{M_i} \gg m_{D_i}$. The mass matrix in Eq. (1.10) can then be block-diagonalized and, at leading order, one can distinguish two neutrino mass eigenstates:

$$\text{a right-handed state:} \quad R = \nu_R + \nu_R^c$$
$$\text{and a left-handed state:} \quad \nu = \nu_L + \nu_L^c. \tag{1.11}$$

The mass matrix of the left-handed state is suppressed by the high-energy scale *M*,

$$m_{\nu_{ij}} = v^2 \lambda_{ik} M_{M_k}^{-1} \lambda_{jk}. \tag{1.12}$$

Thus, with the above mentioned mass scale $M \sim 10^{12} - 10^{14}$ GeV one gets light neutrino masses in the sub-eV range without demanding particularly small Yukawa couplings.

Adding a fermionic singlet representation (type-I) however, is not the only extension of the SM that leads to a successful see-saw mechanism. In the type-II see-saw [78–80] a scalar triplet and in the type-III see-saw [81, 82] a fermionic triplet is added. All of these mechanisms have in common that the resulting neutrino masses are suppressed by a higher mass scale.

In this thesis we concentrate on the right-handed neutrinos added in a type-I see-saw setting. In the next chapter we introduce the leptogenesis framework as a mechanism that creates the matter-antimatter asymmetry of the universe. In Chapter 3 we provide a calculation of the lepton asymmetry generated in heavy neutrino decays using a network of momentum mode equations. The use of single mode equations will lead to significant differences in the final asymmetry compared to the use of momentum integrated Boltzmann equations that are conventionally used in leptogenesis calculations. In Chapter 4 we include scattering of right-handed neutrinos via Yukawa couplings off quarks in our calculation. In leptogenesis these scatterings are important since, on the one hand, they provide an additional production channel for right-handed neutrinos and lead to a more efficient equilibration of their distribution functions. On the other hand, as an additional lepton number violating interaction, they contribute to the wash-out of the produced asymmetry. Finally, in Chapter 5 we apply the calculation of the matter-antimatter

asymmetry with our treatment of complete Boltzmann equations to an alternative scenario of leptogenesis in which the lepton asymmetry is generated in the decays of the next-to-lightest right-handed neutrino.

In Appendix A we show how scattering processes can be implemented in the momentum integrated Boltzmann equations, whereas in Appendix B we provide a method to implement scattering processes in the complete mode equations. In Appendix C the evolution of the top Yukawa coupling from high scales to low scales is calculated.

The main results of Chapters 3 and 4 are based on the research paper [83], whereas in Chapter 5 we present unpublished material.

Chapter 2

Baryogenesis via leptogenesis

Relying on the type-I see-saw mechanism to create small masses for the SM neutrinos, leptogenesis [42] provides an attractive explanation of the baryon asymmetry of the universe. The ingredients of this mechanism are simple: the out-of-equilibrium decay of the heavy neutrino states into leptons and Higgs particles violates CP, from whence a lepton asymmetry can be generated. This lepton asymmetry is then partially transformed into a baryon asymmetry by anomalous processes of the SM called sphalerons [16], introduced earlier in Section 1.2. In this way the three Sakharov conditions are fulfilled and leptogenesis turns out as a consequence of the see-saw mechanism. At this point we will shortly sketch how to calculate the CP asymmetry in the decays of a heavy neutrino state N_i. We will continue with the discussion of the out-of-equilibrium condition and at the end of this section summarize the ideas of the standard thermal leptogenesis scenario.

2.1 CP asymmetry

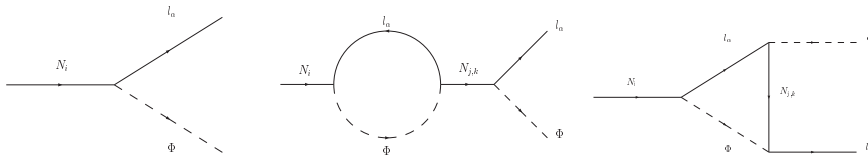**Figure 2.1:** CP violation in interference of tree-level with one-loop diagrams.

In general, the total decay width of a right-handed neutrino generation N_i at tree-level is given by:

$$\Gamma_{D_i} = \sum_\alpha \left(\Gamma(N_i \to \Phi + l_{L\alpha}) + \Gamma(N_i \to \overline{\Phi} + \bar{l}_{L\alpha}) \right) = \frac{1}{8\pi} \left(\lambda^\dagger \lambda \right)_{ii} M_i, \qquad (2.1)$$

where the sum is taken over the single decay rates into lepton flavor α. The CP asymmetry in lepton flavor α is then defined as

$$\varepsilon_{i\alpha} \equiv \frac{\Gamma(N_i \to \Phi + l_{L\alpha}) - \Gamma(N_i \to \overline{\Phi} + \bar{l}_{L\alpha})}{\Gamma(N_i \to \Phi + l_L) + \Gamma(N_i \to \overline{\Phi} + \bar{l}_L)}. \tag{2.2}$$

This asymmetry is due to the interference of the tree-level amplitude and the one-loop vertex and self-energy contributions shown in Figure 2.1. The indices i and α denote the generation of the decaying right-handed neutrino and the flavor of the produced lepton, respectively. Accounting for different lepton generations, the CP asymmetry is a diagonal matrix in flavor space [84]:

$$\varepsilon_{i\alpha} = \frac{3}{16\pi (\lambda^\dagger \lambda)_{ii}} \sum_{j \neq i} \left\{ \operatorname{Im} \left[\lambda_{\alpha i}^* \left(\lambda^\dagger \lambda \right)_{ij} \lambda_{\alpha j} \right] \frac{\xi(x_j/x_i)}{\sqrt{x_j/x_i}} \right. \tag{2.3}$$

$$\left. + \frac{2}{3(x_j/x_i - 1)} \operatorname{Im} \left[\lambda_{\alpha i}^* \left(\lambda^\dagger \lambda \right)_{ji} \lambda_{\alpha j} \right] \right\}, \tag{2.4}$$

where $x_i = M_i^2/M_1^2$ and the function ξ is defined as [85]

$$\xi = \frac{2}{3} x \left[(1+x) \log \left(\frac{1+x}{x} \right) - \frac{2-x}{1-x} \right]. \tag{2.5}$$

For simplicity, we will assume a hierarchical mass spectrum for the heavy right-handed neutrinos with a diagonal mass matrix M_M, i.e., $M_1 \ll M_2, M_3$, called the N_1-dominated scenario. With this assumption the CP asymmetry can be calculated to be [84, 86]:

$$\varepsilon_{1\alpha} = \frac{3}{16\pi} \frac{M_1}{(\lambda^\dagger \lambda)_{11} v^2} \operatorname{Im} \left\{ \lambda_{\alpha 1}^* \left(m_\nu^* \lambda \right)_{\alpha 1} \right\}. \tag{2.6}$$

Neglecting the lepton-flavor structure of the CP asymmetry, i.e., summing over all lepton flavors, $\varepsilon_1 = \sum_\alpha \varepsilon_{1\alpha}$, one can derive an upper bound on the total CP asymmetry [87, 88]:

$$\varepsilon_1^{\max} (M_1, \tilde{m}_1, m_{\min}, m_{\max}) = \varepsilon_1^{\max}(M_1) \beta(\tilde{m}_1, m_{\max}), \tag{2.7}$$

$$\text{with} \quad \beta(\tilde{m}_1, m_{\min}, m_{\max}) = \frac{\left(m_{\max} - m_{\min} \sqrt{1 + \frac{m_{\text{atm}}^2}{\tilde{m}_1}} \right)}{m_{\text{atm}}} \leq 1, \tag{2.8}$$

where $m_{\text{atm}} = \sqrt{\Delta m_{23}^2 - \Delta m_{12}^2} = m_{\max} - m_{\min}$ [85]. The quantity $\tilde{m}_1$ is the effective neutrino mass and we will discuss it later on. The maximal value for the asymmetry, i.e., $\beta = 1$, is reached for fully hierarchical neutrinos with $m_{\min} = 0$, implying

$m_{\text{max}} = \sqrt{m_{\text{atm}}^2}$ and is given by:

$$\varepsilon_1^{\text{max}} = \frac{3}{16\pi} \frac{M_1 m_{\text{atm}}}{v^2} \approx 10^{-6} \left(\frac{M_1}{10^{10}\,\text{GeV}} \right) \left(\frac{m_{\text{atm}}}{0.05\text{eV}} \right). \tag{2.9}$$

2.2 Deviation from thermal equilibrium

The out-of-equilibrium dynamic that is necessary for successful leptogenesis is provided by the expansion of the universe. Interactions are classified to be in (or out-of) equilibrium by comparing their rates to the expansion rate of the universe H. Concerning leptogenesis, one usually compares the total decay rate of the right-handed neutrino state given in Eq. (2.1) to the expansion rate at temperatures $T \sim M_i$,

$$H(T = M_i) = \sqrt{4\pi^3 g^*/45}\,(M_i/M_{\text{Pl}}), \tag{2.10}$$

where $M_{\text{Pl}} = 1.221 \times 10^{19}$ GeV is the Planck mass, and $g^* = 106.75$ corresponds to the number of relativistic degrees of freedom in the SM at temperatures higher than the electroweak scale. For this purpose one introduces the decay parameter as the ratio of the decay rate, Eq. (2.1), over the expansion rate of the universe Eq. (2.10)

$$K_i \equiv \frac{\Gamma_{D_i}}{H(M_i)} = \frac{\tilde{m}_i}{m_*}. \tag{2.11}$$

It proves useful to introduce at this point two dimensionless variables to connect the decay parameter to the neutrino mass scale:

The *effective neutrino mass* [89]:

$$\tilde{m}_i = \frac{(m_D^\dagger m_D)_{ii}}{M_i}, \tag{2.12}$$

where $m_{D_{ij}} = \lambda_{\nu_{ij}} v$, cf. Eq. (1.10). And the *equilibrium neutrino mass*:

$$m_* = \frac{16\pi^{\frac{5}{2}}\sqrt{g^*}}{3\sqrt{5}} \frac{v^2}{M_{\text{Pl}}} \approx 1.08 \times 10^{-3}\,\text{eV}. \tag{2.13}$$

It has been shown [90] that the effective neutrino mass for the lightest right-handed state is always larger than the mass of the lightest SM neutrino state, i.e., $\tilde{m}_1 > m_{\text{min}}$.

The decay parameter controls whether the right-handed neutrino decays in equilibrium ($K_i > 1$) or out of equilibrium ($K_i < 1$) and is a key quantity for the dynamics of leptogenesis.

2.3 Thermal leptogenesis

In the standard scenario of thermal leptogenesis the right-handed neutrinos are produced in the early universe via inverse decays and $2 \leftrightarrow 2$ scatterings with the top quark and electroweak gauge bosons. As initial condition one supposes that after the period of inflation the thermal bath of the universe is produced in the reheating process when the heavy scalar field responsible for inflation decays into light degrees of freedom. The temperature of the thermal bath at the beginning of the radiation dominated phase of the universe is denoted as the reheating temperature T_{RH}. Restricting the discussion to the N_1-dominated scenario, it has been shown in [90, 91] that the Yukawa coupling that describes the right-handed neutrino decay via the decay parameter, Eq. (2.11), alone leads to a sufficient abundance of heavy neutrinos for leptogenesis to be successful. Inverse decays and lepton number violating $2 \leftrightarrow 2$ scatterings, on the other side, contribute to the total wash-out of the lepton asymmetry that was produced in the heavy neutrino decays. This makes the dynamics of leptogenesis more involved and studies by means of Boltzmann equations are needed. In general, the baryon asymmetry produced by leptogenesis can be written as [92]

$$\eta_B = \frac{3}{4} \frac{\alpha_{\mathrm{sph}}}{f} \, \varepsilon_1 \, \kappa_f \equiv d \, \varepsilon_1 \, \kappa_f \simeq 0.96 \times 10^{-2} \, \varepsilon_1 \, \kappa_f. \tag{2.14}$$

Here, κ_f is the final efficiency factor that parametrizes the amount of asymmetry that survives the competing production and wash-out processes. It is a direct result of solving the relevant Boltzmann equations for leptogenesis. In the limit of vanishing wash-out and a thermal initial abundance for the right-handed neutrino, the efficiency factor has a final value $\kappa_f = 1$. The factor $f = 2387/86$ accounts for the dilution of the baryon asymmetry due to photon production from the onset of leptogenesis till recombination and the quantity $\alpha_{\mathrm{sph}} = 28/79$ is the conversion factor of the $B - L$ asymmetry into a baryon asymmetry by the sphalerons processes, see Section 1.2.

Note that, using the maximal CP asymmetry Eq. (2.9), one can derive a lower bound on the heavy neutrino mass M_1 since the produced baryon asymmetry has to be larger (equal) to the observed value, $\eta_B^{\mathrm{max}} \geq \eta_B^{CMB}$, yielding the constraint

$$M_1 > M_1^{\mathrm{min}} = \frac{1}{d} \frac{16\pi}{3} \frac{v^2}{m_{\mathrm{atm}}} \frac{\eta_B^{CMB}}{\kappa_f}$$

$$\approx 6.5 \times 10^8 \ \mathrm{GeV} \left(\frac{\eta_B^{CMB}}{6 \times 10^{10}} \right) \left(\frac{0.05 \ \mathrm{eV}}{m_{\mathrm{atm}}} \right) \kappa_f^{-1}. \tag{2.15}$$

For a successful production of the baryon asymmetry this corresponds to a lower bound on the initial temperature of leptogenesis [92], i.e.,

$$T_{\mathrm{RH}} \gtrsim 1.5 \times 10^9 \ \mathrm{GeV}. \tag{2.16}$$

In the context of supersymmetric theories this might lead to the so-called gravitino problem. The gravitino is the gauge field of local supersymmetry and its thermal production rate [93, 94] is increasing with the reheating temperature $T_{\rm RH}$. If the gravitino is not the lightest supersymmetric particle, a too large abundance of gravitinos might lead to problems with BBN since the decay products of the gravitino can destroy the light nuclei produced in BBN, cf. Figure 1.3. If the gravitino mass is smaller then $20\,{\rm TeV}$, this leads to an upper bound on the reheating temperature [95]

$$T_{\rm RH} \lesssim 10^6 \text{ GeV}. \tag{2.17}$$

On the other hand, if the gravitino is the lightest supersymmetric particle, its abundance is limited by the amount of observed dark matter in the universe, cf. Figure 1.1, leading again to an upper bound on $T_{\rm RH}$[93, 96, 97]

$$T_{\rm RH} \lesssim 10^7 - 10^9 \text{ GeV}. \tag{2.18}$$

From this perspective, it seems very challenging to realize standard thermal leptogenesis in the local supersymmetric framework. Within thermal leptogenesis the bound in Eq. (2.15) can be circumvented assuming a quasi degenerate mass spectrum for the right-handed neutrinos, i.e., $M_1 \simeq M_2 \simeq M_3$. For such a degeneracy the CP asymmetry exhibits a resonance and is remarkably enhanced. As a consequence, the production of the observed value of the baryon asymmetry in this so-called *resonant leptogenesis* [98–100] scenario is possible down to the TeV scale.

Another possibility to reduce the lower bound on $T_{\rm RH}$ is provided in *non-thermal leptogenesis* [87, 101–104], where the right-handed neutrinos are produced in the decays of some heavy scalar field, e.g., the inflaton. The right-handed neutrino contribute then the dominant part of the energy budget of the universe, called a dominant initial abundance [105]. Depending on the coupling of the scalar field and the right-handed neutrino Yukawa coupling, successful leptogenesis in this scenarios demands [106]

$$T_{\rm RH} \gtrsim 10^6 \text{ GeV}. \tag{2.19}$$

Finally, we want to mention the supersymmetric scenario of *soft leptogenesis* [107–109], where the CP violation is not due to flavor physics but to the supersymmetry-breaking terms. A CP violation is induced in the mixing of two neutral sneutrino states. For a certain choice of parameters the lower bound on the reheating temperatures is again given by Eq. (2.19) [105].

Chapter 3

Mode equations for leptogenesis

In the recent past a huge step forward has been made towards understanding in detail the processes of leptogenesis that have been introduced in the last section. Relevant studies include leptogenesis in a supersymmetric context [91], thermal effects [105, 110], analytic formulae for the final efficiency factor [92], the role of flavor [111–114], as well as leptogenesis with CP violation coming only from the measurable low-scale PMNS matrix [115]. Furthermore, it has been pointed out that the classical Boltzmann equations are insufficient to describe the transition region between the flavored and the unflavored regimes [116]; a full quantum-mechanical description in terms of density matrices is necessary. On this front, the quantum-mechanical Kadanoff–Baym equations have been investigated for toy models in extreme out-of-equilibrium situations [117, 118].

On a different front, the classical Boltzmann equations have been solved for the first time for single momentum modes [119]. As one of Sakharov's conditions [14], departure from thermal equilibrium is crucial for the dynamic creation of a baryon asymmetry. In the leptogenesis scenario, out-of-equilibrium conditions are achieved when interactions are no longer able to maintain the momentum distribution function of the right-handed neutrino at its equilibrium value as the universe expands. To simplify the calculation, this non-equilibrium process is traditionally studied by means of the integrated Boltzmann equations [89, 105, 120, 121], whereby the equations of motion for the distribution functions of all particle species involved are integrated over momentum such that only the evolution of the *number densities* is tracked. However, in order for the integrated equations to be in a closed form, it is necessary to neglect quantum statistical behaviors (e.g., Pauli blocking) and assume kinetic equilibrium for all particle species, including the right-handed neutrino. For particle species with gauge interactions these assumptions seem justifiable. For the right-handed neutrino however, their validity is not immediately obvious.

To estimate the effects of kinetic equilibrium and quantum statistics, the Boltzmann

equations for the individual momentum modes have been solved in [119], taking into account only the decay and inverse decay of the right-handed neutrino within the unflavored framework. More recently, the mode equations have been used to study the effect of a pre-existing asymmetry and the soft leptogenesis scenario, again including only decays and inverse decays [122]. In the present thesis, we extend on these previous studies by considering also scattering processes of the right-handed neutrino with the top quark [83].

3.1   Particle kinematics

Boltzmann equations encode the time evolution of the distribution function of particle species. Here, we will give a short derivation of the Boltzmann equation for a particle species Ψ in an isotropic and spatially homogeneous universe described by the Robertson–Walker–Metric [2],

$$ds^2 = dt^2 - a(t)^2 \left\{ \frac{dr^2}{1 - kr^2} + r^2 d\vartheta^2 + r^2 \sin^2 \vartheta d\phi^2 \right\}, \tag{3.1}$$

where $a(t)$ is the cosmic scale factor, which describes the expansion of the universe, $k = \pm 1, 0$ specifies the curvature, and (t, r, ϑ, ϕ) are the comoving coordinates.

The trajectory of a particle Ψ with mass $m_\Psi \geq 0$ moving in a gravitational field is given by the geodesic equations of motion [123]:

$$\frac{dp_\Psi^\mu}{d\tau} + \Gamma^\mu_{\nu\alpha} \, p_\Psi^\nu \, p_\Psi^\alpha = 0, \tag{3.2}$$

$$\frac{dx_\Psi^\mu}{d\tau} = p_\Psi^\mu. \tag{3.3}$$

Since $s = m_\Psi \tau$ is the eigen-time of the particle, τ is fixed and p^μ is the momentum of a particle Ψ.

In the Robertson–Walker–Metric the $\mu = 0$ component of Eq (3.2) is given as:

$$\frac{dp_\Psi^0}{d\tau} + \frac{\dot{a}}{a} \mathbf{p}_\Psi^2 = 0, \qquad \text{with} \quad \dot{a} = \frac{\partial a}{\partial t}. \tag{3.4}$$

Writing $p_\Psi^0 \, dp_\Psi^0 = |\mathbf{p}_\Psi| \, d|\mathbf{p}_\Psi|$, this leads to:

$$|\dot{\mathbf{p}}_\Psi| a + \dot{a} |\mathbf{p}_\Psi| = 0$$
$$\Leftrightarrow \frac{d}{dt} (|\mathbf{p}_\Psi| a) = 0$$
$$\Leftrightarrow |\mathbf{p}_\Psi| = const. \times \frac{1}{a}. \tag{3.5}$$

Therefore the 3-momentum scales as $1/a$.

In general, the Liouville operator describing the evolution of a point particle's phase space in a gravitational field is given by,

$$L = p^\alpha \frac{\partial}{\partial x^\alpha} - \Gamma^\alpha_{\ \beta\gamma} p^\beta p^\gamma \frac{\partial}{\partial p^\alpha}. \tag{3.6}$$

With this operator the equations of motion (3.2) and (3.3) can be written for the momentum as

$$\frac{dp^\mu}{d\tau} = L\left[p^\mu\right], \tag{3.7}$$

and for the space-time one has

$$\frac{dx^\mu}{d\tau} = L\left[x^\mu\right]. \tag{3.8}$$

Furthermore, it is known that the time derivative of the phase space distribution of a non-interacting gas vanishes, i.e.,

$$\frac{df(x,p)}{d\tau} = 0. \tag{3.9}$$

Using now the equations of motion for the particle one obtains the Boltzmann equations for the non-interacting particle species Ψ:

$$L\left[f_\Psi(x,p)\right] = 0. \tag{3.10}$$

Since we are assuming a Robertson–Walker universe, which is isotropic and homogeneous, the distribution function f_Ψ depends only on t and $|\mathbf{p}_\Psi|$. Therefore, the Boltzmann equation can be written as [2]

$$L\left[f_\Psi\right] = E_\Psi \frac{\partial f_\Psi}{\partial t} - H|\mathbf{p}_\Psi|^2 \frac{\partial f_\Psi}{\partial E_\Psi} = 0, \tag{3.11}$$

where we have not written all the arguments to keep the notation clearer.

Since $p_\Psi^2 = m_\Psi^2$ and because of the spatial isotropy of the Robertson–Walker–Metric, one has

$$|\mathbf{p}_\Psi|^2 \frac{\partial f_\Psi}{\partial E_\Psi} = E_\Psi\, |\mathbf{p}_\Psi|\, \frac{\partial f_\Psi}{\partial |\mathbf{p}_\Psi|}. \tag{3.12}$$

After dividing by E_Ψ, Eq. (3.11) gets the following form

$$L'\left[f_\Psi\right] = \frac{\partial f_\Psi}{\partial t} - H\,|\mathbf{p}_\Psi|\, \frac{\partial f_\Psi}{\partial |\mathbf{p}_\Psi|}. \tag{3.13}$$

Interactions can now be introduced on the right-hand side by a collision term $C\left[f_\Psi\right]$ which drives the distribution function towards its equilibrium. Now, the complete Boltzmann equation reads

$$L'\left[f_\Psi\right] = \frac{\partial f_\Psi}{\partial t} - H\left|\mathbf{p}_\Psi\right| \frac{\partial f_\Psi}{\partial\left|\mathbf{p}_\Psi\right|} = C\left[f_\Psi\right]. \tag{3.14}$$

Thus, the Boltzmann equation in a Robertson–Walker universe has the form of a partial differential equation. However, in the radiation dominated phase of the universe, in which leptogenesis takes place, Eq. (3.14) can be written as an ordinary differential equation by transforming to the dimensionless coordinates $z = m_\Psi/T$ and $y_\Psi = \left|\mathbf{p}_\Psi\right|/T$. Using the relation $dT/dt = -HT$, the differential operator $\partial_t - \left|\mathbf{p}_\Psi\right| H \partial_{\left|\mathbf{p}_i\right|}$ becomes $zH\partial_z$, and consequently [124]

$$\frac{\partial f_\Psi(z,y)}{\partial z} = \frac{z}{H\left(m_\Psi\right)} C_D\left[f_\Psi(z,y)\right], \tag{3.15}$$

with $H\left(m_\Psi\right)$ given in Eq. (2.10). Now, the Boltzmann equation can be easily solved numerically on a grid for specific rescaled momenta y.

3.2 Leptogenesis set-up

In this thesis we concentrate mainly on the simplest case of "vanilla leptogenesis", in which a lepton asymmetry is established from the decay and scattering of the lightest heavy right-handed neutrino N_1. We neglect the decay of the two heavier neutrino states $N_{2,3}$ [125], assuming that any lepton asymmetry produced from these decays will be efficiently washed out by the N_1 interactions. This is called the N_1-dominated scenario. [1] Therefore we will drop the subscript "1", and refer to the lightest right-handed neutrino simply as N in the following. Furthermore, we will work in the one-flavor approximation since flavor effects do not change the kinetic consideration for the mode equations.

As shown in the previous section, the Boltzmann equation for a right-handed neutrino (RHN) in a Friedman–Lemaître–Robertson–Walker framework can be written as

$$\frac{\partial f_N(z,y)}{\partial z} = \frac{z}{H(M)} \left(C_D[f_N(z,y)] + C_S[f_N(z,y)]\right). \tag{3.16}$$

On the right-hand side, the collision integrals $C_D\left[f_N\right]$ and $C_S\left[f_N\right]$ encode respectively the interactions of the RHN due to decays into leptons and Higgs (D) and scattering processes via Yukawa interactions with the top quark (S).

The Boltzmann equation for leptons (anti-leptons) with phase space distribution f_l ($f_{\bar{l}}$) has a similar form to Eq. (3.16), save for the replacements $f_N \to f_l$ ($f_N \to f_{\bar{l}}$)

---

[1]For a different scenario, N_2-dominated leptogenesis, see Chapter 5.

and $y_N \to y_l$ ($y_N \to y_{\bar{l}}$). Since we are interested in the asymmetry between leptons and antileptons, it is convenient to define

$$f_{l-\bar{l}} \equiv f_l - f_{\bar{l}}, \tag{3.17}$$

and the corresponding Boltzmann equation

$$\frac{\partial f_{l-\bar{l}}(z,y)}{\partial z} = \frac{z}{H(M)} \left(C_D[f_{l-\bar{l}}(z,y)] + C_S[f_{l-\bar{l}}(z,y)] \right), \tag{3.18}$$

where $C_{D,S}\left[f_{l-\bar{l}}\right] \equiv C_{D,S}\left[f_l\right] - C_{D,S}\left[f_{\bar{l}}\right]$. Integrating $f_{l-\bar{l}}$ over the lepton phase space, i.e.,

$$n_{l-\bar{l}} \equiv \frac{g_l}{(2\pi)^3} \int d^3 p_l \, f_{l-\bar{l}}, \tag{3.19}$$

with $g_l = 2$, gives us the lepton asymmetry per comoving photon,

$$N_{l-\bar{l}} \equiv \frac{n_{l-\bar{l}}}{n_\gamma^{\rm eq}}, \tag{3.20}$$

where $n_\gamma^{\rm eq} = (\zeta(3)/\pi^2) g_\gamma T^3$, with $g_\gamma = 2$, is the equilibrium photon density.

This lepton asymmetry is translated into a baryon asymmetry in sphaleron processes, cf. Section 1.2, giving [126]

$$N_B = \alpha_{\rm sph} N_{B-L} = \frac{\alpha_{\rm sph}}{\alpha_{\rm sph} - 1} N_{l-\bar{l}}, \tag{3.21}$$

with $\alpha_{\rm sph} = 28/79$. The Boltzmann equations (3.16) and (3.18) encode how a lepton asymmetry is generated and washed out in an expanding universe given some specific particle interactions.

3.3   Decay and inverse decay

In this section, which is based on the research paper [83], we consider the simplest possible scenario of thermal leptogenesis, in which only the decay and inverse decay of the RHN into lepton l and Higgs Φ pairs contribute to the evolution of f_N, i.e., we set $C_S = 0$ in Eqs. (3.16) and (3.18). The decay and inverse decay of the RHN violate CP through interference of the tree-level and the one-loop diagrams (cf. Figure 2.1).

The collision integral for the RHN in the decay–inverse decay picture has the following form:

$$C_D\left[f_N\right] = \frac{1}{2\,E_N} \int \frac{d^3 p_l}{2E_l(2\pi)^3} \frac{d^3 p_\Phi}{2E_\Phi(2\pi)^3} (2\pi)^4 \delta^4 \left(p_N - p_l - p_\Phi\right) \tag{3.22}$$
$$\times \left[f_\Phi\, f_l\,(1 - f_N)\left(|\mathcal{M}_{\Phi l \to N}|^2 + |\mathcal{M}_{\Phi \bar{l} \to N}|^2\right)\right.$$
$$\left. - f_N\,(1 - f_l)\,(1 + f_\Phi)\left(|\mathcal{M}_{N \to \Phi l}|^2 + |\mathcal{M}_{N \to \Phi \bar{l}}|^2\right)\right],$$

where E_i and p_i are, respectively, the energy and 4-momenta of the particle species i, and $\mathcal{M}_A$ denotes the matrix element for the process A. At tree-level, the squared matrix element summed over all internal degrees of freedom for the decay of the RHN into a pair of lepton and Higgs particles is given by

$$|\mathcal{M}_{N\to\Phi l}|^2 = 2\,\frac{(m_D^\dagger m_D)_{11}}{v^2}\,p_l p_N, \tag{3.23}$$

where the neutrino mass matrix m_D has been defined in Section 1.5.

The integral (3.22) can be readily reduced to a one dimensional form [127]

$$C_D\,[f_N] = \frac{M\,\Gamma_D}{E_N|\mathbf{p}_N|}\int_{(E_N-p_N)/2}^{(E_N+p_N)/2} dp_\Phi\,[f_\Phi f_l(1-f_N) - f_N(1-f_l)(1+f_\Phi)]\,, \tag{3.24}$$

where

$$\Gamma_D = \frac{\tilde{m}_1 M^2}{8\pi v^2} \tag{3.25}$$

is the total decay rate in the RHN's rest frame written in terms of the effective neutrino mass (cf. Eq. (2.12)).

For leptons participating in the same decay and inverse decay processes, the collision integral is given by

$$C_D\,[f_l] = \frac{1}{2\,E_l}\int\frac{d^3 p_N}{2E_N(2\pi)^3}\frac{d^3 p_\Phi}{2E_\Phi(2\pi)^3}\,(2\pi)^4\,\delta^4\,(p_N - p_l - p_\Phi) \tag{3.26}$$
$$\times\,[f_N\,(1-f_l)\,(1+f_\Phi)\,|\mathcal{M}_{N\to\Phi l}|^2$$
$$-\,f_\Phi f_l\,(1-f_N)\,|\mathcal{M}_{\Phi l\to N}|^2\,]\,.$$

An analogous expression for the anti-leptons can be derived by replacing $f_l \to f_{\bar{l}}$, $\mathcal{M}_{N\to\Phi l} \to \mathcal{M}_{N\to\Phi\bar{l}}$, and $\mathcal{M}_{\Phi l\to N} \to \mathcal{M}_{\Phi\bar{l}\to N}$. Some useful relations exist between the matrix elements following from CPT-invariance [120]:

$$|\mathcal{M}_{N\to\Phi l}|^2 = |\mathcal{M}_{\Phi\bar{l}\to N}|^2 = |\mathcal{M}_0|^2\,(1+\varepsilon), \tag{3.27}$$
$$|\mathcal{M}_{N\to\Phi\bar{l}}|^2 = |\mathcal{M}_{\Phi l\to N}|^2 = |\mathcal{M}_0|^2\,(1-\varepsilon), \tag{3.28}$$

where $|\mathcal{M}_0|^2$ is the tree-level matrix element given in Eq. (3.23).

The collision integral (3.26) suffers from the problem that a lepton asymmetry is produced even in thermal equilibrium. This can be remedied by including contributions from the resonant part of the $\Delta L = 2$ scattering process $l\Phi \leftrightarrow \bar{l}\Phi$ [105, 120]. We implement this remedy following the method developed in [92], and add to the collision integral (3.26) the term

$$f_\Phi f_{\bar{l}}\,(1-f_N)|\mathcal{M}_{\Phi\bar{l}\to N}|^2_{\text{sub}} - f_\Phi f_l\,(1-f_N)|\mathcal{M}_{\Phi l\to N}|^2_{\text{sub}}, \tag{3.29}$$

Table 3.1: Scenarios considered in the decay/inverse decay picture and their associated assumptions. Case D1 corresponds to the conventional integrated Boltzmann approach, while Case D4 was previously investigated by Basbøll and Hannestad [119].

Case	Assumption of kinetic equilibrium	Including quantum statistics	Section
D1	Yes	No	3.3.1
D2	No	No	3.3.2
D3	Yes	Yes	3.3.3
D4	No	Yes	3.3.4

with

$$|\mathcal{M}_{\Phi\bar{l}\to N}|^2_{\text{sub}} = |\mathcal{M}|^2_{\Delta L=2} - \varepsilon\,|\mathcal{M}_0|^2, \tag{3.30}$$

$$|\mathcal{M}_{\Phi l\to N}|^2_{\text{sub}} = |\mathcal{M}|^2_{\Delta L=2} + \varepsilon\,|\mathcal{M}_0|^2, \tag{3.31}$$

where $|\mathcal{M}|^2_{\Delta L=2}$ is negligible for $M \ll 10^{14}$ GeV [128].[2]

In the following subsections, we review first the derivation of the conventional integrated Boltzmann equations, which neglects quantum statistics and assumes kinetic equilibrium for the RHN. We then remove step by step these assumptions, in order to examine their effects on the efficiency factor κ. The scenarios to be examined and their associated assumptions are summarized in Table 3.1.

3.3.1   Case D1: integrated Boltzmann equations

In the integrated approach conventionally used in the literature [92, 105, 120], the time evolution of number densities n_i are tracked in favor of the phase space distributions f_i. This is achieved by integrating the Boltzmann equations (3.16) and (3.18) over momentum. However, the integrated equations have no closed forms unless we make certain simplifying assumptions: First, we neglect factors stemming from Pauli blocking for fermions and induced emission for bosons, i.e., we approximate $1 \pm f_i \approx 1$ [120]. Second, all SM particles are taken to be in thermal equilibrium due to their gauge interactions and their distribution functions approximated by a Maxwell–Boltzmann distribution, $f_i^{\text{eq}} = e^{-E_i/T}$.

---

[2]Reference [122] includes terms in addition to Eq. (3.29) in order to avoid asymmetry production in thermal equilibrium. However, the same analysis also shows that the quantitative difference between this and our approach is negligible.

With these assumptions and using energy conservation, we find

$$f_\Phi f_l = e^{-(E_\Phi + E_l)/T} = e^{-E_N/T} = f_N^{\text{eq}}, \tag{3.32}$$

so that the collision integral (3.24) simplifies to

$$C_D[f_N] = \frac{M \Gamma_D}{E_N \, p_N} \int_{(E_N - p_N)/2}^{(E_N + p_N)/2} dp_\Phi \left[f_N^{\text{eq}} - f_N \right]. \tag{3.33}$$

Integrating (3.33) over p_Φ and inserting into Eq. (3.16), the Boltzmann equation for the RHN distribution function becomes

$$\frac{\partial f_N}{\partial z} = \frac{z \, \Gamma_D \, M}{H(M) \, E_N} \left(f_N^{\text{eq}} - f_N \right). \tag{3.34}$$

To make further inroads, we assume kinetic equilibrium holds for the RHN, i.e., its distribution function f_N can be expressed as $f_N / f_N^{\text{eq}} \approx n_N / n_N^{\text{eq}}$, where n_N is the RHN number density. Then one can easily integrate Eq. (3.34) over the RHN phase space to obtain

$$\frac{\partial n_N}{\partial z} = z \, K \left\langle \frac{M}{E_N} \right\rangle \left(n_N^{\text{eq}} - n_N \right), \tag{3.35}$$

where $K \equiv \Gamma_D / H(M)$ (cf. Eq. (2.11)), and $\Gamma_D \langle M/E_N \rangle \equiv (\Gamma_D / n_N^{\text{eq}}) \int d^3 p_N / (2\pi)^3 \, f_N^{\text{eq}} \, (M/E_N)$ is the thermal average of the decay rate [120]. The thermally averaged dilation factor is given by the ratio of the modified Bessel functions of the second kind of first and second order, $\langle M/E_N \rangle = K_1(z)/K_2(z)$.

Dividing Eq. (3.35) by the equilibrium photon density n_γ^{eq}, we obtain the Boltzmann equation for the quantity $N_N \equiv n_N / n_\gamma^{\text{eq}}$ [92],

$$\frac{\partial N_N}{\partial z} = - D \left(N_N - N_N^{\text{eq}} \right), \tag{3.36}$$

with

$$D \equiv z \, K \left\langle \frac{M}{E_N} \right\rangle, \tag{3.37}$$

and

$$N_N^{\text{eq}}(z) = \frac{3}{8} z^2 K_2 (z). \tag{3.38}$$

Here, an inconsistency in the integrated approach is visible: all particles, i.e., N, l and Φ, are assumed to follow the Maxwell–Boltzmann distribution function. However, when calculating N_N^{eq}, we must use a Fermi–Dirac distribution for the RHN, $n_N^{\text{eq}} = [3 \zeta(3) g_N T M^2 / (8\pi^2)] K_2(z)$, with $\zeta(3) \approx 1.202$ and $g_N = 2$, in order to reproduce a realistic equilibrium RHN to photon density ratio. This leads to an extra

prefactor $(3/4)\zeta(3)$ in the definition of N_N^{eq} compared to a strictly Maxwell–Boltzmann approach.

For the lepton asymmetry, Eqs. (3.18), (3.26) and (3.29) combine to give the Boltzmann equation for the lepton distribution functions,

$$\frac{\partial f_{l-\bar{l}}}{\partial z} = -\frac{z^2\,K}{2\,y_l^2}\int_{\frac{z^2-4y_l^2}{4y_l}}^{\infty}dy_N\,\frac{y_N}{\mathcal{E}_N}\left[f_\Phi\,f_{l-\bar{l}} - 2\,\varepsilon\left(f_N - f_N^{\mathrm{eq}}\right)\right], \qquad (3.39)$$

where $\mathcal{E}_N \equiv E_N/T$. Using energy conservation and assuming kinetic equilibrium for the RHN, Eq. (3.39) can be integrated over y_N to give [119]

$$\frac{\partial f_{l-\bar{l}}}{\partial z} = -\frac{z^2\,K}{2\,y_l^2}\,e^{-\frac{z^2+4y_l^2}{4y_l}}\left[e^{y_l}\,f_{l-\bar{l}} - 2\,\varepsilon\left(\frac{n_N - n_N^{\mathrm{eq}}}{n_N^{\mathrm{eq}}}\right)\right]. \qquad (3.40)$$

We further assume that kinetic equilibrium prevails for the leptons such that

$$f_{l-\bar{l}}^{\mathrm{eq}} = e^{-(E_l-\mu)/T} - e^{-(E_l+\mu)/T} \approx 2\,(\mu/T)\,e^{-E_l/T}, \qquad (3.41)$$

$$n_{l-\bar{l}}^{\mathrm{eq}} \approx 2\,(\mu/T)\,n_l^{\mathrm{eq}}, \qquad (3.42)$$

$$f_{l-\bar{l}} \approx \frac{n_{l-\bar{l}}}{n_l^{\mathrm{eq}}}e^{-y_l}, \qquad (3.43)$$

with chemical potential $\mu \ll 1$ and n_l^{eq} the lepton equilibrium number density. Thus, integrating over the lepton phase space, we obtain the equation of motion for the number density

$$\frac{\partial n_{l-\bar{l}}}{\partial z} = -\frac{z^3\,K\,T^3}{2\,\pi^2}\,K_1(z)\left[\frac{n_{l-\bar{l}}}{n_l^{\mathrm{eq}}} - 2\,\varepsilon\left(\frac{n_N - n_N^{\mathrm{eq}}}{n_N^{\mathrm{eq}}}\right)\right], \qquad (3.44)$$

where $K_1(z)$ is the modified Bessel function of first kind. Following [92] we rewrite Eq. (3.44) in terms of the lepton asymmetry per comoving photon ,

$$\frac{\partial N_{l-\bar{l}}}{\partial z} = -W_{ID}\,N_{l-\bar{l}} + \varepsilon\,D\left(N_N - N_N^{\mathrm{eq}}\right), \qquad (3.45)$$

where

$$W_{ID} \equiv \frac{1}{4}\,K\,z^3\,K_1(z) = \frac{1}{2}\,D\,\frac{N_N^{\mathrm{eq}}}{N_l^{\mathrm{eq}}} \qquad (3.46)$$

quantifies the strength of the wash-out due to inverse decays, and $N_l^{\mathrm{eq}} = 3/4$. Note that, as with the RHN, when evaluating N_l^{eq} it is necessary to use a Fermi–Dirac distribution for the leptons, $n_l^{\mathrm{eq}} = (3/4)\,(\zeta(3)/\pi^2)g_l T^3$, with $g_l = 2$, to ensure a realistic lepton to photon density ratio.

Figure 3.1 shows the final efficiency factor κ_f, defined in Eq. (2.14), as a function of K for several different initial RHN abundances [106].
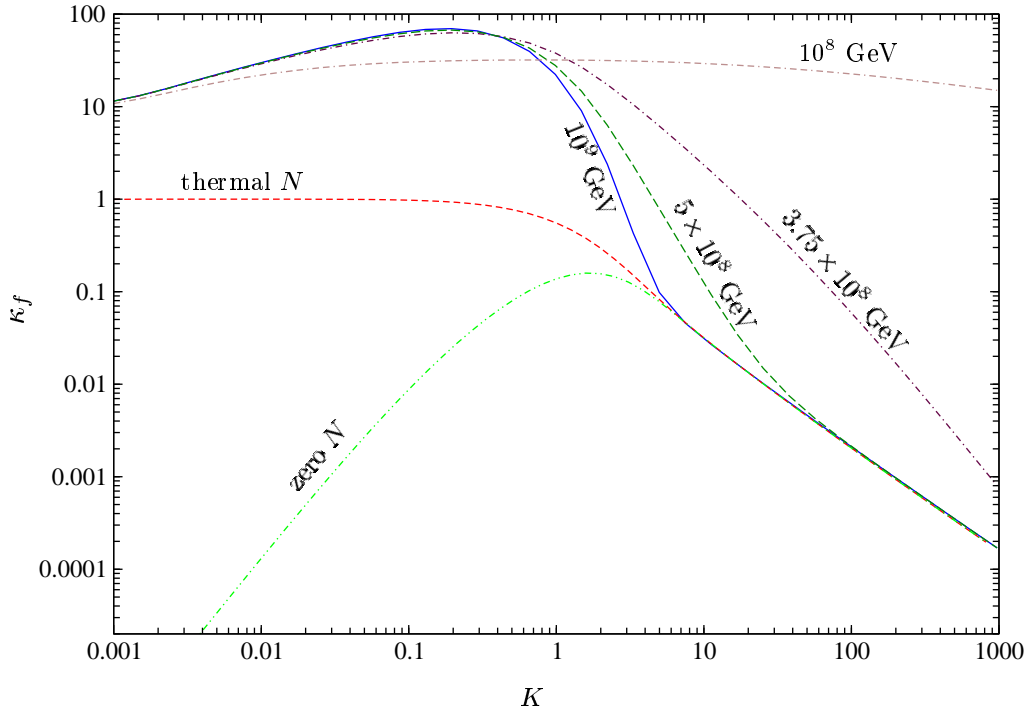
Figure 3.1: Final efficiency factor for different scenarios of thermal and non-thermal leptogenesis. Shown are κ_f for a thermal (dashed/red), a vanishing (dot-dot-dash/light green), and several cases of dominant initial RHN abundance. A dominant initial abundance is realized if a scalar field responsible for inflation decays exclusively into the RHN, which then dominates the energy density of the universe. The coupling strength between the scalar field and the RHN can be connected to an energy scale: 10^9 GeV (solid/blue), 5×10^8 GeV (dashed/dark green), 3.75×10^8 GeV (dot-dash/purple) and 10^8 GeV (dot-dash-dash/taupe). The RHN mass has been set to $M = 10^9$ GeV [106].

It can be seen that thermal leptogenesis is independent of the initial conditions on the RHN abundance in the strong wash-out regime ($K > 1$). Actually, this statement holds even for scenarios of non-thermal leptogenesis, where the RHN abundance is established in the decays of a heavy scalar field, e.g., the inflaton which is responsible for the exponential expansion at the beginning of the universe. After the decay of the scalar field, the RHN dominates the energy density of the universe, realizing a dominant initial abundance. The thermal bath of the radiation dominated phase of the universe is then established in the subsequent decays of the RHN into light degrees of freedom. If the coupling between the RHN and the scalar field, corresponding to an energy scale, is not too weak to account for efficient wash-out, non-thermal leptogenesis yields the same ef-

ficiency factor as thermal leptogenesis for $K \gtrsim 4$. This is true for couplings between the RHN and the inflaton corresponding to energy scales larger than the RHN mass [106]. In the weak wash-out regime, however, different initial conditions on the RHN lead to final efficiency factors varying by several orders of magnitude between the different scenarios. Therefore, we will focus from now on on the case of a vanishing initial RHN abundance.

3.3.2 Case D2: dropping the assumption of kinetic equilibrium

Since the RHN is very heavy—its mass scale corresponds to the temperature of the thermal bath during the period of leptogenesis—it is not *a priori* obvious that decays and inverse decays would occur fast enough to establish kinetic equilibrium. Thus the assumption of kinetic equilibrium for the RHN might lead to sizable deviations from an exact treatment. In this section we drop this assumption in our calculation of the efficiency factor. We retain however our other assumptions: that all equilibrium distribution functions are of the Maxwell–Boltzmann form, and quantum statistical factors are negligible.

Dropping the assumption of kinetic equilibrium for the RHN means that it is now necessary to solve Eq. (3.34), rewritten here as

$$\frac{\partial f_N}{\partial z} = \frac{z^2 \, K}{\mathcal{E}_N} \left(f_N^{\text{eq}} - f_N \right), \tag{3.47}$$

individually for all possible values of the dimensionless RHN energy $\mathcal{E}_N$. For the calculation of the lepton asymmetry, the relevant equation is Eq. (3.39) which we reproduce here:

$$\frac{\partial f_{l-\bar{l}}}{\partial z} = -\frac{z^2 \, K}{2 \, y_l^2} \int_{\frac{z^2 - 4y_l^2}{4y_l}}^{\infty} dy_N \, \frac{y_N}{\mathcal{E}_N} \left[f_\Phi \, f_{l-\bar{l}} - 2 \, \varepsilon \left(f_N - f_N^{\text{eq}} \right) \right]. \tag{3.48}$$

Again, this equation must be solved for all possible values of the lepton momentum y_l, and the resulting $f_{l-\bar{l}}(y_l)$ summed according to Eq. (3.20) to give $N_{l-\bar{l}}$. Alternatively, using energy conservation and assuming kinetic and chemical equilibrium for the SM particles, we can integrate Eq. (3.48) over the lepton phase space to obtain a single equation of motion for $N_{l-\bar{l}}$,

$$\frac{\partial N_{l-\bar{l}}}{\partial z} = -\frac{z^2 \, K}{4} \int_0^\infty dy_l \int_{\frac{z^2 - 4y_l^2}{4y_l}}^{\infty} dy_N \, \frac{y_N}{\mathcal{E}_N} \left[N_{l-\bar{l}} \, f_N^{\text{eq}} - 2 \, \varepsilon \left(f_N - f_N^{\text{eq}} \right) \right]. \tag{3.49}$$

We find the second approach to yield more stable results.

3.3.3   Case D3: Boltzmann equations with quantum statistical factors

In Case D3 we reinstate Pauli blocking factors for fermions and factors due to induced emission for bosons, but adopt again the assumption of kinetic equilibrium for the RHN. Consistency requires that we use the Fermi–Dirac and the Bose–Einstein distribution functions respectively for fermions and bosons in thermal equilibrium, instead of the classical Maxwell–Boltzmann distribution function.

With these assumptions in mind, we integrate the collision integral (3.24) over p_Φ to obtain the Boltzmann equation for the RHN,

$$\frac{\partial f_N}{\partial z} = \frac{z^2\,K}{\mathcal{E}_N\,y_N} \frac{n_N - n_N^{\rm eq}}{n_N^{\rm eq}} f_N^{\rm eq}\,\log\left[\frac{\sinh\left(\left(\mathcal{E}_N - y_N\right)/2\right)}{\sinh\left(\left(\mathcal{E}_N + y_N\right)/2\right)}\right], \tag{3.50}$$

where we have used $f_N/f_N^{\rm eq} = (1 + e^{\mathcal{E}_N})f_N \approx n_N/n_N^{\rm eq}$. Integrating over the RHN phase space and normalizing to the photon number density yields

$$\frac{\partial N_N}{\partial z} = \frac{K}{K_2(z)}\,\left(N_N - N_N^{\rm eq}\right)\int_0^\infty\,dy_N\,\frac{y_N}{\mathcal{E}_N}\,f_N^{\rm eq}\,\log\left[\frac{\sinh\left(\left(\mathcal{E}_N - y_N\right)/2\right)}{\sinh\left(\left(\mathcal{E}_N + y_N\right)/2\right)}\right]. \tag{3.51}$$

We note that the integral over the RHN phase space has no simple analytic form. Therefore it remains necessary to perform the integration numerically.

The Boltzmann equation for the lepton asymmetry including all quantum statistical factors and assuming kinetic equilibrium for all particle species has the following form:

$$\frac{\partial f_{l-\bar{l}}}{\partial z} = -\frac{z^2\,K}{2y_l^2}\int_{\frac{z^2-4y_l^2}{4y_l}}^\infty\,dy_N\,\frac{y_N}{\mathcal{E}_N}\left[\left(f_\Phi + \frac{n_N}{n_N^{\rm eq}}f_N^{\rm eq}\right)(f_{l-\bar{l}} + \varepsilon F^+) - 2\varepsilon\,\frac{n_N}{n_N^{\rm eq}}f_N^{\rm eq}(1 + f_\Phi)\right], \tag{3.52}$$

where $F^+ \equiv f_l + f_{\bar{l}} \approx 2\,f_l^{\rm eq}$. After integrating over the lepton phase space and normalizing to the photon number density we arrive at

$$\frac{\partial N_{l-\bar{l}}}{\partial z} = -\frac{z^2\,K}{4}\int_0^\infty\,dy_l \tag{3.53}$$
$$\times \int_{\frac{z^2-4y_l^2}{4y_l}}^\infty\,dy_N\,\frac{y_N}{\mathcal{E}_N}\left[\left(f_\Phi + \frac{N_N}{N_N^{\rm eq}}f_N^{\rm eq}\right)\left(\frac{4}{3}N_{l-\bar{l}} + 2\varepsilon\right)f_l^{\rm eq} - 2\varepsilon\frac{N_N}{N_N^{\rm eq}}f_N^{\rm eq}\left(1 + f_\Phi\right)\right],$$

with $N_N^{\rm eq}$ given in Eq. (3.38).

3.3.4   Case D4: complete mode equations

Here we include all statistical factors and make no assumption of kinetic equilibrium for the RHN. Integrating Eq. (3.24) over p_Φ gives the Boltzmann equation for the RHN,

$$\frac{\partial f_N}{\partial z} = K\,\frac{z^2}{\mathcal{E}_N\,y_N}\,f_N^{\rm eq}\,\left(-1 + f_N + e^{\mathcal{E}_N}f_N\right)\,\log\left[\frac{\sinh((\mathcal{E}_N - y_N)/2)}{\sinh((\mathcal{E}_N + y_N)/2)}\right]. \tag{3.54}$$

The numerical integration of Eq. (3.54) over the RHN phase space results in the time evolution of the number density N_N. The equation for the lepton asymmetry in this case is similar to Eq. (3.52), except we do not assume kinetic equilibrium for the RHN,

$$\frac{\partial f_{l-\bar{l}}}{\partial z} = -\frac{z^2\,K}{2y_l^2} \int_{\frac{z^2-4y_l^2}{4y_l}}^{\infty} dy_N\,\frac{y_N}{\mathcal{E}_N}\left[(f_\Phi+f_N)(f_{l-\bar{l}}+\varepsilon F^+) - 2\varepsilon\,f_N\,(1+f_\Phi)\right].$$

(3.55)

Integrating over the lepton momentum yields

$$\frac{\partial N_{l-\bar{l}}}{\partial z} = -\frac{z^2\,K}{4} \int_0^{\infty} dy_l \tag{3.56}$$
$$\times \int_{\frac{z^2-4y_l^2}{4y_l}}^{\infty} dy_N\,\frac{y_N}{\mathcal{E}_N}\left[(f_\Phi+f_N)\left(\frac{4}{3}\,N_{l-\bar{l}}+2\,\varepsilon\right)f_l^{\rm eq} - 2\varepsilon\,f_N\,(1+f_\Phi)\right],$$

where we have assumed, as usual, thermal equilibrium for the SM particles.

3.3.5   Results and discussions

Right-handed neutrino

Figure 3.2 shows the time evolution of the comoving number densities of the RHN for the four different cases described above, assuming a vanishing initial RHN abundance. We have picked three values for the decay parameter: (i) $K = 0.1$, lying in the weak wash-out regime, is shown on the upper panel, (ii) $K = 1$, marking the transition regime between the weak and the strong wash-out regime, is shown on the middle panel, and (iii) $K = 10$, lying in the strong wash-out regime, is shown on the lower panel. For reference, we also plot the time evolution of the RHN equilibrium number density $N_N^{\rm eq}$.

The general behavior of the RHN abundance evolution is similar for all four cases. In the weak wash-out regime, there is a net production of RHN by inverse decays at high temperatures $z < 1$. At $z \sim 4$, the RHN abundance overshoots the equilibrium density and continues to grow until $z \sim 5$, when a net destruction of RHN by decays into $l\Phi$ pairs begins to push its abundance slowly back down to the equilibrium value. Equilibrium is reached finally at $z \sim 20$, beyond which the RHN abundance falls off exponentially with z, as expected for all non-relativistic particle species in thermal equilibrium. In the transition regime, all RHN number densities become nearly identical at $z \sim 3$. At the same point they overshoot the equilibrium density. However, RHN decays force the number densities back to their equilibrium value already at $z \sim 10$ from whence the RHN abundances fall off exponentially again. Contrastingly, in the strong wash-out regime, the stronger coupling brings the RHN abundance to its equilibrium
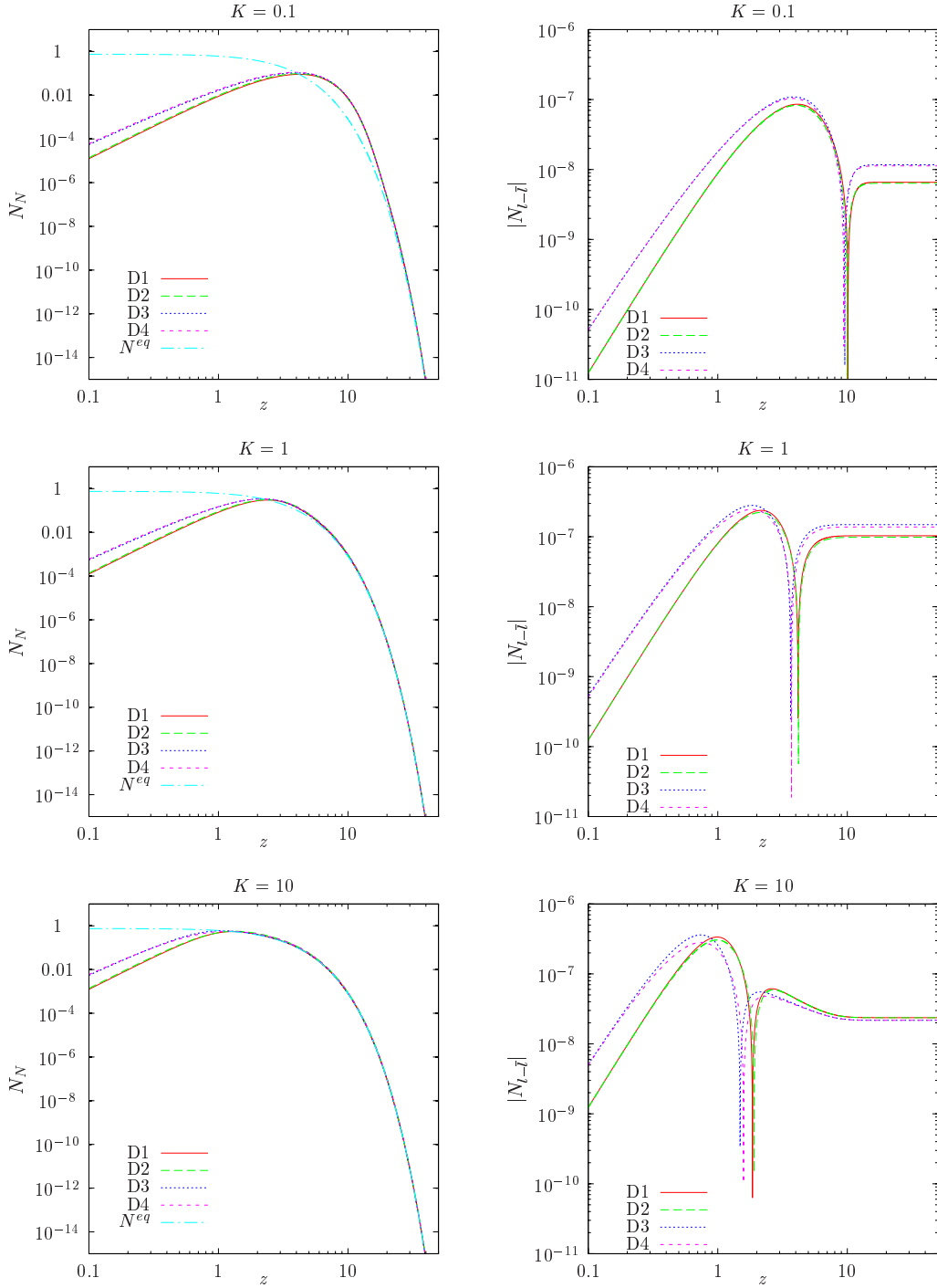
Figure 3.2: Time evolution of the comoving RHN number density N_N and of the absolute value of the lepton asymmetry $N_{l-\bar{l}}$, assuming three different coupling strengths $K = 0.1, 1, 10$, and $\varepsilon = 10^{-6}$. The four scenarios within the decay–inverse decay only framework are shown: Solid/red line denotes Case D1, long dashed/green D2, dotted/blue D3, and short dashed/magenta D4. See Table 3.1 for a short summary of each scenario. For reference, we also indicate the equilibrium RHN number density N_N^{eq} in dot-dash/cyan.

value already at $z \sim 1$. Its subsequent evolution is then simply governed by equilibrium statistics: at $z \sim 4$ the RHN becomes nonrelativistic and hence its abundance is suppressed by $\exp(-M/T)$.

In all three cases, the weak wash-out, the transition, and the strong wash-out regimes, the difference between Cases D1 and D2, which exclude quantum statistical factors, and their counterparts Cases D3 and D4, which include quantum statistics, is most visible at $z \lesssim 1$. The RHN abundance is almost an order of magnitude larger in the latter two cases than in the former. This is because during the high temperature RHN production phase, using the correct Bose–Einstein equilibrium distribution function for the Higgs boson f_Φ substantially enlarges the phase space available for the inverse decay process $\Phi l \to N$ at low E_Φ. This effect is far stronger than the phase space restriction due to Pauli blocking by the final-state RHN, as can be seen from the phase space factors in Eq. (3.24). As the temperature drops and the RHN becomes nonrelativistic, the effects of quantum statistics also diminish, since kinematics now prevents the low energy Φ and l states from contributing to the collision integrals.

Interestingly, the assumption of kinetic equilibrium leads to no visible effects in either the weak, the transition or strong wash-out regime. Comparing Cases D1 and D2 (both assume Maxwell–Boltzmann statistics), their RHN abundances are virtually identical. The same is true for Cases D3 and D4, which include quantum statistical factors.

Lepton asymmetry

The time evolution of the corresponding absolute value of the lepton asymmetry is shown in the right panel of Figure 3.2. A negative lepton asymmetry is produced at high temperatures by RHN production from inverse decays. At $z \sim 5$ in the weak wash-out regime ($z \sim 1$ if strong wash-out), decays come to dominate over inverse decays, thus reversing the direction of the asymmetry production, and eventually flipping the sign of the asymmetry to positive. When the RHN abundance begins to fall off exponentially, the asymmetry also asymptotes to a final, constant value.

In the weak wash-out regime ($K = 0.1$) the asymmetries produced in Cases D3 and D4 which include quantum statistical factors are always larger in magnitude than those produced in Cases D1 and D2 which assume Maxwell–Boltzmann statistics throughout the whole temperature range considered. The change of sign also occurs slightly earlier in D3 and D4. These effects can be understood as follows. From, e.g., Eq. (3.55), we see that the production of a negative lepton asymmetry at high temperatures by inverse RHN decays is significantly enhanced when we take proper account of the Bose–Einstein statistics for the Higgs boson. Like the case of the RHN abundance, this effect dominates over the phase space suppression due to the Fermi–Dirac statistics of the lepton and the
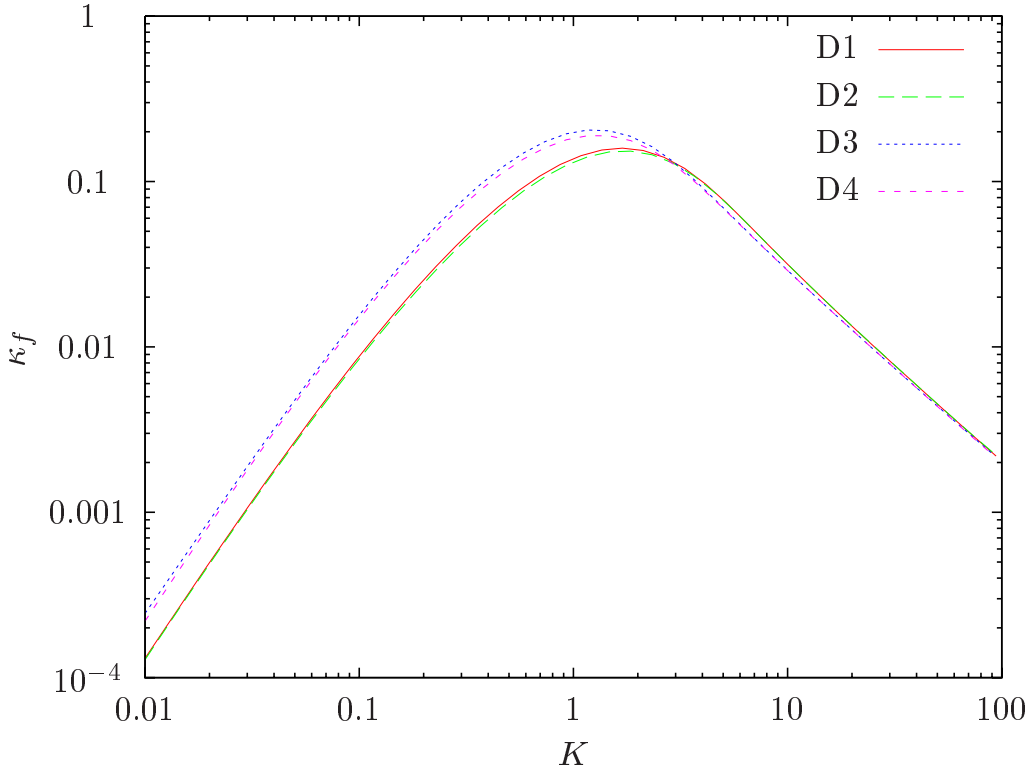
Figure 3.3: The final efficiency factor κ_f as a function of K for the four scenarios within the decay–inverse decay picture, assuming a vanishing initial RHN abundance. Solid/red line denotes Case D1, long dashed/green D2, dotted/blue D3, and short dashed/magenta D4.

RHN. As we progress to lower temperatures, RHN decays begin to dominate over inverse decays, thereby reversing the direction of the lepton asymmetry evolution. Since quantum statistics speeds up RHN production and brings its abundance up to the equilibrium threshold earlier, the transition from decay to inverse decay domination—and hence the turning point in the asymmetry evolution—also happens earlier. As a result, the asymmetry flips sign a little earlier in Cases D3 and D4 than in D1 and D2, and has more time to grow to a larger positive value before the exponential fall-off of the RHN abundance shuts down the asymmetry production.

In the transition regime ($K = 1$) the asymmetry in Cases D3 and D4, where quantum statistics is used, is again always larger than in Cases D1 and D2; however, with a smaller difference than for $K = 0.1$ The change of sign is slightly moved to higher temperatures due to the wash-out becoming more efficient.

In the strong wash-out regime ($K = 10$), a similar behavior is also visible at $z \lesssim 1$. As we progress to lower temperatures, however, Cases D3 and D4 end up producing less

asymmetry than Cases D1 and D2. This is because for $K > 1$, the wash-out rate plays a dominant role in determining the final asymmetry. Here, quantum statistics enlarges the phase space of the wash-out term from $f_\Phi f_{l-\bar{l}}$ in Eq. (3.48) to $(f_\Phi + f_N)f_{l-\bar{l}}$ in Eq. (3.55), thus forcing the lepton asymmetry to flip sign even earlier than for $K = 1$, and continuing on to dampen it to a slightly smaller positive value.

Again, as with the RHN, the assumption of kinetic equilibrium has virtually no effect on the asymmetry evolution: the differences between Cases D1 and D2, and between Cases D3 and D4 are generally at the percent level, only visible in the middle panel of Figure 3.2 in the transition regime for $K = 1$.

Finally, Figure 3.3 summarizes the lepton asymmetry produced in the four cases, in terms of the final efficiency factor κ_f defined in Eq. (2.14), as a function of the decay parameter K. For all values of K considered, the assumption of kinetic equilibrium can be seen to produce a minute ($< 5\%$) difference in κ_f between Cases D1 and D2 and between Cases D3 and D4. Quantum statistics, on the other hand, has a generally stronger effect on the final lepton asymmetry. In the weak wash-out regime ($K \lesssim 1$), inclusion of quantum statistical factors (Cases D3 and D4) enhances κ_f by a factor of ~ 1.5 relative to Cases D1 and D2 which assume Maxwell–Boltzmann statistics. In the strong wash-out regime ($K \gtrsim 1$), the effect of quantum statistics is to suppress κ_f by up to 20% at $K \sim 10$, but reduces to the percent level at $K \sim 100$.

Chapter 4

Mode equations with scattering

4.1 Scattering processes

In this chapter we enlarge our picture of thermal leptogenesis to include tree-level scattering processes of the RHN with the top quark, e.g., $Nl \rightarrow qt$, shown in Figure 4.1, which are of $\mathcal{O}\left(h_t^2 \lambda^2\right)$. These interactions lead to an additional production channel for the RHN and contribute to the wash-out processes. Until recently, these scattering processes have only been considered using the integrated Boltzmann equations [92, 105]. In [83] we provided for the first time a solution of the full set of Boltzmann equations at the mode level taking into account the full energy spectrum of the interactions. This leads to sizable effects on the final asymmetry since small momentum modes can be produced disproportionally compared with an equilibrium distribution, in turn leading to differences in the number densities after integration over the momentum phase space. Furthermore, the inclusion of quantum statistical Pauli-blocking factors modifies the phase space accessible for the scattering interactions. We will confront our findings with the results obtained with mode equations in the decay–inverse decay picture in Section 3.3.4 and with the integrated treatment including scatterings, discussed in the following section.
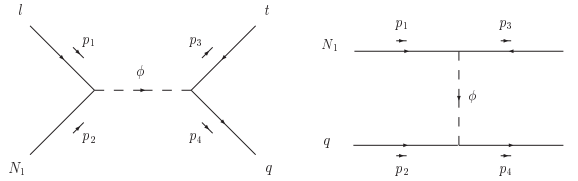

Figure 4.1: Scattering processes with the top quark

We do not consider $\Delta L = 1$ violating interactions with gauge bosons (in spite of

$g_2 > h_t$ at 10^{10} GeV), nor include CP violation in $2 \rightarrow 2$ or $1(2) \rightarrow 3$ processes, which are of higher order in the Yukawa couplings. CP violation from these processes was considered in [100, 112, 129, 130], where it was shown that at high temperatures CP violation from scattering is the main source of lepton asymmetry production. However, the final asymmetry depends also on the strength of the wash-out processes; it turns out that in the weak wash-out regime ($K < 1$) CP violation in the scattering processes tends to suppress the asymmetry production, while in the transition ($K \simeq 1$) and strong ($K > 1$) wash-out regimes its contribution is small to negligible. We do concentrate our considerations in this thesis on the tree-level Yukawa couplings in order to distinguish in detail the effects of quantum statistics and kinetic equilibrium on the final asymmetry. Since the inclusion of several new phenomena would dilute these effects, we compare our results with the findings obtained in [92] providing a consistent study of Yukawa interactions at tree-level.

Including scattering processes based on the Yukawa coupling with the top quark, the basic Boltzmann equation for the distribution function of the RHN is given by

$$\frac{H(M)}{z} \frac{\partial f_N}{\partial z} = C_D \left[f_N \right] + 2\, C_{S,s} \left[f_N \right] + 4\, C_{S,t} \left[f_N \right]. \tag{4.1}$$

The right-hand side of Eq. (4.1) contains two collision integrals from scattering processes coming respectively from scattering in the s-channel and in the t-channel. One factor of 2 stems from contribution from processes involving anti-particles, and another factor of 2 in the t-channel term originates from the u-channel diagram. The decay–inverse decay collision integral C_D is given in Eq. (3.22), the s-channel scattering integral is

$$C_{S,s} \left[f_N \right] = \frac{1}{2E_N} \int \prod_{i=l,q,t} \frac{dp_i^3}{(2\pi)^3 2E_i} (2\pi)^4 \delta^4(p_N + p_l - p_t - p_q) \, |\mathcal{M}_s|^2$$
$$\times \left[(1 - f_N)(1 - f_l) f_t f_q - f_N f_l (1 - f_t)(1 - f_q) \right], \tag{4.2}$$

and a similar expression exists for the t-channel scattering integral $C_{S,t} \left[f_N \right]$, but with the appropriate matrix element $\mathcal{M}_t$, and the replacements $f_l \leftrightarrow f_q$. The explicit expressions of the squared matrix elements $|\mathcal{M}_{s,t}|^2$ can be found in the Appendices B.1 and B.2.

The analogous equation for the lepton asymmetry is

$$\frac{H(M)}{z} \frac{\partial f_{l-\bar{l}}}{\partial z} = C_D \left[f_{l-\bar{l}} \right] + 2\, C_{S,s} \left[f_{l-\bar{l}} \right] + 4\, C_{S,t} \left[f_{l-\bar{l}} \right], \tag{4.3}$$

where $C_D \left[f_{l-\bar{l}} \right] \equiv C_D \left[f_l \right] - C_D \left[f_{\bar{l}} \right]$ can be constructed from Eq. (3.26), and

$$C_{S,s} \left[f_{l-\bar{l}} \right] = \frac{1}{2E_l} \int \prod_{i=N,q,t} \frac{dp_i^3}{(2\pi)^3 \, 2E_i} (2\pi)^4 \delta^4(p_l + p_N - p_q - p_t) \, |\mathcal{M}_s|^2$$
$$\times f_{l-\bar{l}} \left(f_N \left(f_t + f_q - 1 \right) - f_t f_q \right). \tag{4.4}$$

Table 4.1: Scenarios including scattering with the top quark and their associated assumptions. Case S1 corresponds to the conventional integrated Boltzmann approach, while Case S2 involves solving the full set of Boltzmann equations at the mode level.

Case	Assumption of kinetic equilibrium	Including quantum statistics	Section
S1	Yes	No	4.1.1
S2	No	Yes	4.1.2

Replacing $\mathcal{M}_s$ with $\mathcal{M}_t$ and $f_q \leftrightarrow f_N$ in Eq. (4.4) yields the integral $C_{S,t}\left[f_{l-\bar{l}}\right]$.

In the following we first recall the treatment of scattering processes in the integrated picture, before we proceed to write down the full set of mode equations including the relevant scattering terms. Table 4.1 summarizes the assumptions of these two scenarios.

4.1.1 Case S1: scattering in the integrated picture

As done in section 3.3.1 when considering decays and inverse decays only, we derive here the integrated Boltzmann equations for leptogenesis neglecting in the collision integrals, Eqs. (4.2) and (4.4), quantum statistical effects and assuming kinetic equilibrium for all particle species.

Along the lines of a general derivation of scattering rates shown in Appendix A, the integrated Boltzmann equations can be recast in the following form [92],

$$\frac{\partial N_N}{\partial z} = - \left(D + S \right) \left(N_N - N_N^{\text{eq}} \right), \tag{4.5}$$

$$\frac{\partial N_{l-\bar{l}}}{\partial z} = \varepsilon\, D \left(N_N - N_N^{\text{eq}} \right) - W\, N_{l-\bar{l}}, \tag{4.6}$$

where S accounts for the production of RHNs from scattering processes, and the washout rate W contains also a contribution from these processes. The scattering rate S itself consists of two terms, $S = 2\, S_s + 4\, S_t$, coming respectively from scattering in the s-channel and in the t-channel.

The scattering rates for the s- and t-channel, respectively, are defined as

$$S_{s,t} = \frac{\Gamma_{s,t}}{H\, z}, \tag{4.7}$$

where

$$\Gamma_{s,t} = \frac{M}{24\, \zeta(3)\, g_N\, \pi^2} \frac{\mathcal{I}_{s,t}}{K_2(z)\, z^3}. \tag{4.8}$$

Note that an additional factor of $4/(3)\,\zeta(3)$ appears in this definition compared to the definition of reference [92]. This is due to the Fermi–Dirac statistics used for the equilibrium number density in our derivation. The quantity $\mathcal{I}_{s,t}$ is an integral, defined in Eq. (A.9),

$$\mathcal{I}_{s,t} = \int_{z^2}^{\infty} d\Psi \, \hat{\sigma}_{s,t}(\Psi) \sqrt{\Psi} \, K_1\left(\sqrt{\Psi}\right), \tag{4.9}$$

of the reduced cross-section $\hat{\sigma}_{s,t}$, given by [91]

$$\hat{\sigma}_{s,t} = \frac{3\,h_t^2}{4\,\pi} \frac{M\,\tilde{m}_1}{v^2} \chi_{s,t}(x), \tag{4.10}$$

where $x = \Psi/z^2$, and $h_t = h_t(T)$ is the top Yukawa coupling, to be evaluated at the relevant energy scale (or temperature) T by solving the renormalization group equation, cf. Appendix C. Taking the value of the Yukawa coupling at the scale $m_Z = 90\,\text{GeV}$ overestimates the general influence of the scattering processes by about a factor 2 as we show later in Section 4.2. The functions $\chi_{s,t}(x)$ are part of the reduced cross-section, Eq. (4.10), see also Eq. (A.8), and for the RHN scattering off top quarks they are calculated to be [91]

$$\chi_s(x) = \left(\frac{x-1}{x}\right)^2, \tag{4.11}$$

$$\chi_t(x) = \frac{x-1}{x} \left[\frac{x-2+2a_h}{x-1+a_h} + \frac{1-2a_h}{x-1} \log\left(\frac{x-1+a_h}{a_h}\right)\right], \tag{4.12}$$

using the explicit expressions for the squared matrix elements for the s- and t-channel scatterings given in Eqs. (B.3) and (B.69). We have introduced $a_h = m_\Phi/M$ as an infrared cut-off for the t-channel diagram, where m_Φ is the mass of the Higgs boson which presumably receives contributions from interactions with the thermal bath, i.e., its value does not correspond to that potentially measured at the LHC. The value of m_Φ can in principle be deduced from a thermal field theoretic treatment of leptogenesis, and the analysis of [105] found $m_\Phi(T) \simeq 0.4\,T$. However, some open questions still remain and hence in the present work we prefer to adopt a value of $a_h = 10^{-5}$, used first by Luty in [131].

It is convenient to rewrite the s- and t-channel scattering rates $S_{s,t}$ in terms of the functions $f_{s,t}$ defined as

$$f_{s,t}(z) = \frac{\int_{z^2}^{\infty} d\Psi \, \chi_{s,t}\left(\Psi/z^2\right) \sqrt{\Psi} \, K_1\left(\sqrt{\Psi}\right)}{z^2 \, K_2(z)}, \tag{4.13}$$

such that

$$S_{s,t} = \frac{K_s}{9\,\zeta(3)} f_{s,t}, \tag{4.14}$$
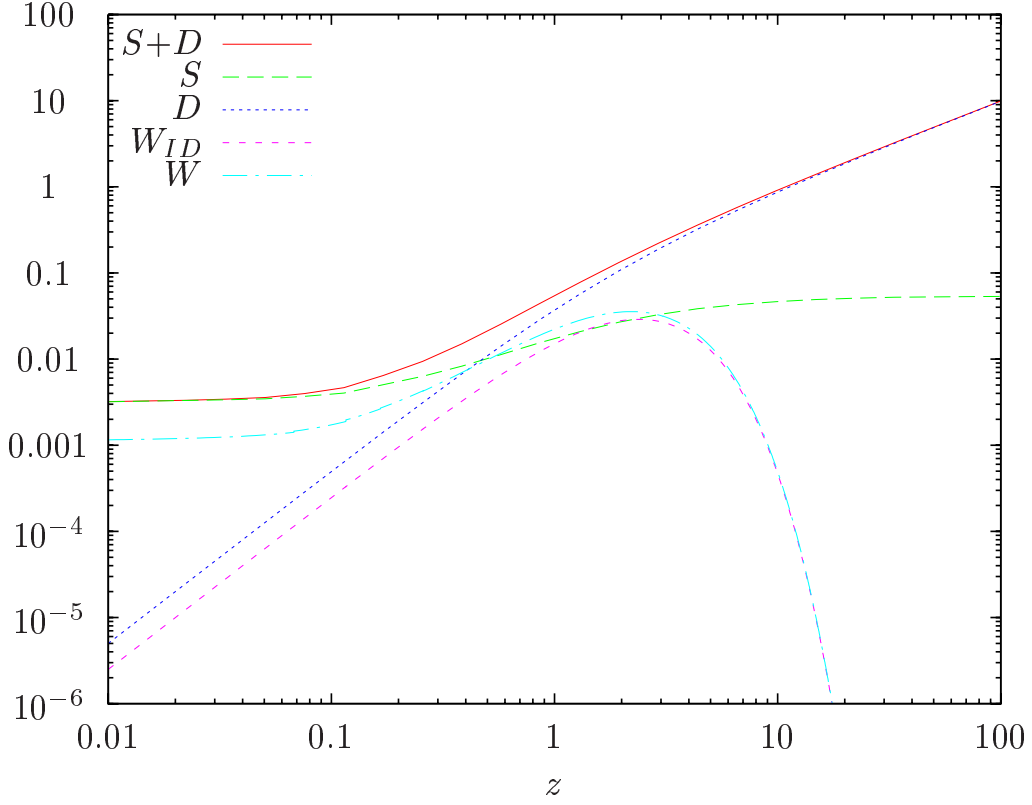
Figure 4.2: The decay D, scattering S, and wash-out rates W and W_{ID} as functions of z in the integrated approach, assuming $K = 0.1$ and $a_h = 10^{-5}$.

and the total scattering rate is given by

$$S = \frac{2\,K_s}{9\,\zeta(3)}\,(f_s(z) + 2\,f_t(z))\,, \tag{4.15}$$

where

$$K_s = \frac{\tilde{m}_1}{m_*^s}, \tag{4.16}$$

with $\tilde{m}_1$ given by Eqs. (2.12), and [92]

$$m_*^s = \frac{4\pi^2}{9}\,\frac{g_N}{h_t^2}\,m_*, \tag{4.17}$$

where m_* has been defined in Eq. (2.13).

Since the scattering processes with the top quark change the lepton number by one unit, they contribute also to the wash-out of the asymmetry. The total wash-out rate is given by

$$W = W_{ID} + W_{\Delta L=1}, \tag{4.18}$$

where W_{ID} denotes the contribution from inverse decay defined in Eq. (3.46), and $W_{\Delta L=1}$ from scattering in the s- and t- channels,

$$W_{\Delta L=1} = W_s + 2\, W_t, \tag{4.19}$$

with

$$W_s = \frac{N_N}{N_N^{\mathrm{eq}}}\, \frac{\Gamma_s^l}{H\, z} = \frac{N_N^{\mathrm{eq}}}{N_l^{\mathrm{eq}}}\, \frac{N_N}{N_N^{\mathrm{eq}}}\, S_s, \tag{4.20}$$

and

$$W_t = \frac{\Gamma_t^l}{H\, z} = \frac{N_N^{\mathrm{eq}}}{N_l^{\mathrm{eq}}}\, S_t. \tag{4.21}$$

The lepton scattering rates are given by $\Gamma_{s,t}^l = N_N^{\mathrm{eq}}/N_l^{\mathrm{eq}}\, \Gamma_{s,t}$. Using Eq. (3.46), the two contributions W_{ID} and $W_{\Delta L=1}$ are related by

$$W_{\Delta L=1} = 2\, W_{ID}\, \frac{1}{D}\, \left(\frac{N_N}{N_N^{\mathrm{eq}}}\, S_s + 2\, S_t \right), \tag{4.22}$$

so that

$$W = W_{ID}\, \left[1 + \frac{1}{D}\, \left(2\, \frac{N_N}{N_N^{\mathrm{eq}}}\, S_s + 4\, S_t \right) \right] \tag{4.23}$$

gives the total wash-out rate.

Figure 4.2 shows the various rates D, S, W, and W_{ID} as functions of z assuming $K = 0.1$. For other choices of K, the corresponding rates evolve with z in a similar fashion, but with magnitudes scaling with K.

4.1.2 Case S2: complete mode equations including scattering

In this section, which is based on the work done in [83], we derive the complete set of mode equations for leptogenesis, including the tree-level scattering processes with the top quark. On that account, we shall solve the collision integrals given in Eqs. (4.2) and (4.4).

The collision integrals are nine-dimensional and can be reduced analytically down to two dimensions. Since this is a rather formal and technical procedure, we provide in Appendix B the full reduction scheme, following the method of [93, 94], as well as the final reduced integrals [1]. The resulting two-dimensional integrals have the general form

$$C_{S,(s,t)}\left[f_N\right] = \sum_\mu \frac{3\, T}{2^6 \pi^3\, \tilde{E}_N\, y_N}\, \frac{h_t^2\, M\, \tilde{m}_1}{v^2}$$

$$\times \int_{w(\tilde{E}_{N,l,q,t})}^{u(\tilde{E}_{N,l,q,t})} d\tilde{E}_l \int_{l(\tilde{E}_{N,l,t,q})}^{k(\tilde{E}_{N,l,t,q})} d\tilde{E}_{(t,q)}\, \Lambda_{(s,t)}^{(N)}\, I_{(s,t)}^{(\mu)} \tag{4.24}$$

---

[1]A general treatment of scattering kernels in kinetic equations can be found in [132].

for the RHN and

$$C_{S,(s,t)}\left[f_{l-\bar{l}}\right] = \sum_{\mu} \frac{3\,T}{2^6\,\pi^3\,\tilde{E}_l^2}\,\frac{h_t^2\,M\,\tilde{m}_1}{v^2}$$

$$\times \int_{w(\tilde{E}_{N,l,q,t})}^{u(\tilde{E}_{N,l,q,t})} d\tilde{E}_N \int_{l(\tilde{E}_{N,l,q,t})}^{k(\tilde{E}_{N,l,t,q})} d\tilde{E}_{(t,q)}\,\Lambda_{(s,t)}^{(l-\bar{l})}\,I_{(s,t)}^{(\mu)}, \qquad (4.25)$$

for the asymmetry. The functions $\Lambda_{(s,t)}^{N}$ and $\Lambda_{(s,t)}^{(l-\bar{l})}$ denote the phase space factors for the RHN (lepton) scatterings in the s- and t-channel, respectively. The integration limits u, w, k, and l depend on the energies of the particles involved in the interactions and give the distinct integration ranges for each integrand in the sums of Eqs. (4.24) and (4.25). The integrands consist of the phase space factors and the analytical functions $I_{(s,t)}^{\mu}$. Both depend on the energies of the particles involved in the process. For the s-channel diagram the sum contains six terms for the RHN and the lepton asymmetry and for the t-channel diagram one counts four terms each. As mentioned above, all explicit expressions can be found in Appendix B. Inserting Eqs. (4.24) and (4.25) in the Boltzmann equations (4.1) and (4.3) yields the complete set of differential equations to be integrated numerically. Once the Boltzmann equations for the distribution functions are solved, one can perform the integration over the RHN (lepton) phase space to obtain the number densities and, in turn, the final efficiency factor κ_f.

Numerical implementation

Since the direct integration of Eqs. (4.1) and (4.3) is very time-consuming, we briefly outline our strategy. In order to receive the distribution functions in dependence of momentum and temperature, we solve the Boltzmann equations on a two-dimensional grid consisting of 500 momentum (y_i) and 5000 temperature (z) bins, respectively. The large number of z-bins is necessary in order to obtain stable results for large values of the decay parameter K at low temperatures (large z). For each momentum bin we use a Runge–Kutta algorithm to integrate the 5000 differential equations between the different z-bins. The most time consuming part is now the two-dimensional integration of the collision integrals Eqs. (4.24) and (4.25) that have to be performed for each step in the Runge–Kutta integration. In order to reduce the run-time, we therefore first integrate all parts of Eqs. (4.24) and (4.25) that do not depend on f_N or $f_{l-\bar{l}}$, respectively, for each point on the (y_i, z)-grid and store the result in a separate file. When solving the differential equations with the Runge–Kutta algorithm, we then read-in the solutions of the collision integrals corresponding to the specific point on the (y_i, z)-grid. In order to find the exact (z) position in the Runge–Kutta algorithm, we interpolate the read-in solutions between the two z-bins corresponding to the explicit initial and final temperature of the
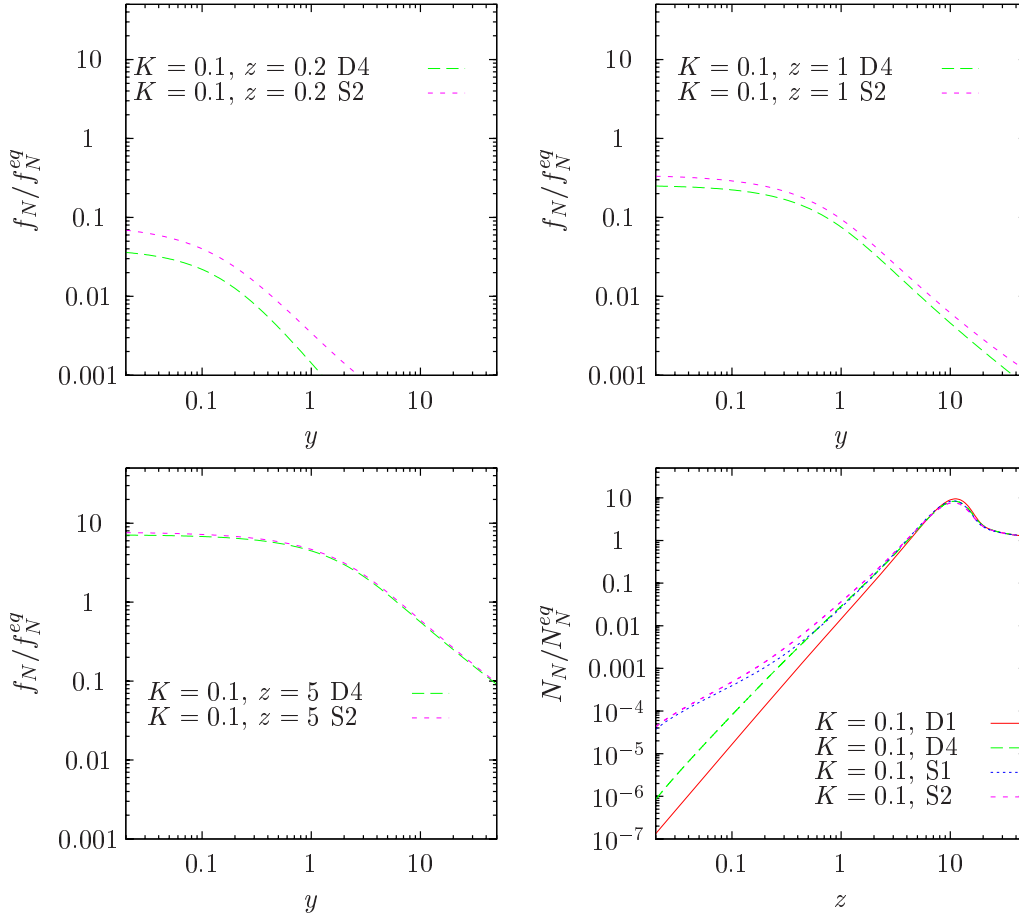
Figure 4.3: Snapshots of the RHN distribution function f_N/f_N^{eq} at $z = 0.2, 1, 5$, and the RHN abundance N_N/N_N^{eq} as a function of z, assuming $K = 0.1$. Solid/red line denotes Case D1, long dashed/green D4, dotted/blue S1, and short dashed/magenta S2. See tables 3.1 and 4.1 for a summary of the scenarios.

Boltzmann equations. Doing so, instead of solving 20 two-dimensional integrals during the integration of the differential equations, we only have to read-in the files containing the solution of the collision integrals once and perform the interpolation for each step in the Runge–Kutta algorithm.

4.1.3   Results and discussions

Scattering vs decay–inverse decay

Figure 4.3 shows snapshots of the RHN distribution function in Case S2 relative to an equilibrium Fermi–Dirac distribution at time $z = 0.2, 1, 5$, as well the RHN number density normalized to its equilibrium value as a function of z for an interaction strength
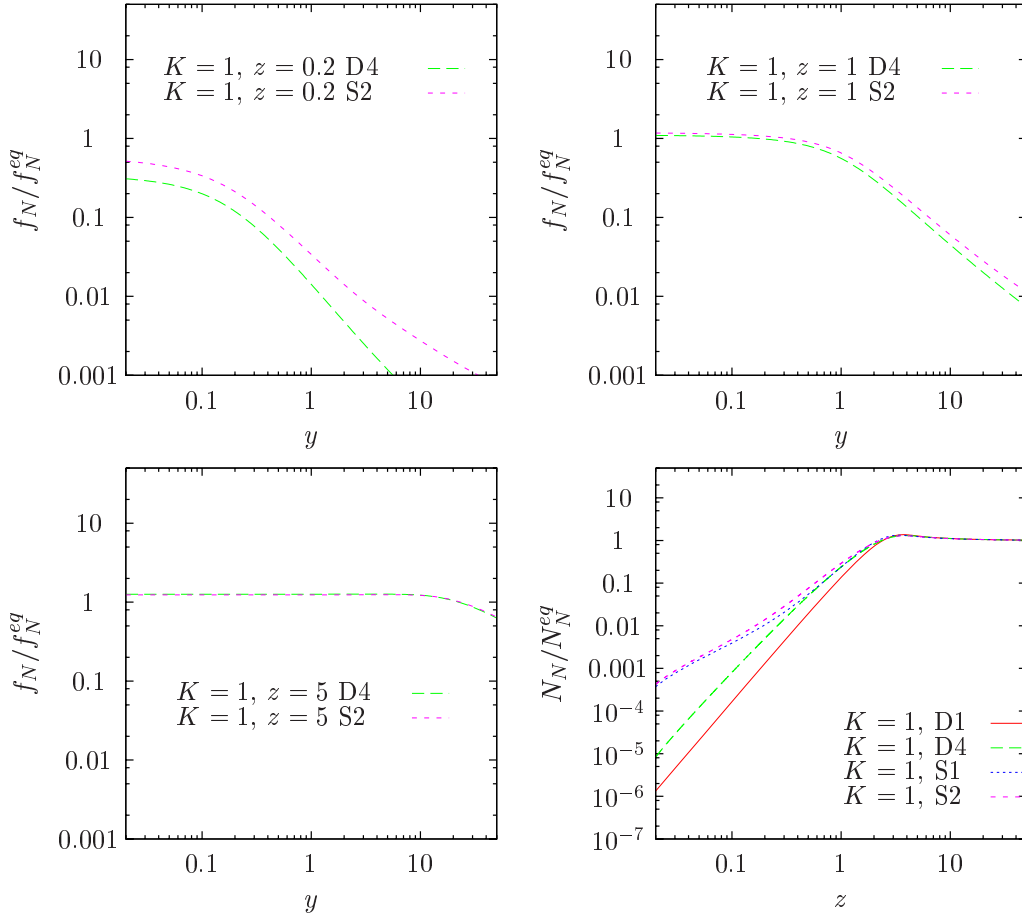
Figure 4.4: Same as Figure 4.3, but for $K = 1$.

of $K = 0.1$. These are compared with their counterparts assuming decay and inverse decay only (Case D4). Figures 4.4 and 4.5 are similar, except for $K = 1$ and $K = 10$, respectively. Clearly, including scattering processes speeds up the equilibration of the RHN distribution function, especially at high temperatures ($z < 1$). This effect is more significant for small values of K since for large K values decays and inverse decays are already fast enough to establish equilibrium.

Looking at the time evolution of the RHN number density, we see a corresponding increase in N_N at high temperatures when scattering is included (Case S2), compared to the case with decays and inverse decays only (Case D4). The equilibrium density is also reached at an earlier time (or higher temperature). The integrated approach shows a similar behavior, with Case S1 predicting a large RHN abundance at high temperatures and hence faster equilibration than Case D1.

Figure 4.6 shows the time evolution of the lepton asymmetry, again for the three
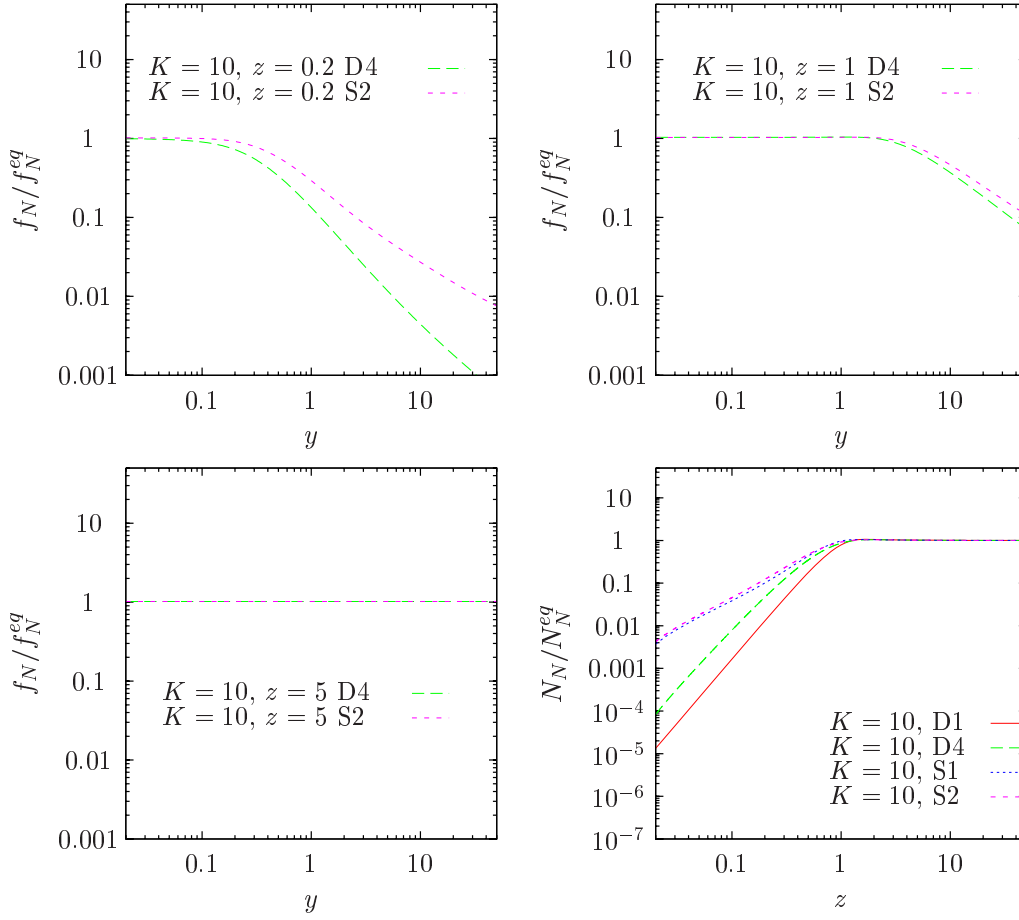
Figure 4.5: Same as Figure 4.3, but for $K = 10$.

characteristic values of the decay parameter $K = 0.1, 1, 10$. As discussed earlier, we have explicitly ignored CP violation in the scattering processes, so that they have no direct influence on the lepton asymmetry. This assumption is the reason why, in the weak wash-out regime ($K = 0.1$), the asymmetry evolution at high temperatures ($z < 1$) in Case S2 is virtually identical to that in its decay–inverse decay only counterpart Case D4. The same behavior can also be seen when comparing Cases S1 and D1. Here, decays and inverse decays of the RHN alone source the creation of a lepton asymmetry. Since for $K < 1$ the asymmetry evolution at high temperatures hinges primarily on inverse decays and is as yet unaffected by such external factors as the RHN abundance and wash-out processes, the inclusion of scattering processes has no visible effect on $N_{l-\bar{l}}$.

However, scattering can still affect the asymmetry production in two indirect and competing ways: (i) the larger RHN abundance produced via scattering processes at high temperatures forces the lepton asymmetry to flip sign earlier, thereby generating a larger
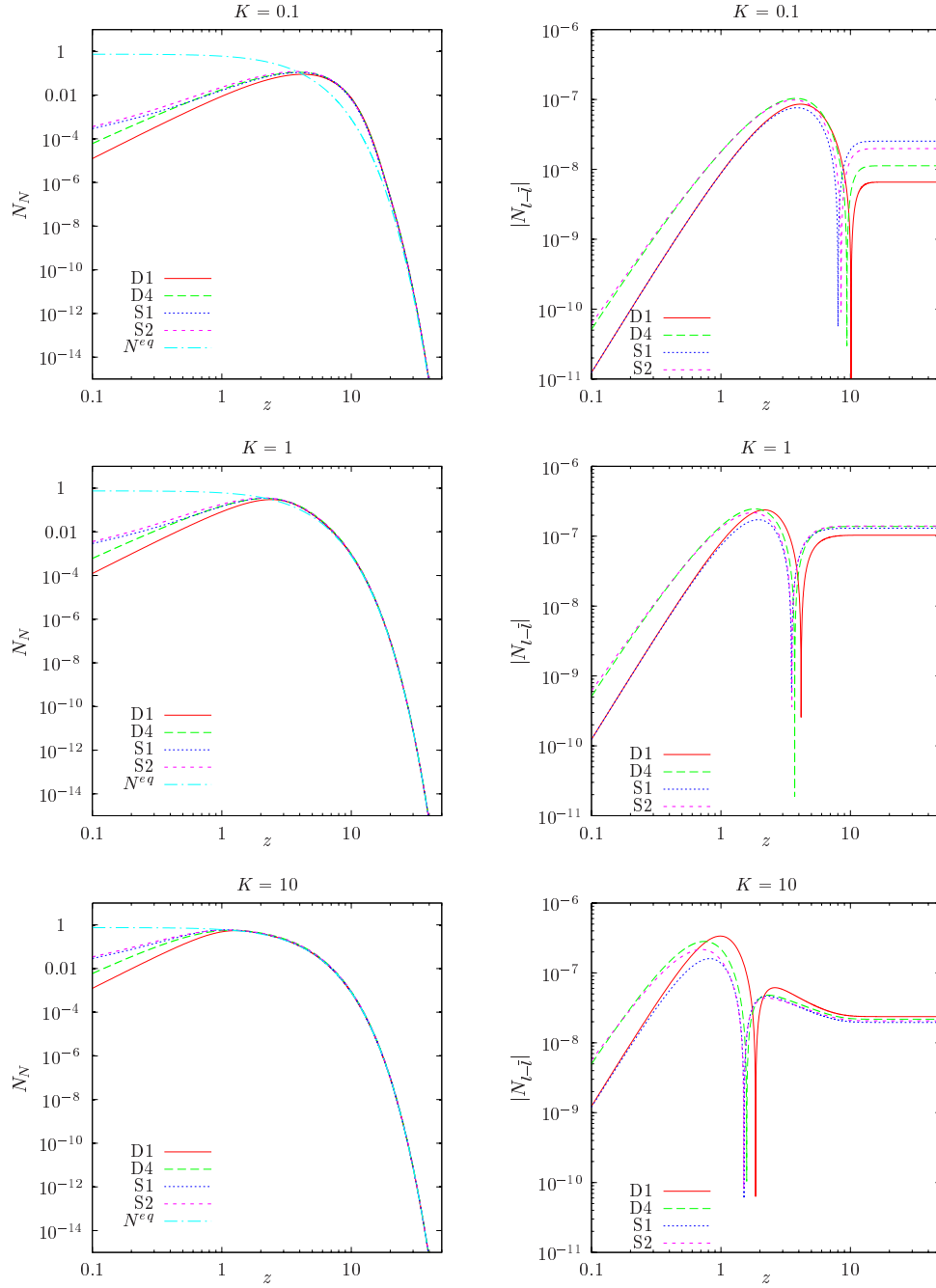
Figure 4.6: Time evolution of the absolute value of the lepton asymmetry $|N_{l-\bar{l}}|$ for three different coupling strengths K. Shown are the two cases including scattering processes S1 (dotted/blue) and S2 (short dashed/magenta), and two scenarios D1 (solid/red) and D4 (long dashed/green) within the decay–inverse decay only framework. For reference we also plot the RHN equilibrium abundance (dot-dash/cyan).

positive lepton asymmetry, and (ii) scattering leads to additional wash-out of the lepton asymmetry. The first effect dominates for coupling strengths lying in the weak wash-out regime ($K < 1$), eventually leading to a larger asymmetry in Cases S1 and S2, compared with their decay–inverse decay only counterparts D1 and D4 as shown in Figure 4.6. For stronger couplings ($K > 1$), the second effect dominates; in fact, Figure 4.6 shows that the additional wash-out due to scattering suppresses the lepton asymmetry production in Cases S1 and S2 already at high temperatures $z < 1$, compared with the decay–inverse decay only scenarios D1 and D4. In the transition regime between weak and strong wash-out, for $K = 1$, the two effects compete with each other: the lepton asymmetry in the Cases D4, S1 and S2 reach almost an identical final value. In the Cases S1 and S2 this is due to the sign flip happening at the same time, earlier than in the decay–inverse decay only scenarios D1 and D4. In Case D4, however, the change of sign occurs only slightly later and the asymmetry grows later on to nearly the same value, since it is not altered by wash-out due to scatterings.

Complete treatment vs integrated approach

The complete treatment differs from the integrated approach in that in the latter case we assume kinetic equilibrium for the RHN and neglect all quantum statistical factors. As we saw in Section 3.3.5, the assumption of kinetic equilibrium tends to underestimate by a tiny amount the RHN abundance at $z < 1$. This can be understood from Figures 4.3 to 4.5 as a result of the more efficient production of low momentum RHN states, which in turn contribute more to the momentum integral.

Quantum statistics, on the other hand, has very different effects on the scattering and the decay–inverse decay collision terms. As we saw in Section 3.3.5, in the decay–inverse decay scenario, quantum statistics always enhances the interaction rates through the enlarged Higgs boson phase space density f_Φ at low E_Φ. For the scattering processes, since all participants are fermions, the role of quantum statistics is to reduce the phase space and hence suppress the interaction rates. In general, however, we expect quantum statistics to be more important for decay/inverse decay than for scattering. This is because in the decay–inverse decay case the enhanced phase space due to f_Φ at low E_Φ can in principle be infinite, while Pauli blocking for fermions participating in scattering, e.g., $1 - f_l$, suppresses the phase space by at most a factor of $1/2$.

The difference between the RHN abundance and the lepton asymmetry evolution in the complete and the integrated treatments can then be understood in terms of a competition between the three aforementioned effects.

Consider first the RHN abundance. At $z \ll 1$ the dominant RHN production channel is scattering. Here, suppression of the production rate due to quantum statistical

factors competes with the small enhancement due to our dropping the assumption of kinetic equilibrium. The net result is that both Cases S1 and S2 give very similar RHN abundances as shown in Figures 4.3 to 4.6. At $z \sim 0.3$, decay/inverse decay becomes comparable to scattering (see Figure 4.2). Here, the enhanced decay rate due to quantum statistics in Case S2 pushes up RHN production relative to Case S1. This effect is more prominent in the weak wash-out regime than in the strong wash-out region since in the former case the RHN abundance is further away from equilibrium. Progressing further in z, we see that the RHN abundances in Cases S1 and S2 become virtually identical already before reaching the equilibrium value. This is in stark contrast with the decay–inverse decay only scenarios, where the RHN abundances in Cases D1 and D4 clearly cross the equilibrium threshold at different times.

Consider now the evolution of the lepton asymmetry (right panel of Figure 4.6). Comparing Cases S1 and S2 in the weak wash-out regime ($K = 0.1$), quantum statistics in the latter scenario enhances the production of a negative lepton asymmetry at high temperatures. This effect is due solely to phase space enhancements in the inverse decay term since we have assumed explicitly that scattering does not violate CP. At $z \sim 4$, the production of lepton asymmetry reverses direction as RHN decays begin to dominate over inverse decays. As mentioned earlier, quantum statistics causes this reversal to happen earlier in the decay–inverse decay only scenario by bringing the RHN abundance to the equilibrium threshold at an earlier time. When including scattering, however, the RHN abundances in both Cases S1 and S2 cross the equilibrium threshold at almost the same time, as discussed in the previous paragraph. This means that the evolution of their corresponding lepton asymmetries also turns around at roughly the same time. Since at the time of the turn-around Case S2 has a more negative asymmetry than Case S1, the net effect is that the asymmetry in Case S2 flips sign at a slightly later time than in Case S1, and subsequently grows to a smaller positive value.

The effects of quantum statistics on the lepton asymmetry evolution in the strong wash-out regime ($K = 10$) can be similarly understood, except that we must consider also the role of the wash-out terms. At $z \lesssim 1$, the wash-out rate is dominated by scattering. However, as shown in Figure 4.2, decay/inverse decay becomes comparable to scattering at $z \sim 0.3$ and is the dominant wash-out process at $z \gtrsim 1$. Thus, from $z \sim 1$ onwards, the net effect of quantum statistics is to enhance the wash-out rate. This effect can be seen at the turn-around of the lepton asymmetry evolution: the stronger wash-out rate in Case S2 forces the lepton asymmetry evolution to reverse direction at a slightly earlier time than in Case S1. However, since at the time of the turn-around Case S2 has a more negative asymmetry than S1, the asymmetries in both cases end up flipping signs at almost the same time and grow to nearly identical values.
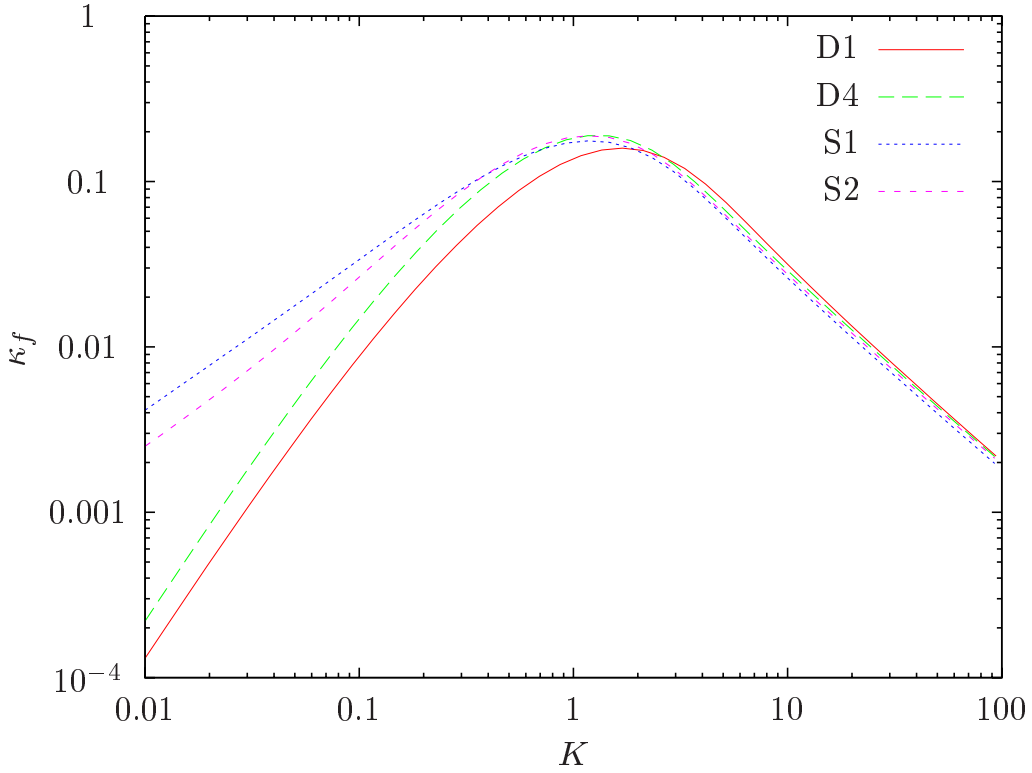
Figure 4.7: The final efficiency factor κ_f without and with scattering terms: D1 (solid), D4 (long dashed), S1 (dotted), and S2 (short dashed).

Having discussed the evolution of the lepton asymmetry in the weak and in the strong wash-out regime, its evolution in the transition regime ($K = 1$) can be understood in a similar fashion. From $z \sim 1$ on the same argumentation than in the strong wash-out is viable: the stronger wash-out in Case S2 forces the lepton asymmetry to turn around at an earlier time than in Case S1. But since it has grown to a larger value, the change of sign happens at almost the same time leading to nearly identical final values.

Finally, Figure 4.7 shows the final efficiency factors as a function of K for the integrated approach and the complete mode treatment, both, including and excluding scattering. For Cases S1 and S2 which include scattering, we note that their difference is rather large in the weak wash-out regime ($K < 1$), with the integrated approach overestimating κ_f by up to a factor ~ 1.5 at $K \sim 0.01$ compared to solving the complete mode equations. But this difference decreases as we increase K. At $K \gtrsim 3$ the integrated approach underestimates κ_f by less than $\sim 10\%$.

It is also interesting to note that the relative contribution of scattering processes to the final efficiency factor is smaller in the complete mode calculation than in the integrated approach. In the weak wash-out regime, including scattering enhances the final efficiency
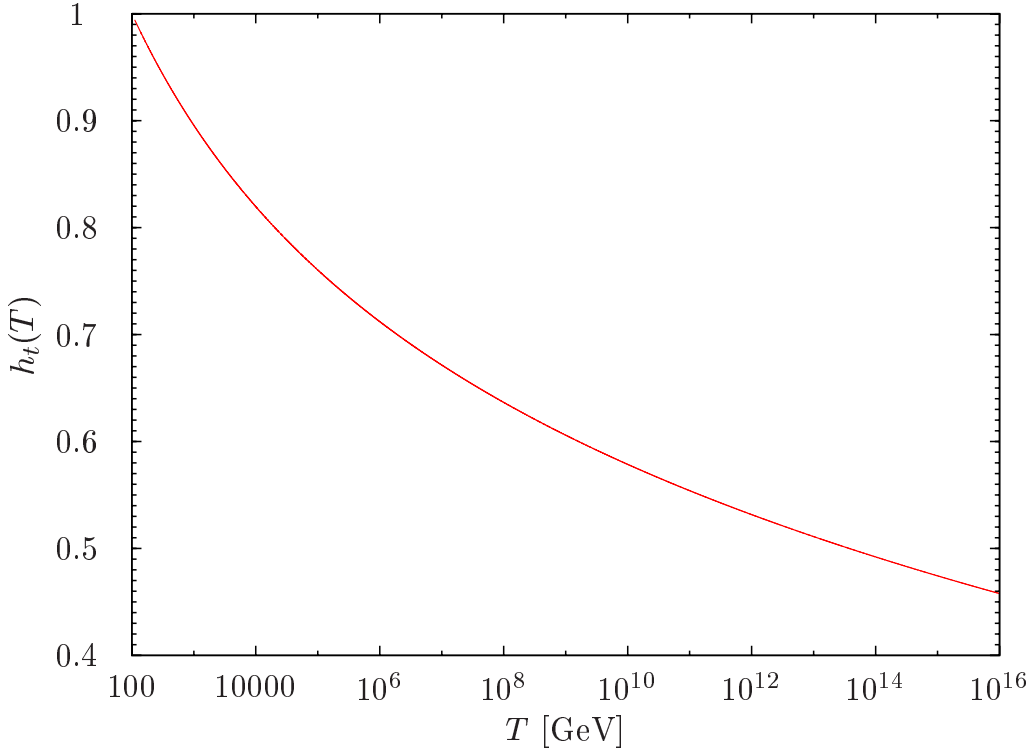
Figure 4.8: The evolution of the top Yukawa coupling from the electroweak scale up to the GUT scale.

factor from decays and inverse decays by up to a factor of ~ 30 in the integrated scenario. In the complete mode calculation, however, the enhancement is only a factor of ~ 15. Similarly, in the strong wash-out regime, scattering reduces κ_f by up to 20% in the integrated picture, compared to below 10% in the complete treatment.

4.2 Influence of energy dependent top Yukawa coupling

In this section we will discuss the influence of the evolution of the top Yukawa coupling on the final efficiency factor. For this purpose, the renormalization group equation for the top Yukawa coupling is set up in Appendix C and the resulting evolution of $h_t(T)$ is shown in Figure 4.8 from the electroweak scale up to the GUT scale.

   As the top Yukawa coupling is a function of temperature, its inclusion in the calculation of the efficiency factor depends on the RHN mass M since in the Boltzmann equations the dimensionless variable $z = M/T$ is used to parametrize the time evolution [2]. The dynamics relevant for leptogenesis take place in the interval $z \in [0.01, 100]$.

---

[2]For values $M \ll 10^{14}$ GeV, the efficiency factor $\kappa\left(\tilde{m}_1, z\right)$ is a function of $\tilde{m}_1$ and z only since
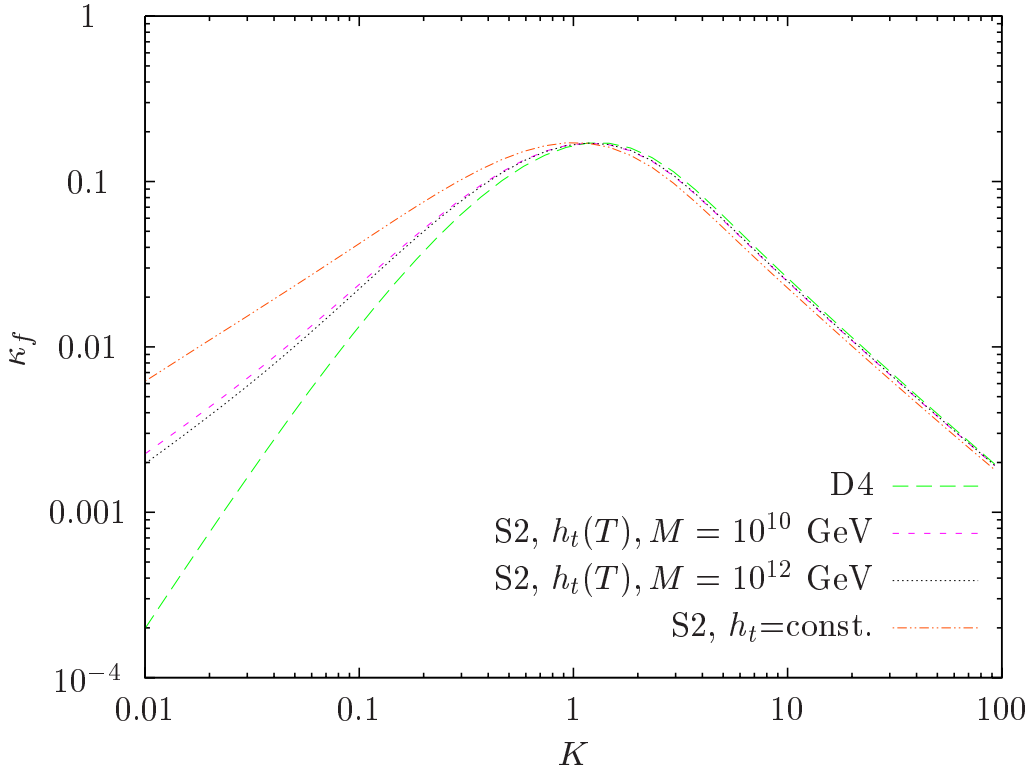
Figure 4.9: Effect of the evolution of the top Yukawa coupling on the final efficiency factor κ_f: h_t fixed at $T = m_Z$ (point-point-dashed/red), $h_t(T)$ with $M = 10^{10}$ GeV (dashed/cyan) and $h_t(T)$ with $M = 10^{12}$ GeV (pointed/grey). For reference, κ_f is shown for Case D4 (long-dashed/green).

Supposing the RHN mass to be in the range 10^8 GeV $\leq M \leq 10^{12}$ GeV, this implies 10^6 GeV $\leq T \leq 10^{14}$ GeV. For the calculations in the previous sections we choose a value $M = 10^{10}$ GeV. As can be clearly seen in Figure 4.8, the coupling at the scale $T = 10^{10}$ GeV has only about half the strength than at the electroweak scale. In turn, the difference at the initial value $z = 0.01$ can be as large as $\sim 20\%$ when changing M by four orders of magnitude. These differences imply that it is important to include the overall evolution of the top Yukawa coupling from the electroweak scale up to the scale where thermal leptogenesis is viable, i.e., $T \gtrsim 10^6$ GeV.

To study the effects of the evolution of the coupling on the final asymmetry, we performed different calculations in the Case S2, using the complete set of Boltzmann equations. In Figure 4.9 we compare the final efficiency factor calculated with the top Yukawa coupling fixed at the electroweak scale $T = m_Z$ with the efficiency factor ob-

---

the wash-out due to $\Delta L = 2$ scatterings with a heavy neutrino $N_{1,2,3}$ in the s- and t-channel can be neglected [128].

tained with a running coupling for chosen values of $M = 10^{10}$ GeV and $M = 10^{12}$ GeV, respectively, in dependence of the decay parameter K. For reference, the decays/inverse scenario D4 is shown as well.

The final efficiency factor calculated with a coupling constant fixed at the electroweak scale is a factor ~ 3 larger in the regime of weak wash-out compared to the scenarios where the evolution of the coupling is accounted for. This is due to the more effective RHN production for stronger couplings. For larger values of the decay parameter, however, the influence of the coupling evolution becomes less important and at $K \sim 1$ the final efficiency factors become virtually identical in all scenarios. Then, in the regime of strong wash-out κ_f is reduced by less than $\sim 10\%$ when the evolution of h_t is neglected. This is due to the additional wash-out in the scattering processes that becomes sizable for larger values of h_t. Concentrating on more realistic scenarios in which the coupling strength depends on the energy scale, we see that changing the RHN mas by two orders of magnitude from $M = 10^{10}$ GeV to $M = 10^{12}$ GeV leads to a reduction of κ_f of 15% in the regime of weak wash-out. However, already at $K \sim 0.3$ the efficiency factors in both cases become virtually identical. In the strong wash-out regime, for $K > 1$, the difference is below the percent level. Overall, this discussion shows that it is important, especially in the regime of weak wash-out, to take the evolution of the top Yukawa coupling into account. Whereas, changing the explicit value of M and hence the explicit leptogenesis scale by two orders of magnitude only leads to minor ($< 15\%$) changes in the final efficiency factor.

Chapter 5

N_2-dominated leptogenesis

5.1 The Ω matrix and different scenarios of leptogenesis

In this thesis we considered up to now leptogenesis exclusively in the N_1-dominated scenario. Qualitatively, this scenario can be realized assuming $M_1 \ll M_2, M_3$. By implication, the CP asymmetries produced in the decays of the heavier states $N_{2,3}$ are small, i.e., $|\varepsilon_{2,3}| \ll |\varepsilon_1|$, as a consequence of light particles running in the loop of the self-energy and vertex corrections to the tree-level decay diagram. This can be seen expressing the CP asymmetry, Eq. (2.3), summed over flavor as [84, 133]

$$\varepsilon_i \approx -\frac{1}{8\pi} \sum_{\substack{j=1,2,3 \\ j \neq i}} \frac{\mathrm{Im}\left[\left(\lambda^\dagger \lambda\right)_{ij}^2\right]}{\left(\lambda^\dagger \lambda\right)_{ii}} \times \left[f_V\left(\frac{M_j^2}{M_i^2}\right) + f_S\left(\frac{M_j^2}{M_i^2}\right)\right], \qquad (5.1)$$

where the functions f_V and f_S describe, respectively, the vertex and self-energy contributions. Indeed, in the limit of massless particles running in the loop, the corresponding CP asymmetry vanishes. Furthermore, due to N_1 interactions following the decay of the heavier right-handed states $N_{2,3}$, a substantial part of the produced lepton asymmetry will presumably be washed-out, especially in the regime of strong wash-out.

To understand how specific scenarios can be realized, we go back to the see-saw mechanism, cf. Section 1.5, and recast the light neutrino mass matrix, Eq. (1.12),

$$m_\nu = -m_D \frac{1}{M} m_D^{\mathrm{T}},$$

with $m_D = \lambda\, v$. Here, it is always possible to choose a basis in which the heavy neutrino mass matrix is diagonal, $D_M = \mathrm{diag}\left(M_1, M_2, M_3\right)$. Using an unitary matrix U, one can simultaneously diagonalize the light neutrino mass matrix

$$D_m = -U^\dagger\, m_\nu\, U^*, \qquad (5.2)$$

where $D_m = \mathrm{diag}\,(m_1, m_2, m_3)$. If one does not account for the running of neutrino parameters from the electroweak scale to the see-saw scale [134, 135], the matrix U corresponds to the PMNS matrix, earlier introduced in Eq. (1.4). With the help of an orthogonal matrix Ω, the Dirac neutrino mass matrix can be written in the so-called *Casas–Ibarra parametrization* [136],

$$m_D = U \sqrt{D_m}\,\Omega\,\sqrt{D_M}. \tag{5.3}$$

The Dirac neutrino mass matrix is fully described by 18 parameters: the mixing matrix U contains six parameters (three mixing angles and three phases), the diagonal matrices D_m and D_M contain three neutrino masses each, and the orthogonal matrix Ω is described by six real (three complex) parameters. It can be written as a product of three rotational matrices [125, 137]

$$\Omega\,(\omega_{21}, \omega_{31}, \omega_{32}) = R_{12}\,(\omega_{21})\,R_{13}\,(\omega_{31})\,R_{23}\,(\omega_{32})\,, \tag{5.4}$$

with

$$R_{12} = \begin{pmatrix} \sqrt{1 - \omega_{21}^2} & -\omega_{21} & 0 \\ \omega_{21} & \sqrt{1 - \omega_{21}^2} & 0 \\ 0 & 0 & 1 \end{pmatrix}, \tag{5.5}$$

$$R_{13} = \begin{pmatrix} \sqrt{1 - \omega_{31}^2} & 0 & -\omega_{31} \\ 0 & 1 & 0 \\ \omega_{31} & 0 & \sqrt{1 - \omega_{31}^2} \end{pmatrix}, \tag{5.6}$$

and

$$R_{23} = \begin{pmatrix} 1 & 0 & 0 \\ 0 & \sqrt{1 - \omega_{32}^2} & -\omega_{32} \\ 0 & \omega_{32} & \sqrt{1 - \omega_{32}^2} \end{pmatrix}. \tag{5.7}$$

In general, one can state that Eq. (5.3) is divided into two parts: (i) a measurable low-energy part, containing the PMNS matrix U and the light neutrino masses D_m (cf. Section 1.4.1), and (ii) a high-scale part, consisting of the orthogonal Ω matrix and the heavy neutrino masses D_M, which is not accessible by current experiments.

The N_1-dominated scenario can now be realized assuming the heavy neutrino mass matrix to be hierarchical, i.e. $M_1 \ll M_{2,3}$, together with a specific choice of the CP asymmetries implemented by a special form of the Ω matrix [125, 137]:

- For $\Omega = R_{13}$, the CP asymmetry in N_2 decays vanishes, i.e., $\varepsilon_2 = 0$, while ε_1 is maximal.

- For $\Omega = R_{12}$, the CP asymmetry ε_1 is suppressed compared to its maximal value, Eq. (2.7), and $|\varepsilon_2| \propto (M_1/M_2)\, |\varepsilon_1|$ is negligible within a strong mass hierarchy [1].

In Figure 3.1 we have seen that the N_1-dominated scenario proves independent of the initial conditions in the regime of strong wash-out. However, in the weak wash-out regime the final asymmetry production depends sensibly on the initial conditions on the N_1 abundance. Furthermore, as discussed in Section 2.3, thermal leptogenesis sets a lower limit of $M_1 \gtrsim 10^9$ GeV, cf. Eq. (2.15), on the mass of the lightest right-handed neutrino in order to explain successfully the observed value of the baryon asymmetry of the universe. This bound is consequently translated into a lower bound on the re-heating temperature after inflation, cf. Eq. (2.16). These lower bounds not only have an issue with the cosmological abundance of gravitinos, mentioned in Section 2.3, but also cause some specific problems in GUTs based on flavor models. Some of these models assume a grand unified symmetry between up-quarks and neutrinos. The neutrino Yukawa couplings are then connected with the up-quark Yukawa matrices leading to right-handed neutrino masses which are proportional to the square of the up-quark masses [138, 139]. Typical values for the mass of the lightest right-handed state fall in the range $10^6 - 10^7$ GeV, see e.g., [140, 141], and masses $M_1 \geq 10^9$ GeV need a specific choice of parameters [142, 143]. This makes thermal leptogenesis difficult to reconcile with this class of models.

In order to circumvent these issues, the N_2-dominated scenario was proposed in [137]. Indeed, for $\Omega = R_{23}$ one can have a maximal CP asymmetry ε_2 coming from N_2 decays while ε_1 vanishes. This means that N_1 is totally decoupled from the heavier states while in the N_2 decay the heavy third state, N_3, is running in the loop. Together with a mass hierarchy in the heavy neutrinos, N_2-dominated leptogenesis can be realized if the wash-out from N_1 interactions does not deplete the produced asymmetry. With the above choice of Ω the effective neutrino mass of the lightest right-handed state is fixed to $\tilde{m}_1 = m_1$. Thus, for hierarchical light neutrino masses the N_1 interactions can be forced to be in the weak wash-out regime where $\tilde{m}_1 \lesssim m^* \approx 10^{-3}$ eV. It is worth noticing that, if the N_1 interactions are in the weak wash-out regime, i.e., $\tilde{m}_1 < m^*$, then the N_2 interactions are constrained to be in the strong wash-out regime, i.e., $\tilde{m}_2 > m^*$. This is due to the orthogonality of the Ω matrix [137]. Therefore, N_2-dominated leptogenesis is independent of the initial conditions on N_2 but might still be down to the initial conditions on N_1. In order to achieve a large enough CP asymmetry, the lower bound on the mass M_1 can be directly translated into a bound on the mass M_2, whereas the lower bound on the reheating temperature remains unchanged. The bound on M_1 is then obsolete and M_1 can be remarkably smaller. However, allowing for small complex

---

[1] If $M_1 \sim M_2$, both CP asymmetries should be taken into account.

rotations R_{12} and R_{13}, both of these bounds become increasingly more stringent leading to a point beyond which the N_2-dominated scenario is not viable anymore.

5.1.1   Note on flavor

Including flavor effects may substantially change the parameter ranges in which the scenarios discussed above are valid. It has been shown that, when the flavor structure of the lepton asymmetry and the wash-out is tracked, it is possible to generate a large enough lepton asymmetry in N_2 decays even if N_1 interactions are effective [143, 144]. The general idea here is that asymmetries in different lepton flavors τ, μ, and e do not mix through interactions in the thermal bath before the wash-out due to N_1 interactions becomes effective. The asymmetries in different lepton flavors will then only be washed-out by the N_1 interactions in the corresponding flavor. When the N_1 decays in the two-flavor regime at temperatures $10^9 \, \text{GeV} \lesssim T \lesssim 10^{12} \, \text{GeV}$, where only the τ Yukawa interactions are in equilibrium, or in the unflavored regime at temperatures $T \gtrsim 10^{12} \, \text{GeV}$, parts of the lepton asymmetry in a distinct flavor are protected from N_1 wash-out [9, 144, 145]. Furthermore, in the first section of this chapter we did not mention the effect of flavor on the CP asymmetry. In Eq. (2.3) we wrote the CP asymmetry as a matrix in flavor space. Indeed, the hierarchy of CP asymmetries, following a mass hierarchy of particles running in the loop, does not necessarily hold when flavored asymmetries are considered [114]. In contrast to the unflavored scenario, where ε_2 is suppressed by M_1/M_2 compared to ε_1, there is the possibility of having a non-negligible asymmetry $\varepsilon_{2\alpha}$ that, in turn, eventually extends the range of the N_2-dominated scenario.

5.2   Mode equations in N_2-dominated leptogenesis

In the last section we discussed the possibility of going beyond the usually considered N_1-dominated scenario of leptogenesis. We have shown that, with a special choice of the Ω matrix, the possibility of a N_2-dominated scenario exists. In this section we want to discuss the effect the complete set of mode equations (Case S2) have in the N_2-dominated scenario. Here, the wash-out due to N_1 interactions is (i) enhanced using mode-equations with decays/inverse decays alone and (ii) enhanced considering scatterings with the top quark. For the N_2-dominated scenario to be realized we will take the following working assumptions [146]: First, a sizable CP asymmetry ε_2 has been generated at the scale $T \sim M_2$ that is not altered by ε_1 generated at the later stage $T \sim M_1$ when the lightest right-handed state decays [2]. Second, the wash-out due to N_1 interactions does not erase the asymmetry produced in N_2 decays.

---

[2]For clarity we keep track of indices corresponding to N_1 and N_2 in this section
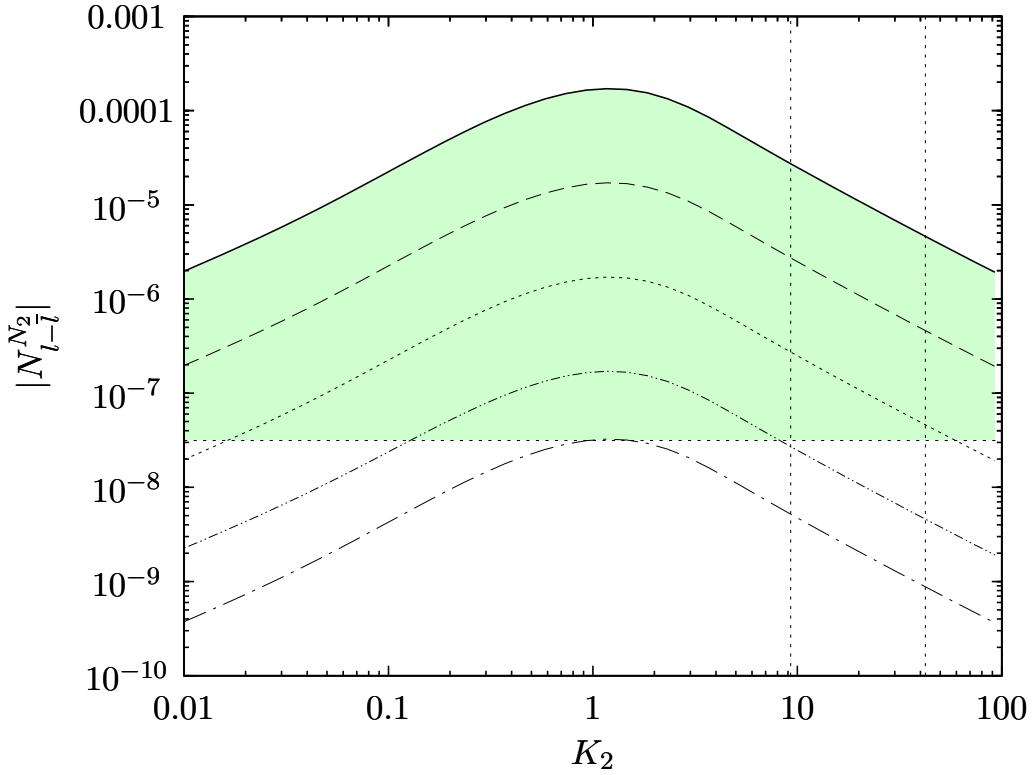
Figure 5.1: Lepton asymmetry generated in N_2 decays for maximal CP violation and different values of M_2: (i) $M_2 = 10^{13}$ GeV, solid line, (ii) $M_2 = 10^{12}$ GeV, long-dashed line, (iii) $M_2 = 10^{11}$ GeV, dashed line, (iv) $M_2 = 10^{10}$ GeV, point-point-dashed line, and (v) $M_2 = 1.9 \times 10^9$ GeV, point-dashed line. Within the considered scenario, the shaded region indicates where the produced baryon asymmetry exceeds η_B^{CMB}.

We will not focus on the first point of an exact evaluation of flavored CP asymmetries within special choices of the Ω matrix but rather discuss the second point within our treatment of complete kinetic equations. The lepton asymmetry that can be generated in N_2 decays is shown in Figure 5.1 in dependence of the decay parameter K_2 for values of M_2 varying between 1.9×10^9 GeV and 10^{13} GeV. The shaded area marks the region where the final asymmetry exceeds the measured value η_B^{CMB}, given in Eq. (1.1). For $M_2 \lesssim 2 \times 10^9$ GeV the CP asymmetry generated in N_2 decays is too small to account for the observed value of the matter–antimatter asymmetry. [3] On the other hand, for $M_2 \gtrsim 10^{13}$ GeV one has to account for $\Delta L = 2$ violating scattering processes with the N_2 in the s- and t-channel. Being an additional contribution to the wash-out, these processes tend to reduce the final amount of asymmetry [128]. The two vertical lines in

---

[3]This bound differs from Eq. (2.15) since for a vanishing initial abundance $\kappa_f < 1$.
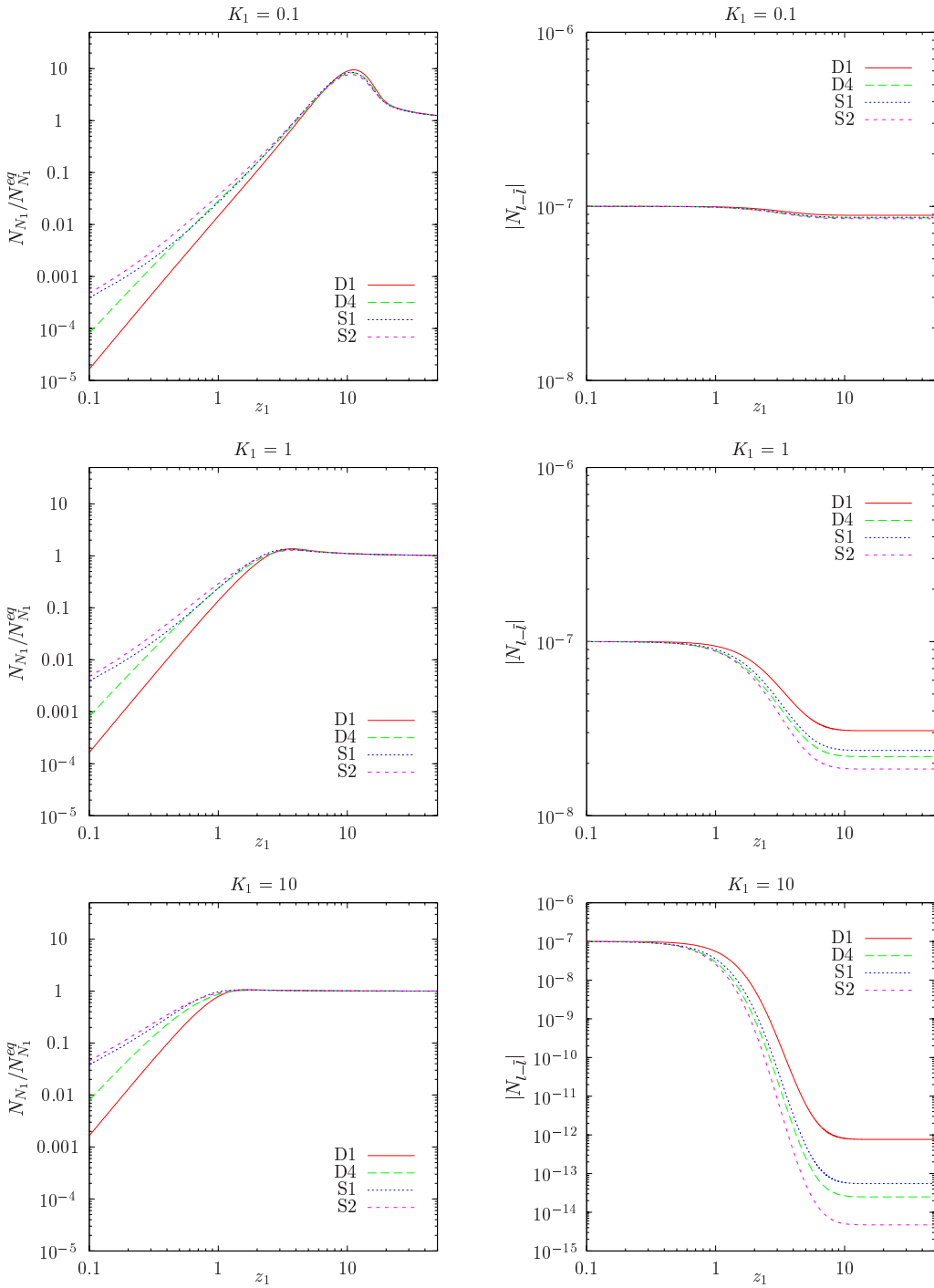
Figure 5.2: Time evolution of the absolute value of the normalized RHN number density $N_{N_1}/N_{N_1}^{\rm eq}$ and the lepton asymmetry $|N_{l-\bar{l}}|$ for three different coupling strengths K_1 in the N_2-dominated scenario for an initial asymmetry $|N_{l-\bar{l}}^{N_2}|_{\rm in} = 10^{-7}$ and $M_1 = 10^7\,{\rm GeV}$. Shown are the two cases including scattering processes S1 (dotted/blue) and S2 (short dashed/magenta), and two scenarios D1 (solid/red) and D4 (long dashed/green) within the decay–inverse decay only framework.

Figure 5.1 correspond to the solar and atmospherics neutrino scale, respectively. Considering the N_2 interactions to be in the strong wash-out regime in the window preferred by neutrino oscillation data demands $M_2 \gtrsim 10^{11}$ GeV to explain the observed value of the baryon asymmetry, Eq. (1.1).

The lepton asymmetry generated in N_2 decays is altered by the subsequent wash-out due to interactions of the lightest right-handed neutrino N_1. According to the considerations of [122], where N_2-dominated leptogenesis has been addressed by means of mode equations within the decay–inverse decay only scenario (Case D4), we choose the following initial conditions at $z_1 = M_1/T$ to calculate the effect of wash-out on an initially produced asymmetry: (i) We take $|N_{l-\bar{l}}^{N_2}|_{\text{in}} = 10^{-7}$ as initial value of the lepton asymmetry generated in N_2 decays, (ii) assume a zero initial N_1 abundance, and (iii) set $\varepsilon_1 \approx 0$. The third condition can be achieved by supposing a small value of the N_1 mass. Anyway, small CP asymmetries stemming from different generations add up linearly and an additional asymmetry ε_1 would not modify our consideration on the N_1-induced wash-out effects. We choose $M_1 = 10^7$ GeV in the numerical implementation in order to fix the evolution of the top Yukawa coupling.

Figure 5.2 shows on the left panel the time evolution of the normalized N_1 number density for the Cases D1, D4, S1, and S2 in dependence of z_1. These plots correspond to the lower right plots in Figures 4.3 to 4.5 save for the difference that for the Cases S1 and S2 we choose $M_1 = 10^7$ GeV here, instead of $M_1 = 10^{10}$ GeV as in Section 4.1.2. On the right panel the time evolution of the lepton asymmetry during N_1 wash-out is shown for the same scenarios. Thus, in addition to the discussion in [122], we include Cases S1 and S2 here. In the weak wash-out regime ($K_1 = 0.1$), the asymmetry is only slightly reduced in the Cases D4, S1, and S2 compared to the integrated approach in the decay/inverse decay only scenario, Case D1. The net wash-out of the initial asymmetry is less than 10%. However, already at $K_1 \sim 1$ the strength of the wash-out in the different scenarios becomes distinguishable. At $z_1 \sim 1$ wash-out becomes effective and is strongest in Case S2 where the complete set of Boltzmann equations including scatterings with the top quark is considered. The difference in the lepton asymmetry between Case D4 and Case S2, both using mode equations, is about a factor of two. However, the net reduction of the initial asymmetry is still less than one order of magnitude. Comparing Case S2 with Case S1, we see that the influence of the additional wash-out factor f_{N_1}, present in the mode equation, cf. Eq. (3.55), is larger than the wash-out due to scatterings in the integrated approach that is present in Case S1. In the strong wash-out regime, for $K_1 = 10$, the initial asymmetry is depleted by up to six orders of magnitude, with the strongest wash-out again in Case S2. Considering the momentum integrated scenarios, the reduction in Case S1 is two orders of magnitude larger than in Case D1.
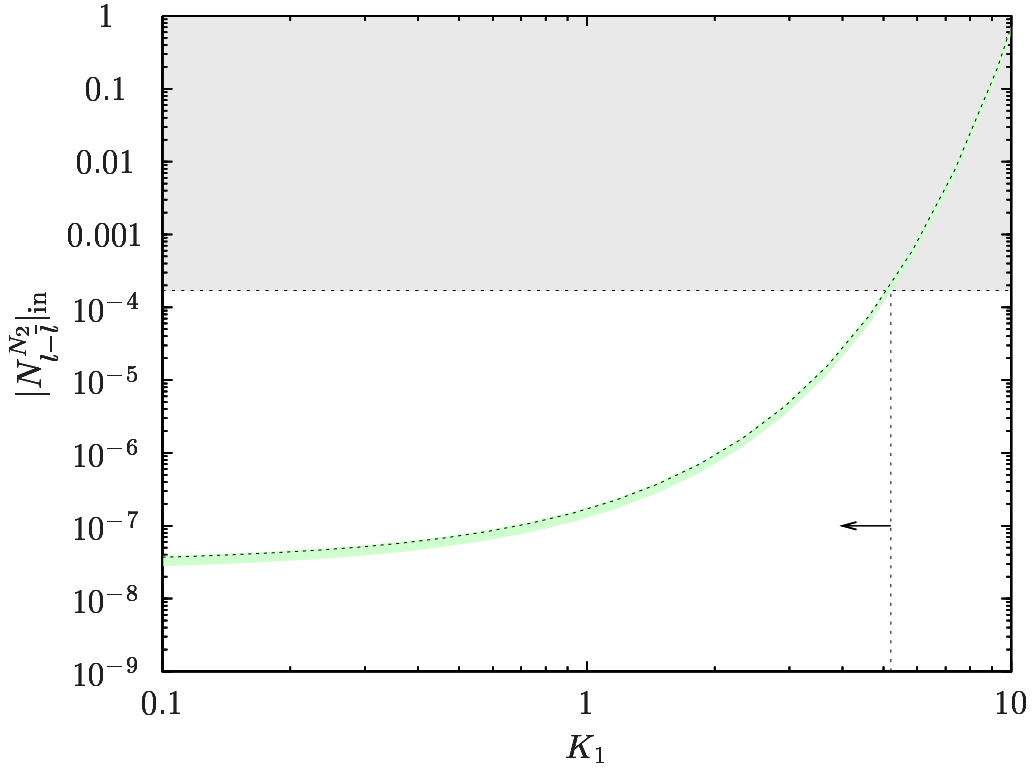
Figure 5.3: Amount of initial asymmetry that has to be generated in N_2 decays in order to survive the subsequent wash-out by N_1 interactions. The mass of the lightest right-handed neutrino was set to $M_1 = 10^7$ GeV and the CP asymmetry generated in N_1 decays was set $\varepsilon_1 = 0$. The asymmetry in the grey shaded region cannot be generated in N_2 decays and the area right of the arrow is excluded due to N_1 wash-out.

Concerning the scenarios in which mode equations are used, the contribution of the scatterings amounts to one order of magnitude as can be seen by comparing Case S2 with Case D4. In general, it can be stated that the wash-out is enhanced more by the use of mode equation than by the inclusion of scattering processes that become important only for values $K_1 \geq 1$.

Figure 5.3 shows the amount of initial asymmetry generated in N_2 decays that is needed to account for the observed value of the baryon asymmetry after wash-out due to N_1 interactions in dependence of K_1. The green colored region corresponds to the value of the baryon asymmetry deduced in BBN within 95% confidence level, Eq. (1.2), and the dashed-line within this region represents the value of the baryon asymmetry deduced from CMB measurements, Eq. (1.1). When N_1 interactions fall into the weak-wash-out regime ($K_1 < 1$), almost all of the initial generated asymmetry survives giving

$|N_{l-\bar{l}}^{N_2}|_{\text{in}} \approx 3 \times 10^8$, i.e., the same limit as can be seen in Figure 5.1. However, increasing the strength of the N_1 interactions, wash-out becomes more and more effective and for $K_1 = 10$ an initial value $|N_{l-\bar{l}}^{N_2}|_{\text{in}} \approx 1$ is needed to account for the observed value of the baryon asymmetry. Though, as can be seen in Figure 5.1, values of the asymmetry lying in the shaded area above the horizontal dashed line at $|N_{l-\bar{l}}^{N_2}|_{\text{in}} = 1.7 \times 10^4$ cannot be generated in N_2 decays. Therefore, for the N_2-dominated scenario to be successful, the N_1 interactions are restricted to $K_1 \lesssim 5$. The upper bound on the initial asymmetry corresponds to values $M_2 = 10^{13}$ GeV and $K_2 \approx 0.3$. For values of K_2 lying in the strong wash-out regime that is preferred by neutrino oscillation data, the generated asymmetry is roughly one order of magnitude smaller, leading to $K_1 \lesssim 3$. When choosing conservative values, $M_2 \sim 10^{11}$ GeV and $\kappa_{2f} \sim 10^{-2}$, the scenarios are forced to $K_1 \lesssim 2$.[4] This corresponds to values of K_1 typically needed in $SO(10)$ inspired GUTs where flavor effects are included. For the limiting scenario, $M_2 \approx 2 \times 10^9$ GeV, the N_1 interactions strength K_1 has to vanish [147].

---

[4]Using typical assumptions, the study in [122] found a limit $K_1 < 3$.

Chapter 6

Conclusions

The absence of antimatter in the universe provides one of the most intriguing problems of particle physics and cosmology. In leptogenesis the explanation of the matter–antimatter asymmetry is connected with the nature of observed neutrino masses via the see-saw mechanism. Here, heavy right-handed neutrino states give rise to light-neutrino masses in the sub-eV range. At the same time a lepton asymmetry may be generated in their decays. This lepton asymmetry is then partially transformed into a baryon asymmetry by so-called sphaleron processes, an anomaly present in the Standard Model of particle physics. The creation and subsequent partial depletion of a lepton asymmetry is usually studied by means of momentum integrated Boltzmann equations since the processes involved in leptogenesis are typically close-to-equilibrium.

In this thesis we have studied leptogenesis by means of the full Boltzmann equations incorporating all quantum statistical terms without the assumption of kinetic equilibrium, and including scatterings of the right-handed neutrino with quarks. This is of particular relevance for the creation of the cosmological baryon asymmetry due to the required deviation from thermal equilibrium and the energy dependence of all interactions. As the simplest possible set-up to study these effects, we have first considered only an asymmetry being created by the lightest right-handed neutrino and have neglected potentially important flavor effects. To this end, in Chapter 3 we provided a thorough study of leptogenesis taking into account exclusively decays and inverse decays where one Yukawa coupling alone controls the production and later decays of right-handed neutrinos.

In the conventional approach, i.e., neglecting quantum statistical factors and assuming kinetic equilibrium, considering only decays and inverse decays is known to give a rather precise approximation of the final baryon asymmetry in the interesting strong wash-out regime. At the same time, this case also offers the possibility to study the influence of various effects separately and in detail.

Interestingly enough, dropping the assumption of kinetic equilibrium has almost no effect on the evolution of the right-handed neutrino number density and the lepton asymmetry. Taking the full energy dependence of interactions into account changes the final efficiency factor by 5% at the most.

Including all quantum statistical factors has somewhat larger effects. These factors tend to enlarge the phase space available for neutrino production by inverse decays, thus significantly boosting the right-handed neutrino abundance and the "wrong-sign" asymmetry being produced at high temperatures. Further, they lead to an earlier domination of decays over inverse decays, thus speeding up the production of the final asymmetry. In the weak wash-out regime this leaves more time for the production of an asymmetry, thus leading to a boost in the final asymmetry by $\sim$50%.

In the strong wash-out regime, on the other hand, the final asymmetry is suppressed by between 20% at $K = 10$ and 1% at $K = 100$. This is again due to the enlarged phase space of inverse decay processes which act as wash-out terms, thus reducing the asymmetry compared to the case where quantum statistical factors are neglected.

In the case of scatterings of right-handed neutrinos off quarks, considered in Chapter 4, in contrast to decays and inverse decays, quantum statistical factors reduce the phase space available, since all external particles in these processes are fermions. Hence, quantum effects generally tend to reduce the importance of these scatterings.

Nonetheless, at high temperatures ($z < 1$) scattering processes increase the amount of right-handed neutrinos being produced, thus making leptogenesis more efficient. On the other hand, at low temperatures ($z > 1$) they act as wash-out terms thereby reducing the produced asymmetry. The first effect, i.e., the more efficient production of right-handed neutrinos dominates in the weak wash-out regime, thus leading to a larger final lepton asymmetry compared to the case where only decays and inverse decays are included. In the strong wash-out regime the effect from increased wash-out dominates, i.e., including scatterings leads to a somewhat reduced asymmetry here.

This is qualitatively in line with results obtained in the integrated picture, i.e., neglecting quantum statistical factors and assuming kinetic equilibrium. However, since quantum statistical factor enhance decays and inverse decays while suppressing scatterings of right-handed neutrinos with quarks, the net influence of these scattering processes is reduced when quantum factors are included. This significantly reduces the spread of results for the final efficiency factor, particularly in the weak wash-out regime.

In general, when including scattering processes of right-handed neutrinos with quarks, it is important to account for the evolution of the top Yukawa coupling from the electroweak scale to the scale of baryogenesis. This energy dependence might change the coupling strength by a factor ~ 2, which, in turn, changes the final asymmetry by

a factor ~ 3. However, changing the right-handed neutrino mass, which determines the precise energy scale of baryogenesis, by up to four orders of magnitude leads only to minor ($< 15\%$) changes in the final asymmetry.

Finally, in Chapter 5, we studied leptogenesis in an alternative scenario in which the lepton asymmetry is created in the decays of the next-to-lightest right-handed neutrino state N_2. Here, the additional wash-out present in the complete set of mode equations leads to a more efficient depletion of the lepton asymmetry in interactions of the lightest right-handed neutrino N_1; these interactions follow the asymmetry generation in the decays of the heavier state. In order to account for the observed value of the matter-antimatter asymmetry, the possible values of the decay parameters K_1 and K_2 of the two right-handed states can be restricted. From the maximal amount of asymmetry that is achievable in N_2 decays, the decay parameter of the lightest right-handed neutrino is forced to $K_1 \lesssim 5$. Furthermore, demanding the decay parameter K_2 to be in the strong wash-out regime favored by neutrino oscillation data, where the asymmetry generation is independent of the initial conditions on N_2, sets the more stringent limit $K_1 \lesssim 2$.

Appendix A

Scattering reaction rates in the integrated approach

In this section we derive the integrated Boltzmann equation for a heavy particle species Ψ interacting via the scattering process $\Psi + a \leftrightarrow b + c$ with light degrees of freedom that are supposed to be in thermal equilibrium. The Boltzmann equation for the distribution function in the radiation dominated epoch is given as (cf. Eq. (3.15))

$$\frac{H(m_\Psi)}{z} \frac{\partial f_\Psi}{\partial z} = C[f_\Psi], \tag{A.1}$$

where $z = m_\Psi/T$ and

$$C[f_\Psi] = \frac{1}{2E_\Psi} \int \prod_{i=a,b,c} \frac{dp_i^3}{(2\pi)^3 2E_i} (2\pi)^4 \delta^4(p_\Psi + p_a - p_b - p_c) \left| \mathcal{M}(\Psi + a \leftrightarrow b + c) \right|^2$$
$$\times \left[(1 \pm f_\Psi)(1 \pm f_a) f_b f_c - f_\Psi f_a (1 \pm f_b)(1 \pm f_c) \right]. \tag{A.2}$$

Here the '+' sign corresponds to bosonic and the '-' sign to fermionic type of particles. In order to receive the Boltzmann equation for the number density, an integration of Eq. (A.1) over the phase space of the particle Ψ has to be performed. For this purpose it proves useful to introduce the reaction density, which is defined as the number of reactions per time and volume element. The reaction density for the process $\Psi + a \rightarrow b + c$, then reads [1]

$$\gamma(\Psi + a \rightarrow b + c) = \int \prod_{i=\Psi,a,b,c} \frac{dp_i^3}{(2\pi)^3 2E_i} (2\pi)^4 \delta^4(p_\Psi + p_a - p_b - p_c)$$
$$\times \left| \mathcal{M}(\Psi + a \rightarrow b + c) \right|^2 f_\Psi f_a. \tag{A.3}$$

---

[1]Since here $|\mathcal{M}|^2$ is summed over all internal degrees of freedom, the factor g_Ψ is included in the definition (A.2).

Here, we already neglected phase space factors stemming from Pauli blocking and Bose emission, assuming $(1 \pm f_i) \approx 1$. The reaction density for the inverse process can analogously be recast by the replacements $f_\Psi f_a \to f_b f_c$. Assuming kinetic equilibrium for the heavy species Ψ, the reaction density can be written in terms of the equilibrium reaction density and the heavy particle's number density, $\gamma = n_\Psi / n_\Psi^{\text{eq}} \, \gamma^{\text{eq}}$, with

$$
\begin{aligned}
\gamma^{\text{eq}} \left(\Psi + a \to b + c \right) &= \int \prod_{i = \Psi, a, b, c} \frac{dp_i^3}{(2\pi)^3 2E_i} (2\pi)^4 \delta^4 \left(p_\Psi + p_a - p_b - p_c \right) \\
&\quad \times \left| \mathcal{M} \left(\Psi + a \to b + c \right) \right|^2 f_\Psi^{\text{eq}} f_a^{\text{eq}} \\
&= \int \prod_{i = \Psi, a} \frac{dp_i^3}{(2\pi)^3 2E_i} f_\Psi^{\text{eq}} f_a^{\text{eq}} \, 4 \sqrt{\left(p_\Psi \cdot p_a \right)^2 - m_\Psi^2 m_a^2} \, \sigma(s),
\end{aligned}
$$
(A.4)

where $s = (p_\Psi + p_a)^2$ and the zero temperature cross-section is denoted by $\sigma(s)$. For the flux-factor one can write [148]

$$
\begin{aligned}
4 \sqrt{\left(p_\Psi \cdot p_a \right)^2 - m_\Psi^2 \, m_a^2} &= 2 \sqrt{\left(s - (m_\Psi + m_a)^2 \right) \left(s - (m_\Psi - m_a)^2 \right)} \\
&= 2 \sqrt{\lambda \left(s, m_\Psi^2, m_a^2 \right)}.
\end{aligned}
$$
(A.5)

With the help of the flux factor and the auxiliary variable $s = Q^2$, we can write for the equilibrium reaction density [149]

$$
\begin{aligned}
\gamma^{\text{eq}} \left(\Psi + a \to b + c \right) &= \int \prod_{i = \Psi, a} \frac{dp_i^3}{(2\pi)^3 2E_i} \, e^{-(E_\Psi + E_a)/T} \, 2 \sqrt{\lambda \left(s, m_\Psi^2, m_a^2 \right)} \, \sigma(s) \\
&= \int \frac{d^4 Q}{(2\pi)^4} (2\pi)^4 \, \delta \left(Q - p_\Psi - p_a \right) \Theta \left(s - (m_\Psi + m_a)^2 \right) \\
&\quad \times \int \prod_{i = \Psi, a} \frac{dp_i^3}{(2\pi)^3 2E_i} \, e^{-(E_\Psi + E_a)/T} \, 2 \sqrt{\lambda \left(s, m_\Psi^2, m_a^2 \right)} \, \sigma(s) \\
&= \int \frac{d^4 Q}{(2\pi)^4} (2\pi)^4 \, \Theta \left(s - (m_\Psi + m_a)^2 \right) \\
&\quad \times e^{-Q_0/T} \, 2 \sqrt{\lambda \left(s, m_\Psi^2, m_a^2 \right)} \, \sigma(s) \, \Phi(s).
\end{aligned}
$$
(A.6)

Here we introduced the phase space volume element $\Phi(s)$ that is accessible for particles in the entrance channel,

$$
\begin{aligned}
\Phi(s) &= \int \prod_{i = \psi, a} \frac{dp_i^3}{(2\pi)^3 2E_i} \, (2\pi)^4 \, \delta \left(Q - p_\Psi - p_a \right) \quad\quad\quad\quad\quad (A.7) \\
&= \frac{1}{8\pi s} \sqrt{\left(s - (m_\Psi + m_a)^2 \right) \left(s - (m_\Psi - m_a)^2 \right)} = \frac{1}{8\pi s} \sqrt{\lambda \left(s, m_\Psi, m_a^2 \right)}.
\end{aligned}
$$

With the help of $\Phi(s)$, the cross-section $\sigma(s)$ can be related to the reduced cross-section

$$\hat{\sigma}(s) = 8\pi\,\Phi(s)\int\prod_{i=b,c}\frac{dp_i^3}{(2\pi)^3 2E_i}\,(2\pi)^4\,\delta\left(p_\Psi + p_a - p_b - p_c\right)\left|\mathcal{M}\left(\Psi + a \to b + c\right)\right|^2$$

$$= 8\pi\,\Phi(s)\,2\sqrt{\lambda\left(s, m_\Psi^2, m_a^2\right)}\,\sigma(s) = \frac{2\lambda\left(s, m_\Psi^2, m_a^2\right)}{s}\,\sigma(s). \tag{A.8}$$

Thus one finds, after introducing another auxiliary variable $\zeta = \sqrt{1 + \mathbf{Q}^2/s}$, for the equilibrium reaction density the 1-dimensional integral

$$\gamma^{\mathrm{eq}}\left(\Psi + a \to b + c\right) = \frac{1}{8\pi}\int\frac{d^4 Q}{(2\pi)^4}\,\Theta\left(s - (m_\Psi + m_a)^2\right)e^{-Q_0/T}\,\hat{\sigma}(s)$$

$$= \frac{1}{64\pi^4}\int\limits_{(m_\Psi + m_a)^2}^{\infty}ds\,\hat{\sigma}(s)\,s\int\limits_{1}^{\infty}d\zeta\,\sqrt{\zeta^2 - 1}\,e^{-\zeta\sqrt{s}/T} \tag{A.9}$$

$$= \frac{T^4}{64\pi^4}\int\limits_{(m_\Psi^2 + m_a^2)/T}^{\infty}d\Psi\,\hat{\sigma}(\Psi)\,\sqrt{\Psi}\,K_1\left(\sqrt{\Psi}\right) = \frac{T^4}{64\pi^4}\,\mathcal{I},$$

where $\Psi = s/T^2$ and $\mathcal{I}$ contains the integral expression. Eq. (A.9) is valid also for the inverse process $b + c \to \Psi + a$ because there is no preferred direction in thermal equilibrium. Furthermore, the reaction density for the inverse process is as well given by Eq. (A.9), i.e., $\gamma\left(b + c \to \Psi + a\right) = \gamma^{\mathrm{eq}}\left(b + c \to \Psi + a\right)$, since, when integrating over the phase space of the incoming particles in Eq. (A.3), the particle species b and c are assumed to be in thermal equilibrium.

Then the Boltzmann equation for the time evolution of the number density of the particle species Ψ reads

$$\frac{dn_\Psi}{dz} = \frac{z}{H(m_\Psi)}\left(\frac{n_\Psi}{n_\Psi^{\mathrm{eq}}}\gamma^{\mathrm{eq}} - \gamma^{\mathrm{eq}}\right) = \frac{z}{H(m_\Psi)}\frac{\gamma^{\mathrm{eq}}}{n_\Psi^{\mathrm{eq}}}\left(n_\Psi - n_\Psi^{\mathrm{eq}}\right)$$

$$= \frac{z}{H(m_\Psi)}\Gamma^{\mathrm{eq}}\left(n_\Psi - n_\Psi^{\mathrm{eq}}\right) = \frac{\Gamma^{\mathrm{eq}}}{Hz}\left(n_\Psi - n_\Psi^{\mathrm{eq}}\right), \tag{A.10}$$

where we used the relations $\Gamma = \gamma/n_\Psi$ to relate the reaction density to the reaction rate and $H(m_\Psi) = H/z^2$. The Boltzmann equation for the comoving number density N_Ψ can be recast dividing Eq. (A.10) by the equilibrium photon number density.

Appendix B

Reduction of the scattering collision integrals

B.1 s-channel

B.1.1 Right-handed neutrino

The full collision term for the s-channel in Eq. (4.1) is

$$C_{S,s}[f_N] = \frac{1}{2E_N} \int \prod_{i=l,q,t} \frac{d^3 p_i}{(2\pi)^3 2E_i} (2\pi)^4 \delta^4(p_N + p_l - p_t - p_q) |\mathcal{M}_s|^2 \, \Lambda_s^{(N)} (f_N, f_l, f_t, f_q),$$

(B.1)

with phase space factor $\Lambda_s^{(N)}$ given by

$$\Lambda_s^{(N)} (f_N, f_l, f_t, f_q) = [(1 - f_N)(1 - f_l)f_t f_q - f_N f_l (1 - f_t)(1 - f_q)].$$
(B.2)

The matrix element $\mathcal{M}_s$ is summed over all internal degrees of freedom of the particles in the initial and final states, including color and isospin, and is given by

$$|\mathcal{M}_s|^2 = 24 \, h_t^2 \frac{M \tilde{m}_1}{v^2} \frac{p_N p_l \, p_t p_q}{s^2},$$
(B.3)

where $\tilde{m}_1 = \left(m_D^\dagger m_D \right) / M$ is the effective neutrino mass [89], $v = 174$ GeV the vacuum expectation value of the Higgs field and h_t^2 the top Yukawa coupling given in Appendix C.

We work in the center-of-mass frame, i.e.,

$$\mathbf{p}_N + \mathbf{p}_l = \mathbf{p}_t + \mathbf{p}_q \equiv \mathbf{q}.$$
(B.4)

In general, the 4-vector delta function can dealt with using the relation

$$\delta\left(p_i^2 - M_i^2\right) = \delta\left(E_i^2 - \left(|\mathbf{p}_i|^2 + M_i^2\right)\right)$$

$$= \left(\frac{\delta\left(E_i - \sqrt{|\mathbf{p}_i|^2 + M_i^2}\right)}{2\sqrt{|\mathbf{p}_i|^2 + M_i^2}} + \frac{\delta\left(E_i + \sqrt{|\mathbf{p}_i|^2 + M_i^2}\right)}{2\sqrt{|\mathbf{p}_i|^2 + M_i^2}}\right). \quad \text{(B.5)}$$

Using this relation, and the fact that we consider all particles except the RHN to be massless, i.e.,

$$\begin{aligned}
E_{l,t,q} &= |\mathbf{p}_{l,t,q}|, \\
E_N &= \sqrt{|\mathbf{p}_N|^2 + M^2},
\end{aligned} \quad \text{(B.6)}$$

we can integrate over the quark energy,

$$\begin{aligned}
\int \frac{d^3 p_q}{2E_q} \delta^4(p_N + p_l - p_t - p_q) &= \int dE_q \, d^3 p_q \, \frac{\delta\left(E_q - |\mathbf{p}_q|\right)}{2|\mathbf{p}_q|} \Theta(E_q) \delta(E_N + E_l - E_t - E_q) \\
&\quad \times \delta^3\left(\mathbf{p}_N + \mathbf{p}_l - \mathbf{p}_t - \mathbf{p}_q\right) \\
&= \frac{\delta\left(E_N + E_l - E_t - |\mathbf{p}_N + \mathbf{p}_l - \mathbf{p}_t|\right)}{2\left|\mathbf{p}_N + \mathbf{p}_l - \mathbf{p}_t\right|} \Theta(E_N + E_l - E_t) \\
&= \frac{\delta\left(E_N + E_l - E_t - |\mathbf{q} - \mathbf{p}_t|\right)}{2\left|\mathbf{q} - \mathbf{p}_t\right|} \Theta(E_N + E_l - E_t) \\
&= \delta\left((E_N + E_l - E_t)^2 - |\mathbf{q} - \mathbf{p}_t|^2\right) \Theta(E_N + E_l - E_t).
\end{aligned} \quad \text{(B.7)}$$

Similarly, we can rewrite

$$\begin{aligned}
\frac{d^3 p_l}{2E_l} &= \int dE_l \, \frac{\delta\left(E_l - |\mathbf{p}_l|\right)}{2|\mathbf{p}_l|} \Theta(E_l) \, d^3 p_l \\
&= \int dE_l \, \delta\left(E_l^2 - |\mathbf{p}_l|^2\right) \Theta(E_l) \, d^3 p_l \\
&= \int dE_l \, \delta\left(E_l^2 - |\mathbf{q} - \mathbf{p}_N|^2\right) \Theta(E_l) \, d^3 q,
\end{aligned} \quad \text{(B.8)}$$

where the last equality follows from changing the variable from $\mathbf{p}_l$ to $\mathbf{q} = \mathbf{p}_N + \mathbf{p}_l$, and hence $d^3 p_l$ to $d^3 q$, and the integration is over the lepton energy E_l.

We choose an explicit coordinate system,

$$\begin{aligned}
\mathbf{q} &= |\mathbf{q}|\,(0, 0, 1), \\
\mathbf{p}_N &= |\mathbf{p}_N|\,(0, \sin\eta, \cos\eta), \\
\mathbf{p}_t &= E_t(\cos\phi\,\sin\vartheta, \sin\phi\,\sin\vartheta, \cos\vartheta),
\end{aligned} \quad \text{(B.9)}$$

and obtain the following quantities:

$$s = (p_N + p_l)^2 = (p_t + p_q)^2 = (E_N + E_l)^2 - |\mathbf{q}|^2,$$

$$p_N p_l = \frac{s - M^2}{2},$$

$$p_q p_t = \frac{s}{2}, \tag{B.10}$$

$$|\mathbf{q} - \mathbf{p}_t|^2 = |\mathbf{q}|^2 + |\mathbf{p}_t|^2 - 2\mathbf{q} \cdot \mathbf{p}_t = |\mathbf{q}|^2 + E_t^2 - 2|\mathbf{q}| E_t \cos \vartheta,$$

$$|\mathbf{q} - \mathbf{p}_N|^2 = |\mathbf{q}|^2 + |\mathbf{p}_N|^2 - 2\mathbf{q} \cdot \mathbf{p}_N = |\mathbf{q}|^2 + |\mathbf{p}_N|^2 - 2|\mathbf{q}| |\mathbf{p}_N| \cos \eta.$$

The matrix element in these coordinates reads

$$|\mathcal{M}_s|^2 = 6 h_t^2 \frac{M \tilde{m}_1}{v^2} \frac{(E_N + E_l)^2 - M^2 - |\mathbf{q}|^2}{(E_N + E_l)^2 - |\mathbf{q}|^2}, \tag{B.11}$$

and the delta functions are given by

$$\delta\left((E_N + E_l - E_t)^2 - |\mathbf{q} - \mathbf{p}_t|^2\right) = \delta\left((E_N + E_l - E_t)^2 - |\mathbf{q}|^2 - E_t^2 + 2|\mathbf{q}| E_t \cos \vartheta\right)$$

$$= \frac{1}{2|\mathbf{q}| E_t} \delta\left(\cos \vartheta - \frac{E_t^2 - (E_N + E_l - E_t)^2 + |\mathbf{q}|^2}{2|\mathbf{q}| E_t}\right),$$

$$\delta\left(E_l^2 - |\mathbf{q} - \mathbf{p}_N|^2\right) = \delta\left(E_l^2 - |\mathbf{q}|^2 - |\mathbf{p}_N|^2 + 2|\mathbf{q}||\mathbf{p}_N| \cos \eta\right)$$

$$= \frac{1}{2|\mathbf{q}||\mathbf{p}_N|} \delta\left(\cos \eta - \frac{|\mathbf{p}_N|^2 - E_l^2 + |\mathbf{q}|^2}{2|\mathbf{q}| |\mathbf{p}_N|}\right). \tag{B.12}$$

Collecting all terms, we get for the collision integral

$$C_{S,s}[f_N] = \frac{1}{2 E_N (2\pi)^5} \int \frac{d\Omega_N}{4\pi} d\cos \vartheta \, d\phi \, \frac{E_t^2}{2 E_t} dE_t \, dE_l \, d^3q \, \frac{1}{2|\mathbf{q}| |\mathbf{p}_N|} \frac{1}{2|\mathbf{q}| E_t} |\mathcal{M}_s|^2$$

$$\times \delta\left(\cos \eta - \frac{|\mathbf{p}_N|^2 - E_l^2 + |\mathbf{q}|^2}{2|\mathbf{q}| |\mathbf{p}_N|}\right) \delta\left(\cos \vartheta - \frac{E_t^2 - (E_l + E_N - E_t)^2 + |\mathbf{q}|^2}{2|\mathbf{q}| E_t}\right)$$

$$\times \Lambda_s^{(N)}(f_N, f_l, f_t, f_q) \, \Theta(E_l) \, \Theta(E_t) \, \Theta(E_l + E_N - E_t)$$

$$= \frac{1}{2^7 \pi^3} \frac{1}{E_N |\mathbf{p}_N|} \int d\cos \vartheta \, d\cos \eta \, dE_t \, dE_l \, d|\mathbf{q}| \, |\mathcal{M}_s|^2$$

$$\times \delta\left(\cos \eta - \frac{|\mathbf{p}_N|^2 - E_l^2 + |\mathbf{q}|^2}{2|\mathbf{q}| |\mathbf{p}_N|}\right) \delta\left(\cos \vartheta - \frac{E_t^2 - (E_l + E_N - E_t)^2 + |\mathbf{q}|^2}{2|\mathbf{q}| E_t}\right)$$

$$\times \Lambda_s^{(N)}(f_N, f_l, f_t, f_q) \, \Theta(E_l) \, \Theta(E_t) \, \Theta(E_l + E_N - E_t). \tag{B.13}$$

Here, in the first equality, we take $d^3 p_t = E_t^2 dE_t \, d\cos \vartheta \, d\phi$, and average over the direction of the incoming RHN by integrating over $d\Omega_N/(4\pi)$, where $d\Omega_N = d\theta \, d\cos \eta$,

because of rotational invariance (cf. Eq (B.9)). In the second equality, we take $d^3q = 4\pi |\mathbf{q}|^2 d|\mathbf{q}|$, and integrate over all azimuthal angles.

The two remaining angles ϑ and η run in the range

$$\cos \vartheta, \cos \eta \in [-1, 1]. \tag{B.14}$$

Since apart from the delta functions the integrand does not depend on either angle, integrating over these ranges effectively lead to new integration limits for the q-integral:

$$\begin{aligned}
\cos \vartheta = 1 &\quad\Rightarrow\quad q \in [E_l + E_N, -E_l - E_N + 2E_t], \\
\cos \vartheta = -1 &\quad\Rightarrow\quad q \in [-E_l - E_N, E_l + E_N - 2E_t], \\
\cos \eta = 1 &\quad\Rightarrow\quad q \in [-E_l + p_N, E_l + p_N], \\
\cos \eta = -1 &\quad\Rightarrow\quad q \in [-E_l - p_N, E_l - p_N],
\end{aligned} \tag{B.15}$$

where $p_N \equiv |\mathbf{p}_N|$, and $q \equiv |\mathbf{q}|$. Putting these conditions together we get

$$\sup\left[|2E_t - E_l - E_N|, |E_l - p_N|\right] \leq q \leq \inf\left[E_l + E_N, E_l + p_N\right]. \tag{B.16}$$

Since $E_l + E_N > E_l + p_N$ this reduces to

$$\sup\left[|2E_t - E_l - E_N|, |E_l - p_N|\right] \leq q \leq E_l + p_N. \tag{B.17}$$

Thus, the integration over $\cos \eta$ and $\cos \vartheta$ effectively gives rise to a combination of Θ functions in the remaining 3-dimensional integral. Together with existing Θ functions in Eq. (B.13), we define

$$\Omega \equiv \Theta\left(q - |2E_t - E_l - E_N|\right)\ \Theta\left(q - |E_l - p_N|\right)\ \Theta\left(E_l + p_N - q\right) \Theta(E_l + E_N - E_t) \tag{B.18}$$

to collectively denote all Θ functions appearing in the remaining integral. Note that we have omitted writing out $\Theta(E_l)\Theta(E_t)$, since positive particle energies are understood.

Next, we use the relations

$$\Theta\left(q - |2E_t - E_l - E_N|\right) = 1 - \Theta\left(|2E_t - E_l - E_N| - q\right), \tag{B.19}$$

and

$$\Theta\left(|2E_t - E_l - E_N| - q\right)\ \Theta\left(E_l + p_N - q\right) = \Theta\left(|2E_t - E_l - E_N| - q\right), \tag{B.20}$$

the latter following from the fact that Ω in Eq. (B.18) vanishes unless $|2E_t - E_l - E_N| < E_l + p_N$. With these we split the function Ω into two parts (i.e., $\Omega = \Omega_1 + \Omega_2$):

$$\Omega_1 = \Theta(E_l + E_N - E_t)\ \Theta\left(q - |E_l - p_N|\right)\ \Theta\left(E_l + p_N - q\right), \tag{B.21}$$

$$\Omega_2 = -\ \Theta(E_l + E_N - E_t)\ \Theta\left(q - |E_l - p_N|\right)\ \Theta\left(|2E_t - E_l - E_N| - q\right). \tag{B.22}$$

Equation (B.21) can be further split into two parts at $\Theta\left(q - |E_l - p_N|\right)$ using the relation

$$\Theta\left(E_l - p_N\right) + \Theta\left(p_N - E_l\right) = 1, \tag{B.23}$$

from which we find

$$\Omega_{1a} = \Theta(E_l + E_N - E_t)\ \Theta\left(q - (E_l - p_N)\right)\ \Theta\left(E_l + p_N - q\right)\ \Theta\left(E_l - p_N\right), \tag{B.24}$$

$$\Omega_{1b} = \Theta(E_l + E_N - E_t)\ \Theta\left(q - (p_N - E_l)\right)\ \Theta\left(E_l + p_N - q\right)\ \Theta\left(p_N - E_l\right), \tag{B.25}$$

so that $\Omega_1 = \Omega_{1a} + \Omega_{1b}$.

Similarly, Eq. (B.22) can be split at $\Theta\left(q - |E_l - p_N|\right)$ into two parts, $\Omega_2 = \Omega_{2a} + \Omega_{2b}$, by way of the relation (B.23):

$$\Omega_{2a} = -\ \Theta(E_l + E_N - E_t)\ \Theta\left(q - (E_l - p_N)\right) \Theta\left(|2E_t - E_l - E_N| - q\right)\ \Theta\left(E_l - p_N\right), \tag{B.26}$$

$$\Omega_{2b} = -\ \Theta(E_l + E_N - E_t)\ \Theta\left(q - (p_N - E_l)\right)\ \Theta\left(|2E_t - E_l - E_N| - q\right)\ \Theta\left(p_N - E_l\right). \tag{B.27}$$

One further split is possible at $\Theta\left(|2E_t - E_l - E_N| - q\right)$ using

$$\Theta\left(E_l + E_N - 2E_t\right) + \Theta\left(2E_t - E_l - E_N\right) = 1. \tag{B.28}$$

Putting this relation in Eqs. (B.26) and (B.27), we find the combinations

$$
\begin{aligned}
\Theta\left(q - (E_l - p_N)\right)\ \Theta(E_l + E_N - 2E_t - q) &\Rightarrow E_t \leq \frac{1}{2}\left(E_N + p_N\right), \\
\Theta\left(q - (E_l - p_N)\right)\ \Theta(2E_t - E_l - E_N - q) &\Rightarrow E_t \geq \frac{1}{2}\left(2E_l + (E_N - p_N)\right), \\
\Theta\left(q - (p_N - E_l)\right)\ \Theta(E_l + E_N - 2E_t - q) &\Rightarrow E_t \leq \frac{1}{2}\left(2E_l + (E_N - p_N)\right), \\
\Theta\left(q - (p_N - E_l)\right)\ \Theta(2E_t - E_N - E_l - q) &\Rightarrow E_t \geq \frac{1}{2}\left(E_N + p_N\right),
\end{aligned}
\tag{B.29}
$$

with which we can write down the four parts of Ω_2:

$$
\Omega_{2a,i} = - \Theta \left(\frac{1}{2}(E_N + p_N) - E_t \right) \Theta \left(q - (E_l - p_N) \right) \Theta \left(E_l + E_N - 2E_t - q \right)
$$
$$
\times \Theta(E_l - p_N), \tag{B.30}
$$

$$
\Omega_{2a,ii} = - \Theta(E_l + E_N - E_t) \Theta \left(E_t - \frac{1}{2}(2E_l + E_N - p_N) \right) \Theta \left(2E_t - E_l - E_N - q \right)
$$
$$
\times \Theta \left(q - (E_l - p_N) \right) \Theta(E_l - p_N), \tag{B.31}
$$

$$
\Omega_{2b,i} = - \Theta \left(\frac{1}{2}(2E_l + E_N - p_N) - E_t \right) \Theta \left(E_l + E_N - 2E_t - q \right)
$$
$$
\times \Theta \left(q - (p_N - E_l) \right) \Theta(p_N - E_l), \tag{B.32}
$$

$$
\Omega_{2b,ii} = - \Theta(E_l + E_N - E_t) \Theta \left(E_t - \frac{1}{2}(E_N + p_N) \right) \Theta \left(2E_t - E_l - E_N - q \right)
$$
$$
\times \Theta \left(q - (p_N - E_l) \right) \Theta(p_N - E_l), \tag{B.33}
$$

such that $\Omega_{2a} = \Omega_{2a,i} + \Omega_{2a,ii}$ and $\Omega_{2b} = \Omega_{2b,i} + \Omega_{2b,ii}$.

Finally, collecting all terms we obtain the relation

$$
\Omega = \sum_\mu \Omega_\mu = \Omega_{1a} + \Omega_{1b} + \Omega_{2a,i} + \Omega_{2a,ii} + \Omega_{2b,i} + \Omega_{2b,ii}, \tag{B.34}
$$

so that the remaining 3-dimensional integration in the collision integral (B.13) can be equivalently written as

$$
C_{S,s}[f_N] = \sum_\mu \frac{1}{2^7 \pi^3 E_N |\mathbf{p}_N|} \int dE_t \, dE_l \, dq \, |\mathcal{M}_s|^2 \, \Lambda_s^{(N)} (f_N, f_l, f_t, f_q) \, \Omega_\mu. \tag{B.35}
$$

The phase space factor reads

$$
\Lambda_s^{(N)} (f_N, f_l, f_t, f_q) = - \frac{e^{\mathcal{E}_l + \mathcal{E}_t} \left(-1 + f_N + e^{\mathcal{E}_N} f_N \right)}{\left(1 + e^{\mathcal{E}_l} \right) \left(1 + e^{\mathcal{E}_t} \right) \left(e^{\mathcal{E}_l + \mathcal{E}_N} + e^{\mathcal{E}_t} \right)}, \tag{B.36}
$$

where we have used energy conservation, and Fermi–Dirac statistics for the leptons and quarks.

The integration over q can now be performed analytically, reducing the dimensions of the collision integrals to two. These final integrals must be evaluated numerically and then summed to give $C_{S,s}[f_N]$,

$$
C_{S,s}[f_N] = C_s^{(1)} + C_s^{(2)} + C_s^{(3)} + C_s^{(4)} + C_s^{(5)} + C_s^{(6)}. \tag{B.37}
$$

The integrals $C_{S,s}^{(1,\ldots,6)}$ are as follows:

- The first integral comes from evaluating the Θ function Ω_{1a}, and we have defined $\tilde{q} \equiv q/T$:

$$C_{S,s}^{(1)} = \frac{3\,T}{2^6\,\pi^3\,\mathcal{E}_N\,y_N}\,\frac{h_t^2\,M\,\tilde{m}_1}{v^2}\int_{y_N}^{\infty}d\mathcal{E}_l\int_0^{\mathcal{E}_l+\mathcal{E}_N}d\mathcal{E}_t\,\Lambda_s^{(N)}\,I_s^{(1)}, \qquad \text{(B.38)}$$

$$\begin{aligned}
I_s^{(1)} &= \int_{\mathcal{E}_l-y_N}^{\mathcal{E}_l+y_N}d\tilde{q}\,\frac{(\mathcal{E}_N+\mathcal{E}_l)^2-z^2-\tilde{q}^2}{(\mathcal{E}_N+\mathcal{E}_l)^2-\tilde{q}^2} \\
&= \frac{4\,y_N\,(\mathcal{E}_l+\mathcal{E}_N)+z^2\,\log\left[\frac{(\mathcal{E}_N-y_N)\,(2\mathcal{E}_l+\mathcal{E}_N-y_N)}{(\mathcal{E}_N+y_N)\,(2\mathcal{E}_l+\mathcal{E}_N+y_N)}\right]}{2\,(\mathcal{E}_l+\mathcal{E}_N)}.
\end{aligned} \qquad \text{(B.39)}$$

- The second integral comes from evaluation of Ω_{1b}:

$$C_{S,s}^{(2)} = \frac{3\,T}{2^6\,\pi^3\,\mathcal{E}_N\,y_N}\,\frac{h_t^2\,M\,\tilde{m}_1}{v^2}\int_0^{y_N}d\mathcal{E}_l\int_0^{\mathcal{E}_l+\mathcal{E}_N}d\mathcal{E}_t\,\Lambda_s^{(N)}\,I_s^{(2)}, \qquad \text{(B.40)}$$

$$\begin{aligned}
I_s^{(2)} &= \int_{y_N-\mathcal{E}_l}^{\mathcal{E}_l+y_N}d\tilde{q}\,\frac{(\mathcal{E}_N+\mathcal{E}_l)^2-z^2-\tilde{q}^2}{(\mathcal{E}_N+\mathcal{E}_l)^2-\tilde{q}^2} \\
&= \frac{4\,\mathcal{E}_l\,(\mathcal{E}_l+\mathcal{E}_N)+z^2\,\log\left[\frac{\mathcal{E}_N^2-y_N^2}{(2\mathcal{E}_l+\mathcal{E}_N)^2-y_N^2}\right]}{2\,(\mathcal{E}_l+\mathcal{E}_N)}.
\end{aligned} \qquad \text{(B.41)}$$

- The third integral comes from the $\Omega_{2a,i}$ term:

$$C_{S,s}^{(3)} = \frac{3\,T}{2^6\,\pi^3\,\mathcal{E}_N\,y_N}\,\frac{h_t^2\,M\,\tilde{m}_1}{v^2}\int_{y_N}^{\infty}d\mathcal{E}_l\int_0^{\frac{1}{2}\,(\mathcal{E}_N+y_N)}d\mathcal{E}_t\,\Lambda_s^{(N)}\,I_s^{(3)}, \qquad \text{(B.42)}$$

$$\begin{aligned}
I_s^{(3)} &= -\int_{\mathcal{E}_l-y_N}^{\mathcal{E}_l+\mathcal{E}_N-2\mathcal{E}_t}d\tilde{q}\,\frac{(\mathcal{E}_N+\mathcal{E}_l)^2-z^2-\tilde{q}^2}{(\mathcal{E}_N+\mathcal{E}_l)^2-\tilde{q}^2} \\
&= -\frac{2\,(\mathcal{E}_l+\mathcal{E}_N)\,(\mathcal{E}_N-2\,\mathcal{E}_t+y_N)+z^2\,\log\left[\frac{\mathcal{E}_t\,(2\,\mathcal{E}_l+\mathcal{E}_N-y_N)}{(\mathcal{E}_l+\mathcal{E}_N-\mathcal{E}_t)\,(\mathcal{E}_N+y_N)}\right]}{2\,(\mathcal{E}_l+\mathcal{E}_N)}.
\end{aligned}$$
$$\text{(B.43)}$$

- Integral four originates from the $\Omega_{2a,ii}$ term:

$$C_{S,s}^{(4)} = \frac{3\,T}{2^6\,\pi^3\,\mathcal{E}_N\,y_N}\,\frac{h_t^2\,M\,\tilde{m}_1}{v^2}\int_{y_N}^{\infty}d\mathcal{E}_l\int_{\frac{1}{2}\,(2\,\mathcal{E}_l+\mathcal{E}_N-y_N)}^{\mathcal{E}_l+\mathcal{E}_N}d\mathcal{E}_t\,\Lambda_s^{(N)}\,I_s^{(4)}, \qquad \text{(B.44)}$$

$$\begin{aligned}
I_s^{(4)} &= -\int_{\mathcal{E}_l-y_N}^{2\mathcal{E}_t-\mathcal{E}_l-\mathcal{E}_N}d\tilde{q}\,\frac{(\mathcal{E}_N+\mathcal{E}_l)^2-z^2-\tilde{q}^2}{(\mathcal{E}_N+\mathcal{E}_l)^2-\tilde{q}^2} \\
&= \frac{2\,(\mathcal{E}_l+\mathcal{E}_N)\,(2\,\mathcal{E}_l+\mathcal{E}_N-2\,\mathcal{E}_t-y_N)-z^2\,\log\left[\frac{(\mathcal{E}_l+\mathcal{E}_N-\mathcal{E}_t)\,(2\,\mathcal{E}_l+\mathcal{E}_N-y_N)}{\mathcal{E}_t\,(\mathcal{E}_N+y_N)}\right]}{2\,(\mathcal{E}_l+\mathcal{E}_N)}.
\end{aligned}$$
$$\text{(B.45)}$$

- Integral five relates to $\Omega_{2b,i}$:

$$C_{S,s}^{(5)} = \frac{3\,T}{2^6\,\pi^3\,\mathcal{E}_N\,y_N}\,\frac{h_t^2\,M\,\tilde{m}_1}{v^2}\int_0^{y_N}d\mathcal{E}_l\int_0^{\frac{1}{2}\,(2\,\mathcal{E}_l+\mathcal{E}_N-y_N)}d\mathcal{E}_t\,\Lambda_s^{(N)}\,I_s^{(5)},$$

(B.46)

$$\begin{aligned}
I_s^{(5)} &= -\int_{y_N-\mathcal{E}_l}^{\mathcal{E}_l+\mathcal{E}_N-2\mathcal{E}_t}d\tilde{q}\,\frac{(\mathcal{E}_N+\mathcal{E}_l)^2-z^2-\tilde{q}^2}{(\mathcal{E}_N+\mathcal{E}_l)^2-\tilde{q}^2}\\
&= -\frac{2\,(\mathcal{E}_l+\mathcal{E}_N)\,(2\,\mathcal{E}_l+\mathcal{E}_N-2\,\mathcal{E}_t-y_N)-z^2\,\log\left[\frac{(\mathcal{E}_l+\mathcal{E}_N-\mathcal{E}_t)\,(2\,\mathcal{E}_l+\mathcal{E}_N-y_N)}{\mathcal{E}_t\,(\mathcal{E}_N+y_N)}\right]}{2\,(\mathcal{E}_l+\mathcal{E}_N)}.
\end{aligned}$$

(B.47)

- Finally, the sixth integral derives from $\Omega_{2b,ii}$:

$$C_{S,s}^{(6)} = \frac{3\,T}{2^6\,\pi^3\,\mathcal{E}_N\,y_N}\,\frac{h_t^2\,M\,\tilde{m}_1}{v^2}\int_0^{y_N}d\mathcal{E}_l\int_{\frac{1}{2}\,(\mathcal{E}_N+y_N)}^{\mathcal{E}_l+\mathcal{E}_N}d\mathcal{E}_t\,\Lambda_s^{(N)}\,I_s^{(6)}, \quad\text{(B.48)}$$

$$\begin{aligned}
I_s^{(6)} &= -\int_{y_N-\mathcal{E}_l}^{2\mathcal{E}_t-\mathcal{E}_l-\mathcal{E}_N}d\tilde{q}\,\frac{(\mathcal{E}_N+\mathcal{E}_l)^2-z^2-\tilde{q}^2}{(\mathcal{E}_N+\mathcal{E}_l)^2-\tilde{q}^2}\\
&= \frac{2\,(\mathcal{E}_l+\mathcal{E}_N)\,(\mathcal{E}_N-2\,\mathcal{E}_t+y_N)-z^2\,\log\left[\frac{(\mathcal{E}_l+\mathcal{E}_N-\mathcal{E}_t)\,(\mathcal{E}_N+y_N)}{\mathcal{E}_t\,(2\,\mathcal{E}_l+\mathcal{E}_N-y_N)}\right]}{2\,(\mathcal{E}_l+\mathcal{E}_N)}.
\end{aligned}$$

(B.49)

B.1.2   Lepton asymmetry

The s-channel collision term in Eq. (4.3) for tracking the lepton asymmetry is

$$C_{S,s}[f_{l-\bar{l}}] = \frac{1}{2E_l}\int\prod_{i=N,q,t}\frac{dp_i^3}{(2\pi)^3\,2E_i}(2\pi)^4\delta^4(p_l+p_N-p_q-p_t)|\mathcal{M}_s|^2\Lambda_s^{(l-\bar{l})}\left(f_{l-\bar{l}},f_N,f_t,t_q\right),$$

(B.50)

with phase space factor

$$\Lambda_s^{(l-\bar{l})}\left(f_{l-\bar{l}},f_N,f_t,t_q\right) = f_{l-\bar{l}}\left(f_N\,(f_t+f_q-1)-f_tf_q\right), \quad\text{(B.51)}$$

and matrix element $\mathcal{M}_s$ given by Eq. (B.11). As in Section B.1.2 we work in the center-of-mass frame Eq. (B.4)

$$\mathbf{p}_N+\mathbf{p}_l = \mathbf{p}_t+\mathbf{p}_q \equiv \mathbf{q}. \quad\text{(B.52)}$$

and integrate first over the quark energy E_q as in Eq. (B.7) and rewrite

$$
\begin{aligned}
\frac{d^3 p_N}{2E_N} &= \int dE_N \, \frac{\delta\left(E_N - \sqrt{\mathbf{p}_N^2 + M^2}\right)}{2\sqrt{\mathbf{p}_N^2 + M^2}} \, \Theta(E_N) \, d^3 p_N \\
&= \int dE_N \, \delta\left(E_N - (\mathbf{p}_N^2 + M^2)\right) \, \Theta(E_N) \, d^3 p_N \\
&= \int dE_N \, \delta\left(E_N^2 - |\mathbf{q} - \mathbf{p}_l|^2 - M^2\right) \, \Theta(E_N) \, d^3 q,
\end{aligned}
\tag{B.53}
$$

where the last equality follows from changing the variable from $\mathbf{p}_N$ to $\mathbf{q} = \mathbf{p}_N + \mathbf{p}_l$, and hence $d^3 p_N$ to $d^3 q$, and the integration is over the RHN energy E_N.

Again we choose an explicit coordinate system and use rotational invariance

$$
\begin{aligned}
\mathbf{q} &= |\mathbf{q}| \, (0, 0, 1), \\
\mathbf{p}_l &= E_l \, (0, \sin\eta, \cos\eta), \\
\mathbf{p}_t &= E_t (\cos\phi \, \sin\vartheta, \sin\phi \, \sin\vartheta, \cos\vartheta).
\end{aligned}
\tag{B.54}
$$

In Eq. (B.10) we have the modifications

$$
\begin{aligned}
|\mathbf{q} - \mathbf{p}_t|^2 &= |\mathbf{q}|^2 + |\mathbf{p}_t|^2 - 2\mathbf{q} \cdot \mathbf{p}_t = |\mathbf{q}|^2 + E_t^2 - 2|\mathbf{q}| \, E_t \, \cos\vartheta \\
|\mathbf{q} - \mathbf{p}_l|^2 &= |\mathbf{q}|^2 + |\mathbf{p}_l|^2 - 2\mathbf{q} \cdot \mathbf{p}_l = |\mathbf{q}|^2 + E_l^2 - 2|\mathbf{q}| \, E_l \, \cos\eta.
\end{aligned}
\tag{B.55}
$$

The matrix element in theses coordinates is still given in Eq. (B.11) and for the delta function in Eq. (B.53) one gets:

$$
\begin{aligned}
\delta\left(E_N^2 - |\mathbf{q} - \mathbf{p}_l|^2 - M^2\right) &= \delta\left(E_N^2 - |\mathbf{q}|^2 - E_l^2 + 2|\mathbf{q}| E_l \, \cos\eta - M^2\right) \\
&= \frac{1}{2|\mathbf{q}| \, E_l} \, \delta\left(\cos\eta - \frac{E_l^2 - E_N^2 + M^2 + |\mathbf{q}|^2}{2|\mathbf{q}| \, E_l}\right).
\end{aligned}
\tag{B.56}
$$

Following the same procedure as in Section B.1.1, we reduce the collision integral (B.50) to

$$
C_{S,s}[f_{l-\bar{l}}] = \frac{1}{2^7 \pi^3 \, E_l^2} \int d\cos\vartheta \, d\cos\eta \, dE_t \, dE_N \, dq \, |\mathcal{M}_s|^2
\tag{B.57}
$$

$$
\times \, \delta\left(\cos\eta - \frac{E_l^2 - E_N^2 + M + |\mathbf{q}|^2}{2|\mathbf{q}|E_l}\right) \delta\left(\cos\vartheta - \frac{E_t^2 - (E_l + E_N - E_t)^2 + |\mathbf{q}|^2}{2|\mathbf{q}|E_t}\right)
$$

$$
\times \, \Lambda_s^{(l-\bar{l})}\left(f_{l-\bar{l}}, f_N, f_t, t_q\right) \Theta\left(E_N\right) \Theta\left(E_t\right) \Theta\left(E_l + E_N - E_t\right),
$$

with phase space element

$$
\Lambda_s^{(l-\bar{l})}\left(f_{l-\bar{l}}, f_N, f_t, t_q\right) = - f_{l-\bar{l}} \, \frac{e^{\mathcal{E}_t} \left(1 + \left(e^{\mathcal{E}_l + \mathcal{E}_N} - 1\right) f_N\right)}{\left(1 + e^{\mathcal{E}_t}\right) \left(e^{\mathcal{E}_l + \mathcal{E}_N} + e^{\mathcal{E}_t}\right)},
\tag{B.58}
$$

using as usual energy conservation, and Fermi–Dirac statistics for the leptons and quarks.

In analogy to Section B.1.1, we further reduce the collision integral (B.57) to a sum of six integrals with distinct integration ranges,

$$C_{S,s}[f_{l-\bar{l}}] = C_{S,s}^{(1)} + C_{S,s}^{(2)} + C_{S,s}^{(3)} + C_{S,s}^{(4)} + C_{S,s}^{(5)} + C_{S,s}^{(6)}, \tag{B.59}$$

to be integrated numerically over two remaining degrees of freedom. To account for the difference to Section B.1.1, we have to replace the integration over dE_l by an integration over dE_N which leads to

$$E_l \geq p_N \Rightarrow E_N \leq \sqrt{E_l^2 + M^2}$$

$$\text{and} \quad E_l \leq p_N \Rightarrow E_N \geq \sqrt{E_l^2 + M^2}. \tag{B.60}$$

The explicit integrals in Eq. (B.59) are:

- First integral

$$C_{S,s}^{(1)} = \frac{3\,T}{2^6 \pi^3\,\mathcal{E}_l^2} \frac{h_t^2\,M\,\tilde{m}_1}{v^2} \int_z^{\sqrt{\mathcal{E}_l^2 + z^2}} d\mathcal{E}_N \int_0^{\mathcal{E}_l + \mathcal{E}_N} d\mathcal{E}_t \, \Lambda_s^{(l-\bar{l})}\, I_s^{(1)}, \tag{B.61}$$

  where $I_s^{(1)}$ is given by Eq. (B.39).

- Second integral with $I_s^{(2)}$ given by Eq. (B.41):

$$C_{S,s}^{(2)} = \frac{3\,T}{2^6 \pi^3\,\mathcal{E}_l^2} \frac{h_t^2\,M\,\tilde{m}_1}{v^2} \int_{\sqrt{\mathcal{E}_l^2 + z^2}}^{\infty} d\mathcal{E}_N \int_0^{\mathcal{E}_l + \mathcal{E}_N} d\mathcal{E}_t \, \Lambda_s^{(l-\bar{l})}\, I_s^{(2)}. \tag{B.62}$$

- Third integral ($I_s^{(3)}$ given by Eq. (B.43)):

$$C_{S,s}^{(3)} = \frac{3\,T}{2^6 \pi^3\,\mathcal{E}_l^2} \frac{h_t^2\,M\,\tilde{m}_1}{v^2} \int_z^{\sqrt{\mathcal{E}_l^2 + z^2}} d\mathcal{E}_N \int_0^{\frac{1}{2}(\mathcal{E}_N + y_N)} d\mathcal{E}_t \, \Lambda_s^{(l-\bar{l})}\, I_s^{(3)}. \tag{B.63}$$

- Fourth integral ($I_s^{(4)}$ given by Eq. (B.45)):

$$C_{S,s}^{(4)} = \frac{3\,T}{2^6 \pi^3\,\mathcal{E}_l^2} \frac{h_t^2\,M\,\tilde{m}_1}{v^2} \int_z^{\sqrt{\mathcal{E}_l^2 + z^2}} d\mathcal{E}_N \int_{\frac{1}{2}(2\mathcal{E}_l + \mathcal{E}_N - y_N)}^{\mathcal{E}_l + \mathcal{E}_N} d\mathcal{E}_t \, \Lambda_s^{(l-\bar{l})}\, I_s^{(4)}. \tag{B.64}$$

- Fifth integral ($I_s^{(5)}$ given by Eq. (B.47)):

$$C_{S,s}^{(5)} = \frac{3\,T}{2^6 \pi^3\,\mathcal{E}_l^2} \frac{h_t^2\,M\,\tilde{m}_1}{v^2} \int_{\sqrt{\mathcal{E}_l^2 + z^2}}^{\infty} d\mathcal{E}_N \int_0^{\frac{1}{2}(2\mathcal{E}_l + \mathcal{E}_N - y_N)} d\mathcal{E}_t \, \Lambda_s^{(l-\bar{l})}\, I_s^{(5)}. \tag{B.65}$$

- sixth integral ($I_s^{(6)}$ given by Eq. (B.49)):

$$C_{S,s}^{(6)} = \frac{3\,T}{2^6 \pi^3\,\mathcal{E}_l^2} \frac{h_t^2\,M\,\tilde{m}_1}{v^2} \int_{\sqrt{\mathcal{E}_l^2 + z^2}}^{\infty} d\mathcal{E}_N \int_{\frac{1}{2}(\mathcal{E}_N + y_N)}^{\mathcal{E}_l + \mathcal{E}_N} d\mathcal{E}_t \, \Lambda_s^{(l-\bar{l})}\, I_s^{(6)}. \tag{B.66}$$

B.2 t-channel

B.2.1   Right-handed neutrino

The collision integral for the t-channel process appearing in Eq. (4.1) is given by

$$C_{S,t}[f_N] = \frac{1}{2E_N} \int \prod_{i=l,q,t} \frac{dp_i^3}{(2\pi)^3 2E_i} (2\pi)^4 \delta^4(p_N + p_q - p_t - p_l) |\mathcal{M}_t|^2 \Lambda_t^{(N)} (f_N, f_q, f_l, f_t),$$

(B.67)

with phase space factor

$$\Lambda_t^{(N)} (f_N, f_q, f_l, f_t) = [(1 - f_N)(1 - f_q)f_t f_l - f_N f_q (1 - f_t)(1 - f_l)], \quad \text{(B.68)}$$

and

$$|\mathcal{M}_t|^2 = 24 \, h_t^2 \frac{M \tilde{m}_1}{v^2} \frac{p_N p_l \, p_q p_t}{t^2}$$

(B.69)

is the matrix element.

The reduction of the collision integral proceeds in the same way as for the analogous s-channel collision integral in Section B.1. We use the momentum

$$\mathbf{k} \equiv \mathbf{p}_N - \mathbf{p}_l = \mathbf{p}_q - \mathbf{p}_t,$$

(B.70)

and integrate over the quark energy,

$$\int \frac{d^3 p_t}{2E_t} \delta^4(p_N + p_q - p_l - p_t) = \int dE_t \, d^3 p_t \frac{\delta(E_t - |\mathbf{p}_t|)}{2|\mathbf{p}_t|} \Theta(E_t) \, \delta(E_N + E_q - E_l - E_t)$$

$$\times \delta^3(\mathbf{p}_N + \mathbf{p}_q - \mathbf{p}_l - \mathbf{p}_t)$$

$$= \frac{\delta(E_N + E_q - E_l - |\mathbf{p}_N + \mathbf{p}_q - \mathbf{p}_l|)}{2|\mathbf{p}_N + \mathbf{p}_q - \mathbf{p}_l|} \Theta(E_N + E_q - E_l)$$

$$= \frac{\delta(E_N + E_q - E_l - |\mathbf{k} + \mathbf{p}_q|)}{2|\mathbf{k} + \mathbf{p}_q|} \Theta(E_N + E_q - E_l)$$

$$= \delta\left((E_N + E_q - E_l)^2 - |\mathbf{k} + \mathbf{p}_q|^2\right) \Theta(E_N + E_q - E_l).$$

(B.71)

Similarly, we can rewrite

$$\frac{d^3 p_l}{2E_l} = \int dE_l \frac{\delta(E_l - |\mathbf{p}_l|)}{2|\mathbf{p}_l|} \Theta(E_l) \, d^3 p_l$$

$$= \int dE_l \, \delta\left(E_l^2 - |\mathbf{p}_l|^2\right) \Theta(E_l) \, d^3 p_l$$

(B.72)

$$= \int dE_l \, \delta\left(E_l^2 - |\mathbf{p}_N - \mathbf{k}|^2\right) \Theta(E_l) \, d^3 k,$$

where the last equality follows from changing the variable from $\mathbf{p}_l$ to $\mathbf{k} = \mathbf{p}_N - \mathbf{p}_l$, and hence $d^3 p_l$ to $d^3 k$, and the integration is over the lepton energy E_l.

As for the s-channel we stick to a specific coordinate system

$$
\begin{aligned}
\mathbf{k} &= |\mathbf{k}|\,(0, 0, 1), \\
\mathbf{p}_q &= E_q\,(0, \sin\eta, \cos\eta), \\
\mathbf{p}_N &= |\mathbf{p}_N|(\cos\phi\,\sin\vartheta, \sin\phi\,\sin\vartheta, \cos\vartheta),
\end{aligned}
\tag{B.73}
$$

and obtain the following quantities:

$$
\begin{aligned}
t = (p_N - p_l)^2 &= (p_q - p_t)^2 = (E_N - E_l)^2 - |\mathbf{k}|^2, \\
p_N p_l &= -\frac{t - M^2}{2}, \\
p_q p_t &= -\frac{t}{2}, \\
|\mathbf{k} + \mathbf{p}_q|^2 = |\mathbf{k}|^2 + |\mathbf{p}_q|^2 + 2\mathbf{k}\cdot\mathbf{p}_q &= |\mathbf{k}|^2 + E_q^2 + 2|\mathbf{k}|\,E_q\,\cos\eta, \\
|\mathbf{k} - \mathbf{p}_N|^2 = |\mathbf{k}|^2 + |\mathbf{p}_N|^2 - 2\mathbf{k}\cdot\mathbf{p}_N &= |\mathbf{k}|^2 + |\mathbf{p}_N|^2 - 2\,|\mathbf{k}|\,|\mathbf{p}_N|\,\cos\vartheta.
\end{aligned}
\tag{B.74}
$$

The matrix element in these coordinates reads

$$
|\mathcal{M}_t|^2 = 6\,h_t^2\,\frac{M\,\tilde{m}_1}{v^2}\,\frac{(E_N - E_l)^2 - M^2 - |\mathbf{k}|^2}{(E_N - E_l)^2 - |\mathbf{k}|^2}.
\tag{B.75}
$$

Averaging over the incoming RHN direction and integrating over all azimuthal angles leads to the following 5-dimensional integral:

$$
\begin{aligned}
C_{S,t}[f_N] = \frac{1}{2^7\,\pi^3\,E_N\,p_N} \int &\; d\cos\vartheta\,d\cos\eta\,dE_q\,dE_l\,d|\mathbf{k}|\,|\mathcal{M}_t|^2 \\
\times\; &\delta\left(\cos\eta - \frac{(E_N + E_q - E_l)^2 - E_q^2 - |\mathbf{k}^2|}{2|\mathbf{k}|\,E_q}\right) \delta\left(\cos\vartheta - \frac{E_l^2 - E_N^2 + M - |\mathbf{k}^2|}{2|\mathbf{k}|\,|\mathbf{p}_N|}\right) \\
\times\; &\Lambda_t^{(N)}\left(f_N, f_q, f_l, f_t\right)\,\Theta\left(E_q\right)\,\Theta\left(E_l\right)\,\Theta\left(E_N + E_q - E_l\right),
\end{aligned}
\tag{B.76}
$$

with

$$
\Lambda_t^{(N)}\left(f_N, f_q, f_l, f_t\right) = -\frac{e^{\mathcal{E}_l + \mathcal{E}_q}\left(-1 + f_N + e^{\mathcal{E}_N}\,f_N\right)}{\left(1 + e^{\mathcal{E}_l}\right)\left(1 + e^{\mathcal{E}_q}\right)\left(e^{\mathcal{E}_l} + e^{\mathcal{E}_l + \mathcal{E}_q}\right)},
\tag{B.77}
$$

assuming thermal equilibrium for the standard model particles.

The two remaining angles ϑ and η run in the range

$$
\cos\vartheta, \cos\eta \in [-1, 1],
\tag{B.78}
$$

and the integrals over $\cos\eta$ and $\cos\vartheta$ in Eq. (B.76) can be readily performed. In the process, integration limits are derived for the integral over $k = |\mathbf{k}|$:

$$
\begin{aligned}
\cos\eta = 1 \quad &\Rightarrow \quad k \in [E_N - E_l, E_l - E_N - 2E_q], \\
\cos\eta = -1 \quad &\Rightarrow \quad k \in [-E_N + E_l, 2E_q + E_N - E_l], \\
\cos\vartheta = 1 \quad &\Rightarrow \quad k \in [-E_l + p_N, E_l + p_N], \\
\cos\vartheta = -1 \quad &\Rightarrow \quad k \in [E_l - p_N, -E_l - p_N],
\end{aligned}
\tag{B.79}
$$

where $p_N \equiv |\mathbf{p}_N|$, and $k \equiv |\mathbf{k}|$. Putting these conditions together we get

$$
\sup\left[|E_N - E_l|, |E_l - p_N|\right] \leq k \leq \inf\left[|2E_q + E_N - E_l|, E_l + p_N\right]. \tag{B.80}
$$

Since

$$
\begin{aligned}
E_t &= E_N + E_q - E_l > 0 \\
&\Rightarrow -E_N - E_q + E_l < 0 \\
&\Rightarrow -E_N - 2E_q + E_l < 0,
\end{aligned}
$$

this reduces to

$$
\sup\left[|E_N - E_l|, |E_l - p_N|\right] \leq k \leq \inf\left[2E_q + E_N - E_l, E_l + p_N\right]. \tag{B.81}
$$

Thus, the integration over $\cos\eta$ and $\cos\vartheta$ effectively gives rise to a combination of Θ functions in the remaining 3-dimensional integral. Together with existing Θ functions in Eq. (B.76), we define

$$
\begin{aligned}
\Omega \equiv \ &\Theta\left(E_N + E_q - E_l\right) \ \Theta\left(2E_l - (E_N - p_N)\right) \ \Theta\left(2E_q + E_N - E_l - |p_N - E_l|\right) \\
&\times \Theta\left(k - |E_N - E_l|\right) \Theta\left(k - |p_N - E_l|\right) \\
&\times \Theta\left(E_l + p_N - k\right) \ \Theta(2E_q + E_N - E_l - k)
\end{aligned}
\tag{B.82}
$$

to collectively denote all Θ functions appearing in the remaining integral. Note that we have omitted writing out $\Theta(E_l)\Theta(E_q)$, since positive particle energies are understood. The functions

$$
\Theta\left(2E_l - (E_N - p_N)\right) \quad \text{and} \quad \Theta\left(2E_q + E_N - E_l - |p_N - E_l|\right)
$$

have been introduced to assure that the upper limit on k is always larger than the lower limit.

Now we use the following relations to eliminate the absolute values

$$
1 = \Theta\left(E_N - E_l\right) + \Theta\left(E_l - E_N\right), \quad 1 = \Theta\left(p_N - E_l\right) + \Theta\left(E_l - p_N\right), \tag{B.83}
$$

and can now write $\Omega = \Omega_1 + \Omega_2 + \Omega_3 + \Omega_4$, with:

$$
\begin{aligned}
\Omega_1 &= \Theta\left(E_N + E_q - E_l\right)\Theta\left(E_N - E_l\right)\Theta\left(p_N - E_l\right)\Theta\left(2E_l - \left(E_N - p_N\right)\right) \\
&\quad \times \Theta\left(2E_q + E_N - E_l - \left(p_N - E_l\right)\right)\Theta\left(E_l + p_N - k\right) \\
&\quad \times \Theta\left(2E_q + E_N - E_l - k\right)\Theta\left(k - \left(E_N - E_l\right)\right)\Theta\left(k - \left(p_N - E_l\right)\right) \\
&= \Theta\left(p_N - E_l\right)\Theta\left(2E_l - \left(E_N - p_N\right)\right)\Theta\left(3p_N - E_N\right) \\
&\quad \times \Theta\left(E_l + p_N - k\right)\Theta\left(2E_q + E_N - E_l - k\right)\Theta\left(k - \left(E_N - E_l\right)\right).
\end{aligned}
$$
(B.84)

At this point we introduced $\Theta\left(3p_N - E_N\right)$ to assure that $2p_N > E_N - p_N$ and used

$$
\Theta\left(E_N - E_l\right)\Theta\left(p_N - E_l\right) = \Theta\left(p_N - E_l\right).
$$

Further we have

$$
\begin{aligned}
\Omega_2 &= \Theta\left(E_N + E_q - E_l\right)\Theta\left(E_N - E_l\right)\Theta\left(E_l - p_N\right)\Theta\left(2E_l - \left(E_N - p_N\right)\right) \\
&\quad \times \Theta\left(2E_q + E_N - E_l - \left(E_l - p_N\right)\right)\Theta\left(E_l + p_N - k\right) \\
&\quad \times \Theta\left(2E_q + E_N - E_l - k\right)\Theta\left(k - \left(E_N - E_l\right)\right)\Theta\left(k - \left(E_l - p_N\right)\right) \\
&= \Theta\left(E_N - E_l\right)\Theta\left(E_l - p_N\right)\Theta\left(2E_l - \left(E_N - p_N\right)\right) \\
&\quad \times \Theta\left(2E_q + E_N - E_l - \left(E_l - p_N\right)\right)\Theta\left(E_l + p_N - k\right) \\
&\quad \times \Theta\left(2E_q + E_N - E_l - k\right)\Theta\left(k - \left(E_N - E_l\right)\right)\Theta\left(k - \left(E_l - p_N\right)\right),
\end{aligned}
$$
(B.85)

$$
\begin{aligned}
\Omega_3 &= \Theta\left(E_N + E_q - E_l\right)\Theta\left(E_l - E_N\right)\Theta\left(p_N - E_l\right)\Theta\left(2E_l - \left(E_N - p_N\right)\right) \\
&\quad \times \Theta\left(2E_q + E_N - E_l - \left(p_N - E_l\right)\right)\Theta\left(E_l + p_N - k\right) \\
&\quad \times \Theta\left(2E_q + E_N - E_l - k\right)\Theta\left(k - \left(E_l - E_N\right)\right)\Theta\left(k - \left(p_N - E_l\right)\right),
\end{aligned}
$$
(B.86)

and

$$
\begin{aligned}
\Omega_4 &= \Theta\left(E_N + E_q - E_l\right)\Theta\left(E_l - E_N\right)\Theta\left(E_l - p_N\right)\Theta\left(2E_l - \left(E_N - p_N\right)\right) \\
&\quad \times \Theta\left(2E_q + E_N - E_l - \left(E_l - p_N\right)\right)\Theta\left(E_l + p_N - k\right) \\
&\quad \times \Theta\left(2E_q + E_N - E_l - k\right)\Theta\left(k - \left(E_l - E_N\right)\right)\Theta\left(k - \left(E_l - p_N\right)\right) \\
&= \Theta\left(E_l - E_N\right)\Theta\left(E_q - \left(E_l - E_N\right)\right)\Theta\left(2E_q - \left(2E_l - E_N - p_N\right)\right) \\
&\quad \times \Theta\left(E_l + p_N - k\right)\Theta\left(2E_q + E_N - E_l - k\right)\Theta\left(k - \left(E_l - p_N\right)\right) \\
&= \Theta\left(E_l - E_N\right)\Theta\left(2E_q - \left(2E_l - E_N - p_N\right)\right)\Theta\left(E_l + p_N - k\right) \\
&\quad \times \Theta\left(2E_q + E_N - E_l - k\right)\Theta\left(k - \left(E_l - p_N\right)\right).
\end{aligned}
$$
(B.87)

Here we used

$$
\Theta\left(E_l - E_N\right)\Theta\left(E_l - p_N\right) = \Theta\left(E_l - E_N\right).
$$

We see instantaneously that Ω_3 gives no contributions since its Θ-functions lead to the wrong condition $E_N < E_l < p_N$.

In Ω_1 to Ω_4 we encounter for the upper limit on k the function

$$\Theta\left(E_l + p_N - k\right) \Theta\left(2E_q + E_N - E_l - k\right).$$

With a short calculation

$$E_l + p_N \lessgtr 2E_q + E_N - E_l$$
$$2E_l - E_N + p_N \lessgtr 2E_q, \tag{B.88}$$

follow the combinations

$$\Theta\left(2E_q + E_N - E_l - k\right) \Theta\left(2E_l - E_N + p_N - 2E_q\right) \tag{B.89}$$

and

$$\Theta\left(E_l + p_N - k\right) \Theta\left(2E_q - \left(2E_l - E_N + p_N\right)\right). \tag{B.90}$$

So we can split the Ω-functions further up:

First Ω_1:

$$\Omega_{1a} = \Theta\left(3p_N - E_N\right) \Theta\left(p_N - E_l\right) \Theta\left(2E_l - \left(E_N - p_N\right)\right) \tag{B.91}$$
$$\times \Theta\left(2E_q - \left(2E_l - E_N + p_N\right)\right) \Theta\left(k - \left(E_N - E_l\right)\right) \Theta\left(E_l + p_N - k\right)$$
$$\Omega_{1b} = \Theta\left(3p_N - E_N\right) \Theta\left(p_N - E_l\right) \Theta\left(2E_l - \left(E_N - p_N\right)\right) \tag{B.92}$$
$$\times \Theta\left(2E_l - E_N + p_N - 2E_q\right) \Theta\left(k - \left(E_N - E_l\right)\right) \Theta\left(2E_q + E_N - E_l - k\right).$$

In Ω_2 the situation is slightly more involved since we have to care about the lower limit on k, finding

$$\Theta\left(k - \left(E_N - E_l\right)\right) \Theta\left(k - \left(E_l - p_N\right)\right) \Theta\left(E_N - E_l\right) \Theta\left(E_l - p_N\right) \tag{B.93}$$
$$= \begin{cases} & \Theta\left(k - \left(E_N - E_l\right)\right) \Theta\left(E_N + p_N - 2E_l\right) \Theta\left(E_l - p_N\right) \\ + & \\ & \Theta\left(k - \left(E_l - p_N\right)\right) \Theta\left(2E_l - \left(E_N + p_N\right)\right) \Theta\left(E_N - E_l\right). \end{cases}$$

Using Eq. (B.93), we split Ω_2 for the lower k-limit into two parts

$$\Omega_{2,i} = \Theta\left(E_N + p_N - 2E_l\right) \Theta\left(E_l - p_N\right) \Theta\left(2E_l - \left(E_N - p_N\right)\right)$$
$$\times \Theta\left(2E_q - \left(2E_l - E_N - p_N\right)\right) \Theta\left(E_l + p_N - k\right) \tag{B.94}$$
$$\times \Theta\left(2E_q + E_N - E_l - k\right) \Theta\left(k - \left(E_N - E_l\right)\right)$$

and

$$
\begin{aligned}
\Omega_{2,ii} = {} & \Theta\left(E_N - E_l\right) \Theta\left(2E_l - \left(E_N + p_N\right)\right) \Theta\left(2E_q - \left(2E_l - E_N - p_N\right)\right) \\
& \times \Theta\left(E_l + p_N - k\right) \Theta\left(2E_q + E_N - E_l - k\right) \Theta\left(k - \left(E_l - p_N\right)\right).
\end{aligned}
\tag{B.95}
$$

In $\Omega_{2,i}$ we encounter

$$
\Theta\left(E_l - p_N\right) \Theta\left(2E_l - \left(E_N - p_N\right)\right),
$$

leading with the conditions $2p_N \lessgtr E_N - p_N$ to the two combinations

$$
\begin{aligned}
\Omega_{2,i}^{I} = {} & \Theta\left(3p_N - E_N\right) \Theta\left(E_l - p_N\right) \Theta\left(E_N + p_N - 2E_l\right) \\
& \times \Theta\left(2E_q - \left(2E_l - E_N - p_N\right)\right) \Theta\left(E_l + p_N - k\right) \\
& \times \Theta\left(2E_q + E_N - E_l - k\right) \Theta\left(k - \left(E_N - E_l\right)\right) \\
= {} & \Theta\left(3p_N - E_N\right) \Theta\left(E_l - p_N\right) \Theta\left(E_N + p_N - 2E_l\right) \\
& \times \Theta\left(E_l + p_N - k\right) \Theta\left(2E_q + E_N - E_l - k\right) \Theta\left(k - \left(E_N - E_l\right)\right)
\end{aligned}
\tag{B.96}
$$

and

$$
\begin{aligned}
\Omega_{2,i}^{II} = {} & \Theta\left(E_N - 3p_N\right) \Theta\left(2E_l - \left(E_N - p_N\right)\right) \Theta\left(E_N + p_N - 2E_l\right) \\
& \times \Theta\left(2E_q - \left(2E_l - E_N - p_N\right)\right) \Theta\left(E_l + p_N - k\right) \\
& \times \Theta\left(2E_q + E_N - E_l - k\right) \Theta\left(k - \left(E_N - E_l\right)\right) \\
= {} & \Theta\left(E_N - 3p_N\right) \Theta\left(2E_l - \left(E_N - p_N\right)\right) \Theta\left(E_N + p_N - 2E_l\right) \\
& \times \Theta\left(E_l + p_N - k\right) \Theta\left(2E_q + E_N - E_l - k\right) \Theta\left(k - \left(E_N - E_l\right)\right).
\end{aligned}
\tag{B.97}
$$

Now we can use Eqs. (B.89) and (B.90) to specify the upper integration limits on k for Ω_2:

$$
\begin{aligned}
\Omega_{2,1a}^{I} = {} & \Theta\left(3p_N - E_N\right) \Theta\left(E_l - p_N\right) \Theta\left(E_N + p_N - 2E_l\right) \\
& \times \Theta\left(2E_q - \left(2E_l - E_N + p_N\right)\right) \Theta\left(k - \left(E_N - E_l\right)\right) \Theta\left(E_l + p_N - k\right) \\
= {} & \Theta\left(3p_N - E_N\right) \Theta\left(E_l - p_N\right) \Theta\left(E_N + p_N - 2E_l\right) \\
& \times \Theta\left(k - \left(E_N - E_l\right)\right) \Theta\left(E_l + p_N - k\right)
\end{aligned}
\tag{B.98}
$$

$$
\begin{aligned}
\Omega_{2,ib}^{I} = {} & \Theta\left(3p_N - E_N\right) \Theta\left(E_l - p_N\right) \Theta\left(E_N + p_N - 2E_l\right) \\
& \times \Theta\left(2E_l - E_N + p_N - 2E_q\right) \Theta\left(k - \left(E_N - E_l\right)\right) \Theta\left(2E_q + E_N - E_l - k\right).
\end{aligned}
\tag{B.99}
$$

and

$$
\begin{aligned}
\Omega_{2,ia}^{II} = {} & \Theta\left(E_N - 3p_N\right) \Theta\left(E_N + p_N - 2E_l\right) \Theta\left(2E_l - \left(E_N - p_N\right)\right) \\
& \times \Theta\left(2E_q - \left(2E_l - E_N + p_N\right)\right) \Theta\left(k - \left(E_N - E_l\right)\right) \Theta\left(E_l + p_N - k\right)
\end{aligned}
\tag{B.100}
$$

$$
\begin{aligned}
\Omega_{2,ib}^{II} = {} & \Theta\left(E_N - 3p_N\right) \Theta\left(E_N + p_N - 2E_l\right) \Theta\left(2E_l - \left(E_N - p_N\right)\right) \\
& \times \Theta\left(2E_l - E_N + p_N - 2E_q\right) \Theta\left(k - \left(E_N - E_l\right)\right) \Theta\left(2E_q + E_N - E_l - k\right).
\end{aligned}
\tag{B.101}
$$

Then with Eqs. (B.89) and (B.90) we split $\Omega_{2,ii}$ to get

$$
\begin{aligned}
\Omega_{2,iia} &= \Theta\left(E_N - E_l\right) \Theta\left(2E_l - (E_N + p_N)\right) \Theta\left(2E_q - (2E_l - E_N + p_N)\right) \\
&\quad \times \Theta\left(2E_q - (2E_l - E_N - p_N)\right) \Theta\left(k - (E_l - p_N)\right) \Theta\left(E_l + p_N - k\right) \\
&= \Theta\left(E_N - E_l\right) \Theta\left(2E_l - (E_N + p_N)\right) \Theta\left(2E_q - (2E_l - E_N + p_N)\right) \\
&\quad \times \Theta\left(k - (E_l - p_N)\right) \Theta\left(E_l + p_N - k\right) \tag{B.102} \\
\Omega_{2,iib} &= \Theta\left(E_N - E_l\right) \Theta\left(2E_l - (E_N + p_N)\right) \Theta\left(2E_l - E_N + p_N - 2E_q\right) \tag{B.103} \\
&\quad \times \Theta\left(2E_q - (2E_l - E_N - p_N)\right) \Theta\left(k - (E_l - p_N)\right) \Theta\left(2E_q + E_N - E_l - k\right).
\end{aligned}
$$

For Ω_4 we use again directly Eqs. (B.89) and (B.90) for specifying the upper limit on k

$$
\begin{aligned}
\Omega_{4a} &= \Theta\left(E_l - E_N\right) \Theta\left(2E_q - (2E_l - E_N - p_N)\right) \tag{B.104} \\
&\quad \times \Theta\left(2E_q - (2E_l - E_N + p_N)\right) \Theta\left(k - (E_l - p_N)\right) \Theta\left(E_l + p_N - k\right) \\
&= \Theta\left(E_l - E_N\right) \Theta\left(2E_q - (2E_l - E_N + p_N)\right) \Theta\left(k - (E_l - p_N)\right) \Theta\left(E_l + p_N - k\right) \\
\Omega_{4b} &= \Theta\left(E_l - E_N\right) \Theta\left(2E_q - (2E_l - E_N - p_N)\right) \Theta\left(2E_l - E_N + p_N - 2E_q\right) \\
&\quad \times \Theta\left(k - (E_l - p_N)\right) \Theta\left(2E_q + E_N - E_l - k\right). \tag{B.105}
\end{aligned}
$$

Several of these equations are equal apart of the limit on E_l, so we can write

$$
\begin{aligned}
\Omega^1 &= \Omega_{1a} + \Omega_{2,ia}^I + \Omega_{2,ia}^{II} \\
&= \Big\{\Theta\left(3p_N - E_N\right) \\
&\qquad \times \left[\Theta\left(p_N - E_l\right) \Theta\left(2E_l - (E_N - p_N)\right) + \Theta\left(E_N + p_N - 2E_l\right) \Theta\left(E_l - p_N\right)\right] \\
&\quad + \Theta\left(E_N - 3p_N\right) \Theta\left(2E_l - (E_N - p_N)\right) \Theta\left(E_N + p_N - 2E_l\right)\Big\} \\
&\quad \times \Theta\left(2E_q - (2E_l - E_N + p_N)\right) \Theta\left(k - (E_N - E_l)\right) \Theta\left(E_l + p_N - k\right) \\
&= \Big\{\Theta\left(3p_N - E_N\right) \Theta\left(2E_l - (E_N - p_N)\right) \Theta\left(E_N + p_N - 2E_l\right) \\
&\quad + \Theta\left(E_N - 3p_N\right) \Theta\left(2E_l - (E_N - p_N)\right) \Theta\left(E_N + p_N - 2E_l\right)\Big\} \\
&\quad \times \Theta\left(2E_q - (2E_l - E_N + p_N)\right) \Theta\left(k - (E_N - E_l)\right) \Theta\left(E_l + p_N - k\right) \\
&= \Theta\left(2E_l - (E_N - p_N)\right) \Theta\left(E_N + p_N - 2E_l\right) \\
&\quad \times \Theta\left(2E_q - (2E_l - E_N + p_N)\right) \Theta\left(k - (E_N - E_l)\right) \Theta\left(E_l + p_N - k\right),
\end{aligned}
$$

$$\Omega^2 = \Omega_{1,b} + \Omega^I_{2,ib} + \Omega^{II}_{2,ib} \tag{B.106}$$

$$= \{\Theta\left(3p_N - E_N\right)$$

$$\times \left[\Theta\left(p_N - E_l\right)\Theta\left(2E_l - \left(E_N - p_N\right)\right) + \Theta\left(E_N + p_N - 2E_l\right)\Theta\left(E_l - p_N\right)\right]$$

$$+ \Theta\left(E_N - 3p_N\right)\Theta\left(2E_l - \left(E_N - p_N\right)\right)\Theta\left(E_N + p_N - 2E_l\right)\}$$

$$\times \Theta\left(2E_l - E_N + p_N - 2E_q\right)\Theta\left(k - \left(E_N - E_l\right)\right)\Theta\left(2E_q + E_N - E_l - k\right)$$

$$= \{\Theta\left(3p_N - E_N\right)\Theta\left(2E_l - \left(E_N - p_N\right)\right)\Theta\left(E_N + p_N - 2E_l\right)$$

$$+ \Theta\left(E_N - 3p_N\right)\Theta\left(2E_l - \left(E_N - p_N\right)\right)\Theta\left(E_N + p_N - 2E_l\right)\}$$

$$\times \Theta\left(2E_l - E_N + p_N - 2E_q\right)\Theta\left(k - \left(E_N - E_l\right)\right)\Theta\left(2E_q + E_N - E_l - k\right)$$

$$= \Theta\left(2E_l - \left(E_N - p_N\right)\right)\Theta\left(E_N + p_N - 2E_l\right)$$

$$\times \Theta\left(2E_l - E_N + p_N - 2E_q\right)\Theta\left(k - \left(E_N - E_l\right)\right)\Theta\left(2E_q + E_N - E_l - k\right),$$

$$\Omega^3 = \Omega_{2,iia} + \Omega_{4a} \tag{B.107}$$

$$= \left[\Theta\left(E_N - E_l\right)\Theta\left(2E_l - \left(E_N + p_N\right)\right) + \Theta\left(E_l - E_N\right)\right]$$

$$\times \Theta\left(2E_q - \left(2E_l - E_N + p_N\right)\right)\Theta\left(k - \left(E_l - p_N\right)\right)\Theta\left(E_l + p_N - k\right)$$

$$= \Theta\left(2E_l - \left(E_N + p_N\right)\right)$$

$$\times \Theta\left(2E_q - \left(2E_l - E_N + p_N\right)\right)\Theta\left(k - \left(E_l - p_N\right)\right)\Theta\left(E_l + p_N - k\right),$$

and finally

$$\Omega^4 = \Omega_{2,iib} + \Omega_{4b} \tag{B.108}$$

$$= \left[\Theta\left(E_N - E_l\right)\Theta\left(2E_l - \left(E_N + p_N\right)\right) + \Theta\left(E_l - E_N\right)\right]$$

$$\times \Theta\left(2E_l - E_N + p_N - 2E_q\right)\Theta\left(2E_q - \left(2E_l - E_N - p_N\right)\right)$$

$$\times \Theta\left(k - \left(E_l - p_N\right)\right)\Theta\left(2E_q + E_N - E_l - k\right)$$

$$= \Theta\left(2E_l - \left(E_N + p_N\right)\right)$$

$$\times \Theta\left(2E_l - E_N + p_N - 2E_q\right)\Theta\left(2E_q - \left(2E_l - E_N - p_N\right)\right)$$

$$\times \Theta\left(k - \left(E_l - p_N\right)\right)\Theta\left(2E_q + E_N - E_l - k\right).$$

Summing all these terms up, we obtain

$$\Omega = \sum_{\mu}\Omega^{\mu} = \Omega^1 + \Omega^2 + \Omega^3 + \Omega^4 \tag{B.109}$$

and the collision integral (B.76) can equivalently be written as

$$C_{S,t}[f_N] = \sum_{\mu}\frac{1}{2^7\pi^3 E_N |\mathbf{p}_N|}\int dE_q\, dE_l\, d|\mathbf{k}|\,|\mathcal{M}_t|^2\,\Lambda\left(f_N, f_q, f_l, f_t\right)\Omega^{\mu}. \tag{B.110}$$

As it turns out, there are two possible lower limits for the k-integration: $k_{\min,1} = E_N - E_l$ and $k_{\min,2} = E_l - p_N$. Here, a comment on the infrared cut-off is in order. In the integrated picture, a divergence occurs in the integral over t at $t = 0$, whose regulation requires the introduction of a Higgs mass in the propagator, i.e., $|\mathcal{M}_t|^2 \propto 1/t \to |\mathcal{M}_t|^2 \propto 1/(t - m_\Phi^2)$. In the full treatment, the matrix element has the form $|\mathcal{M}_t|^2 \propto 1/((E_N - E_l)^2 - |k^2)$, so that the equivalent divergence occurs in the integration over k at $k = E_N - E_l$, i.e., at $k = k_{\min,1}$. This divergence can be avoided simply by modifying by hand the integration limit $\int_{k_{\min,1}} \to \int_{k_{\min,1}+m_\Phi}$. There are no changes for those integrals with $k_{\min} = k_{\min,2}$.

It is also possible to regulate the divergence by introducing a Higgs mass in the propagator, such as in the integrated picture. This modifies the integration over k not only for $E_N > E_l$ (i.e., $k_{\min} = k_{\min,1}$), but also for $E_l > p_N$ (i.e., $k_{\min} = k_{\min,2}$). In physical terms this procedure corresponds to giving the Higgs particle a mass whose magnitude can vary from zero up to possible thermal contributions, i.e., $0 \le m_\Phi/M \lesssim 0.4\,T/M$, where $m_\Phi(T) \sim 0.4\,T$ is the thermal Higgs mass [105]. In the temperature regime relevant to leptogenesis, electroweak symmetry is unbroken and therefore leptons are massless.

Since we have so far not included thermal corrections in the present work, for consistency we prefer not to use the thermal Higgs mass. Furthermore, in a full thermal treatment, RHN decay into a lepton and Higgs pairs become kinematically forbidden at high enough temperatures, and the decay of a Higgs particle into a neutrino and lepton pair becomes viable [105]. Thus, in addition to determining the value of the infrared cut-off there is also the question of its interpretation. In view of these issues, we choose to deal with the infrared divergence using the simpler method of cutting off the integration over k at $k_{\min} = k_{\min,1} + m_\Phi$, with $a_h = m_\Phi/M = 10^{-5}$. In turn one has to add a_h in the corresponding conditions for E_q and E_l, where the changes in $k_{\min,1}$ are propagated.

After integrating over $\cos\eta$ and $\cos\vartheta$, the original integral (B.76) is now split into four parts

$$C_{S,t}[f_N] = C_{S,t}^{(1)} + C_{S,t}^{(2)} + C_{S,t}^{(3)} + C_{S,t}^{(4)}, \tag{B.111}$$

where the constituent integrals are as follows:

- First integral (with $\tilde{k} \equiv k/T$):

$$C_{S,t}^{(1)} = \frac{3\,T}{2^6\,\pi^3\,\mathcal{E}_N\,y_N}\,\frac{h_t^2\,M\,\tilde{m}_1}{v^2}\int_{\frac{1}{2}(\mathcal{E}_N - y_N + a_h z)}^{\frac{1}{2}(\mathcal{E}_N + y_N)} d\mathcal{E}_l \int_{\frac{1}{2}a_h z}^{\frac{1}{2}(2\mathcal{E}_l - \mathcal{E}_N + y_N)} d\mathcal{E}_q\,\Lambda_t^{(N)}\,I_t^{(1)},$$

(B.112)

$$\begin{aligned} I_t^{(1)} &= \int_{\mathcal{E}_N - \mathcal{E}_l + a_h z}^{2\mathcal{E}_q + \mathcal{E}_N - \mathcal{E}_l} d\tilde{k}\,\frac{(\mathcal{E}_N - \mathcal{E}_l)^2 - z^2 - \tilde{k}^2}{(\mathcal{E}_N - \mathcal{E}_l)^2 - \tilde{k}^2} \\ &= \frac{2\,(\mathcal{E}_N - \mathcal{E}_l)\,(2\mathcal{E}_q - a_h z) - z^2\,\log\left[\frac{(\mathcal{E}_N + \mathcal{E}_q - \mathcal{E}_l)\,a_h z}{\mathcal{E}_q(2(\mathcal{E}_N - \mathcal{E}_l) + a_h z)}\right]}{2\,(\mathcal{E}_N - \mathcal{E}_l)}. \end{aligned}$$

- Second integral:

$$C_{S,t}^{(2)} = \frac{3\,T}{2^6\,\pi^3\,\mathcal{E}_N\,y_N}\,\frac{h_t^2\,M\,\tilde{m}_1}{v^2}\int_{\frac{1}{2}(\mathcal{E}_N - y_N + a_h z)}^{\frac{1}{2}(\mathcal{E}_N + y_N)} d\mathcal{E}_l \int_{\frac{1}{2}(2\mathcal{E}_l - \mathcal{E}_N + y_N)}^{\infty} d\mathcal{E}_q\,\Lambda_t^{(N)}\,I_t^{(2)},$$

(B.113)

$$\begin{aligned} I_t^{(2)} &= \int_{\mathcal{E}_N - \mathcal{E}_l + a_h z}^{\mathcal{E}_l + y_N} d\tilde{k}\,\frac{(\mathcal{E}_N - \mathcal{E}_l)^2 - z^2 - \tilde{k}^2}{(\mathcal{E}_N - \mathcal{E}_l)^2 - \tilde{k}^2} \\ &= \frac{2\,(\mathcal{E}_N - \mathcal{E}_l)\,(2\mathcal{E}_l - \mathcal{E}_N + y_N - a_h z) - z^2\,\left(\log\left[\frac{-a_h z\,(\mathcal{E}_N + y_N)}{(\mathcal{E}_N - 2\mathcal{E}_l - y_N)\,(2(\mathcal{E}_N - \mathcal{E}_l) + a_h z)}\right]\right)}{2\,(\mathcal{E}_N - \mathcal{E}_l)}. \end{aligned}$$

- Third integral:

$$C_{S,t}^{(3)} = \frac{3\,T}{2^6\,\pi^3\,\mathcal{E}_N\,y_N}\,\frac{h_t^2\,M\,\tilde{m}_1}{v^2}\int_{\frac{1}{2}(\mathcal{E}_N + y_N)}^{\infty} d\mathcal{E}_l \int_{\frac{1}{2}(2\mathcal{E}_l - \mathcal{E}_N - y_N)}^{\frac{1}{2}(2\mathcal{E}_l - \mathcal{E}_N + y_N)} d\mathcal{E}_q\,\Lambda_t^{(N)}\,I_t^{(3)},$$

(B.114)

$$\begin{aligned} I_t^{(3)} &= \int_{\mathcal{E}_l - y_N}^{2\mathcal{E}_q + \mathcal{E}_N - \mathcal{E}_l} d\tilde{k}\,\frac{(\mathcal{E}_N - \mathcal{E}_l)^2 - z^2 - \tilde{k}^2}{(\mathcal{E}_N - \mathcal{E}_l)^2 - \tilde{k}^2} \\ &= \frac{2\,(\mathcal{E}_N - \mathcal{E}_l)\,(\mathcal{E}_N + y_N + 2\,(\mathcal{E}_q - \mathcal{E}_l)) + z^2\,\left(\log\left[-\frac{-\mathcal{E}_q(\mathcal{E}_N - y_N)}{(\mathcal{E}_N + \mathcal{E}_q - \mathcal{E}_l)\,(\mathcal{E}_N - 2\mathcal{E}_l + y_N)}\right]\right)}{2\,(\mathcal{E}_N - \mathcal{E}_l)}. \end{aligned}$$

- Fourth integral:

$$C_{S,t}^{(4)} = \frac{3\,T}{2^6\,\pi^3\,\mathcal{E}_N\,y_N}\,\frac{h_t^2\,M\,\tilde{m}_1}{v^2}\int_{\frac{1}{2}(\mathcal{E}_N + y_N)}^{\infty} d\mathcal{E}_l \int_{\frac{1}{2}(\mathcal{E}_l - \mathcal{E}_N + y_N)}^{\infty} d\mathcal{E}_q\,\Lambda_t^{(N)}\,I_t^{(4)},$$

(B.115)

$$\begin{aligned} I_t^{(4)} &= \int_{\mathcal{E}_l - y_N}^{\mathcal{E}_l + y_N} d\tilde{k}\,\frac{(\mathcal{E}_N - \mathcal{E}_l)^2 - z^2 - \tilde{k}^2}{(\mathcal{E}_N - \mathcal{E}_l)^2 - \tilde{k}^2} \\ &= \frac{4\,(\mathcal{E}_N - \mathcal{E}_l)\,y_N + z^2\,\log\left[\frac{(\mathcal{E}_N - y_N)\,(\mathcal{E}_N - y_N - 2\mathcal{E}_l)}{(\mathcal{E}_N + y_N)\,(\mathcal{E}_N + y_N - 2\mathcal{E}_l)}\right]}{2\,(\mathcal{E}_N - \mathcal{E}_l)}. \end{aligned}$$

B.2.2 Lepton asymmetry

The t-channel collision integral for the lepton asymmetry evolution is

$$C_{S,t}[f_{l-\bar{l}}] = \frac{1}{2E_l} \int \prod_{i=N,q,t} \frac{dp_i^3}{(2\pi)^3 \, 2E_i} (2\pi)^4 \delta^4(p_l + p_q - p_N - p_t)|\mathcal{M}_t|^2 \Lambda_t^{(l-\bar{l})} \left(f_{l-\bar{l}}, f_t, f_N, f_q\right),$$

(B.116)

with

$$\Lambda_t^{(l-\bar{l})} \left(f_{l-\bar{l}}, f_t, f_N, f_q\right) = f_{l-\bar{l}} \left(f_q \left(f_t + f_N - 1\right) - f_t f_N\right).$$

(B.117)

The matrix element is the same as for the RHN given in Eq. (B.69), and we use the momentum

$$\mathbf{k} \equiv \mathbf{p}_l - \mathbf{p}_N = \mathbf{p}_q - \mathbf{p}_t,$$

(B.118)

and Eq.(B.5) to integrate over the top-energy. We rewrite the integration over now the RHN energy, respectively:

$$\begin{aligned}
\int \frac{d^3 p_t}{2E_t} \, \delta^4(p_l + p_q - p_N - p_t) &= \int dE_t \, d^3 p_t \, \frac{\delta \left(E_t - |\mathbf{p}_t|\right)}{2|\mathbf{p}_t|} \, \Theta(E_t) \, \delta(E_l + E_q - E_N - E_t) \\
&\quad \times \delta^3 \left(\mathbf{p}_l + \mathbf{p}_q - \mathbf{p}_N - \mathbf{p}_t\right) \\
&= \frac{\delta \left(E_l + E_q - E_N - |\mathbf{p}_l + \mathbf{p}_q - \mathbf{p}_N|\right)}{2 \left|\mathbf{p}_l + \mathbf{p}_q - \mathbf{p}_N\right|} \, \Theta(E_l + E_q - E_N) \\
&= \frac{\delta \left(E_l + E_q - E_N - |\mathbf{k} + \mathbf{p}_q|\right)}{2 \left|\mathbf{k} + \mathbf{p}_q\right|} \, \Theta(E_l + E_q - E_N) \\
&= \delta \left((E_l + E_q - E_N)^2 - |\mathbf{k} + \mathbf{p}_q|^2\right) \, \Theta(E_l + E_q - E_N).
\end{aligned}$$

(B.119)

Similarly, we can rewrite

$$\begin{aligned}
\frac{d^3 p_N}{2E_N} &= \int dE_N \, \frac{\delta \left(E_N - \sqrt{|\mathbf{p}_N|^2 + M^2}\right)}{2\sqrt{|\mathbf{p}_N|^2 + M^2}} \Theta(E_N) \, d^3 p_N \\
&= \int dE_N \, \delta \left(E_N^2 - |\mathbf{p}_N|^2 - M^2\right) \, \Theta(E_N) \, d^3 p_N \\
&= \int dE_N \delta \left(E_N^2 - |\mathbf{p}_l - \mathbf{k}|^2 - M^2\right) \, dE_N \, d^3 k,
\end{aligned}$$

(B.120)

where the last equality follows from changing the variable from $\mathbf{p}_N$ to $\mathbf{k} = \mathbf{p}_l - \mathbf{p}_N$, and hence $d^3 p_N$ to $d^3 k$, and the integration is over the RHN energy E_N.

We specify an explicit coordinate system

$$\mathbf{k} = |\mathbf{k}|\,(0,0,1), \tag{B.121}$$

$$\mathbf{p}_q = E_q\,(0, \sin\eta, \cos\eta),$$

$$\mathbf{p}_l = E_l\,(\cos\phi\,\sin\vartheta, \sin\phi\,\sin\vartheta, \cos\vartheta),$$

to get the absolute values of the momentum differences (we only quote quantities that differ from that in Eq. (B.74))

$$|\mathbf{k} + \mathbf{p}_q|^2 = |\mathbf{k}|^2 + |\mathbf{p}_q|^2 + 2\mathbf{k}\mathbf{p}_q = |\mathbf{k}|^2 + E_q^2 + 2|\mathbf{k}|\,E_q\,\cos\eta$$

$$|\mathbf{p}_l - \mathbf{k}|^2 = |\mathbf{k}|^2 + |\mathbf{p}_l|^2 - 2\mathbf{k}\mathbf{p}_l = |\mathbf{k}|^2 + E_l^2 - 2\,|\mathbf{k}|\,E_l\,\cos\vartheta \tag{B.122}$$

and the delta-functions:

$$\delta\left((E_l + E_q - E_N)^2 - |\mathbf{k} + \mathbf{p}_q|^2\right) = \delta\left((E_l + E_q - E_N)^2 - E_q^2 - |\mathbf{k}|^2 - 2|\mathbf{k}|\,E_q\,\cos\eta\right)$$

$$= \frac{1}{2|\mathbf{k}|\,E_q}\,\delta\left(\cos\eta - \frac{(E_l + E_q - E_N)^2 - E_q^2 - |\mathbf{k}|^2}{2|\mathbf{k}|\,E_q}\right)$$

$$\delta\left(E_N^2 - M^2 - |\mathbf{p}_l - \mathbf{k}|^2\right) = \delta\left(E_N^2 - M^2 - E_l^2 - |\mathbf{k}|^2 + 2|\mathbf{k}|E_l\,\cos\vartheta\right)$$

$$= \frac{1}{2|\mathbf{k}|\,E_l}\,\delta\left(\cos\vartheta + \frac{E_N^2 - E_l^2 - M^2 - |\mathbf{k}|^2}{2|\mathbf{k}|\,E_l}\right). \tag{B.123}$$

Following the method of the previous sections, we reduce the integral (B.116) to

$$C_{S,t}[f_{l-\bar{l}}] = \frac{1}{2^7\pi^3\,E_l^2}\int d\cos\vartheta\,d\cos\eta\,dE_q\,dE_N\,d|\mathbf{k}|\,|\mathcal{M}_t|^2$$

$$\times\,\delta\left(\cos\eta - \frac{(E_l + E_q - E_N)^2 - E_q^2 - |\mathbf{k}^2|}{2|\mathbf{k}|\,E_q}\right)\delta\left(\cos\vartheta + \frac{E_N^2 - E_l^2 - M^2 - |\mathbf{k}^2|}{2|\mathbf{k}|\,E_l}\right)$$

$$\times\,\Lambda_t^{(l-\bar{l})}\left(f_{l-\bar{l}}, f_t, f_N, f_q\right)\,\Theta\left(E_q\right)\,\Theta\left(E_N\right)\,\Theta\left(E_l + E_q - E_N\right), \tag{B.124}$$

with

$$\Lambda_t^{(l-\bar{l})}\left(f_{l-\bar{l}}, f_t, f_N, f_q\right) = f_{l-\bar{l}}\,\frac{e^{\mathcal{E}_q}\left(e^{\mathcal{E}_l}\left(-1 + f_N\right) - e^{\mathcal{E}_N}\,f_N\right)}{\left(1 + e^{\mathcal{E}_q}\right)\left(e^{\mathcal{E}_N} + e^{\mathcal{E}_q + \mathcal{E}_l}\right)} \tag{B.125}$$

as the phase space factor.

In analogy to Section B.2.1, we integrate over $\cos\eta$ and $\cos\vartheta$ to get the integration ranges on k, but compared to Section B.1.2 here the situation is more involved. Again, the two angles ϑ and η run in the range

$$\cos\vartheta, \cos\eta \in [-1, 1], \tag{B.126}$$

and the explicit derived integration limits for the integral over $k = |\mathbf{k}|$ are:

$$
\begin{aligned}
\cos \eta = 1 \quad &\Rightarrow \quad k \in [E_l - E_N, E_N - E_l - 2E_q], \\
\cos \eta = -1 \quad &\Rightarrow \quad k \in [E_N - E_l, 2E_q + E_l - E_N], \\
\cos \vartheta = 1 \quad &\Rightarrow \quad k \in [E_l - p_N, E_l + p_N], \\
\cos \vartheta = -1 \quad &\Rightarrow \quad k \in [-E_l + p_N, -E_l - p_N],
\end{aligned}
\tag{B.127}
$$

where $p_N \equiv |\mathbf{p}_N|$, and $k \equiv |\mathbf{k}|$. Putting these conditions together and demanding $k \geq 0$ and $E_t \geq 0$ we get

$$
\sup \left[|E_N - E_l|, |E_l - p_N| \right] \leq k \leq \inf \left[2E_q - E_N - E_N, E_l + p_N \right]. \tag{B.128}
$$

Compared to Eq. (B.81) one of the upper integration limits on k has changed since we interchanged E_l and E_N in the final and initial state, respectively. Together with existing Θ functions in Eq. (B.124), we now define

$$
\begin{aligned}
\Omega \equiv \; &\Theta \left(E_l + E_q - E_N \right) \; \Theta \left(2E_l - (E_N - p_N) \right) \; \Theta \left(2E_q + E_l - E_N - |p_N - E_l| \right) \\
&\times \Theta \left(k - |E_N - E_l| \right) \Theta \left(k - |p_N - E_l| \right) \\
&\times \Theta \left(E_l + p_N - k \right) \; \Theta (2E_q + E_l - E_N - k),
\end{aligned}
\tag{B.129}
$$

to collectively denote all Θ functions appearing in the remaining integral. Note again, that we have omitted writing out $\Theta(E_N)\Theta(E_q)$, since positive particle energies are understood. The functions

$$
\Theta \left(2E_l - (E_N - p_N) \right) \quad \text{and} \quad \Theta \left(2E_q + E_l - E_N - |p_N - E_l| \right)
$$

have been introduced to assure that the upper limit on k is always larger than the lower limit.

Heron, the reduction of Eq. (B.129) goes in analogy to Section B.2.1 with some modifications:

- $\Theta \left(2E_q + E_l - E_N - |p_N - E_l| \right)$ reduces to

$$
\Theta \left(2E_q - (E_N - p_N) \right), \tag{B.130}
$$

  whenever $E_l > p_N$.

- For the upper limit we encounter now

$$
\Theta \left(E_l + p_N - k \right) \; \Theta \left(2E_q + E_l - E_N - k \right), \tag{B.131}
$$

leading to the combinations

$$\Theta\left(2E_q + E_l - E_N - k\right)\Theta\left(E_N + p_N - 2E_q\right) \tag{B.132}$$

and

$$\Theta\left(E_l + p_N - k\right)\Theta\left(2E_q - \left(E_N + p_N\right)\right). \tag{B.133}$$

- With the above modifications we arrive again at for cases for $\Omega^1 - \Omega^4$. Now, we have to change the integration limits on E_l to limits on E_N, where we find

$$\Theta\left(2E_l - \left(E_N - p_N\right)\right)\Theta\left(E_N + p_N - 2E_l\right) = \Theta\left(\frac{4E_l^2 + M^2}{4E_l} - E_N\right) \tag{B.134}$$

and

$$\Theta\left(E_N + p_N - 2E_l\right) = \Theta\left(E_N - \frac{4E_l^2 + M^2}{4E_l}\right). \tag{B.135}$$

At this point we can write down the four parts of $\Omega_\mu = \sum\limits_\mu = \Omega^1 + \Omega^2 + \Omega^3 + \Omega^4$:

$$\begin{aligned}\Omega^1 =& \Theta\left(E_N - \frac{4E_l^2 + M^2}{4E_l}\right)\Theta\left(2E_q - \left(E_N + p_N\right)\right)\\ & \times \Theta\left(k - \left(E_N - E_l\right)\right)\Theta\left(E_l + p_N - k\right),\end{aligned} \tag{B.136}$$

$$\begin{aligned}\Omega^2 =& \Theta\left(E_N - \frac{4E_l^2 + M^2}{4E_l}\right)\Theta\left(E_q - \left(E_N - E_l\right)\right)\Theta\left(E_N + p_N - 2E_q\right)\\ & \times \Theta\left(k - \left(E_N - E_l\right)\right)\Theta\left(2E_q + E_l - E_N - k\right),\end{aligned} \tag{B.137}$$

$$\begin{aligned}\Omega^3 =& \Theta\left(\frac{4E_l^2 + M^2}{4E_l} - E_N\right)\Theta\left(2E_q - \left(E_N + p_N\right)\right)\\ & \times \Theta\left(k - \left(E_l - p_N\right)\right)\Theta\left(E_l + p_N - k\right)\end{aligned} \tag{B.138}$$

and

$$\begin{aligned}\Omega^4 =& \Theta\left(\frac{4E_l^2 + M^2}{4E_l} - E_N\right)\Theta\left(2E_q - \left(E_N - p_N\right)\right)\Theta\left(E_N + p_N - 2E_q\right)\\ & \times \Theta\left(k - \left(E_l - p_N\right)\right)\Theta\left(E_l + p_N - k\right).\end{aligned} \tag{B.139}$$

As in Section B.2.1 we cut-off the integrand in $C_{S,t}^{(1)}$ and $C_{S.t}^{(2)}$ by adding a_h in the lower integration limit of k (modifying the limits of E_q and E_N accordingly) .

The collision integral (B.124) can then equivalently be written as

$$C_{S,t}\left[f_{l-\bar{l}}\right] = \sum_\mu \frac{1}{2^7 \pi^3 E_l^2}\int dE_q \, dE_N \, d|\mathbf{k}| \, |\mathcal{M}_t|^2 \, \Lambda\left(f_l, f_q, f_N, f_t\right)\Omega^\mu. \tag{B.140}$$

The four integrals have again to be integrated numerically and the summed up to give

$$C_{S,t}[f_{l-\bar{l}}] = C_{S,t}^{(1)} + C_{S,t}^{(2)} + C_{S,t}^{(3)} + C_{S,t}^{(4)}, \qquad (B.141)$$

with:

- First integral:

$$C_{S,t}^{(1)} = \frac{3\,T}{2^6\,\pi^3\,\mathcal{E}_N\,y_N} \frac{h_t^2\,M\,\tilde{m}_1}{v^2} \int_{\frac{(2\mathcal{E}_l - a_h z)^2 + z^2}{2(2\mathcal{E}_l - a_h z)}}^{\infty} d\mathcal{E}_N \int_{\mathcal{E}_N - \mathcal{E}_l + \frac{1}{2} a_h z}^{\frac{1}{2}(\mathcal{E}_N + y_N)} d\mathcal{E}_q\, \Lambda_t^{(l-\bar{l})}\, I_t^{(1)}, $$

$$(B.142)$$

$$\begin{aligned} I_t^{(1)} &= \int_{\mathcal{E}_N - \mathcal{E}_l + a_h z}^{2\mathcal{E}_q + \mathcal{E}_l - \mathcal{E}_N} d\tilde{k}\, \frac{(\mathcal{E}_N - \mathcal{E}_l)^2 - z^2 - \tilde{k}^2}{(\mathcal{E}_N - \mathcal{E}_l)^2 - \tilde{k}^2} \\ &= -\frac{2\,(\mathcal{E}_N - \mathcal{E}_l)\,(2\,(\mathcal{E}_N - \mathcal{E}_q - \mathcal{E}_l) + a_h z) + z^2\,\log\left[\frac{\mathcal{E}_q\,a_h z}{(\mathcal{E}_q - \mathcal{E}_N + \mathcal{E}_l)\,(2(\mathcal{E}_N - \mathcal{E}_l) + a_h z)}\right]}{2\,(\mathcal{E}_N - \mathcal{E}_l)}. \end{aligned}$$

- Second integral:

$$C_{S,t}^{(2)} = \frac{3\,T}{2^6\,\pi^3\,\mathcal{E}_N\,y_N} \frac{h_t^2\,M\,\tilde{m}_1}{v^2} \int_{\frac{(2\mathcal{E}_l - a_h z)^2 + z^2}{2(2\mathcal{E}_l - a_h z)}}^{\infty} d\mathcal{E}_N \int_{\frac{1}{2}(\mathcal{E}_N + y_N)}^{\infty} d\mathcal{E}_q\, \Lambda_t^{(l-\bar{l})}\, I_t^{(2)}, $$

$$(B.143)$$

$$\begin{aligned} I_t^{(2)} &= \int_{\mathcal{E}_N - \mathcal{E}_l + a_h z}^{\mathcal{E}_l + y_N} d\tilde{k}\, \frac{(\mathcal{E}_N - \mathcal{E}_l)^2 - z^2 - \tilde{k}^2}{(\mathcal{E}_N - \mathcal{E}_l)^2 - \tilde{k}^2} \\ &= \frac{2\,(\mathcal{E}_N - \mathcal{E}_l)\,(2\mathcal{E}_l - \mathcal{E}_N + y_N - a_h z) - z^2\,\log\left[\frac{(\mathcal{E}_N + y_N)\,a_h z}{(2\mathcal{E}_l - \mathcal{E}_N + y_N)\,(2(\mathcal{E}_N - \mathcal{E}_l) + a_h z)}\right]}{2\,(\mathcal{E}_N - \mathcal{E}_l)}. \end{aligned}$$

- Third integral:

$$C_{S,t}^{(3)} = \frac{3\,T}{2^6\,\pi^3\,\mathcal{E}_N\,y_N} \frac{h_t^2\,M\,\tilde{m}_1}{v^2} \int_z^{\frac{4\mathcal{E}_l^2 + z^2}{4\mathcal{E}_l}} d\mathcal{E}_N \int_{\frac{1}{2}(\mathcal{E}_N - y_N)}^{\frac{1}{2}(\mathcal{E}_N + y_N)} d\mathcal{E}_q\, \Lambda_t^{(l-\bar{l})}\, I_t^{(3)}, $$

$$(B.144)$$

$$\begin{aligned} I_t^{(3)} &= \int_{\mathcal{E}_l - y_N}^{2\mathcal{E}_q + \mathcal{E}_l - \mathcal{E}_N} d\tilde{k}\, \frac{(\mathcal{E}_N - \mathcal{E}_l)^2 - z^2 - \tilde{k}^2}{(\mathcal{E}_N - \mathcal{E}_l)^2 - \tilde{k}^2} \\ &= \frac{2\,(\mathcal{E}_N - \mathcal{E}_l)\,(2\mathcal{E}_q - \mathcal{E}_N + y_N) + z^2\,\log\left[\frac{(\mathcal{E}_N - \mathcal{E}_q - \mathcal{E}_l)\,(\mathcal{E}_N - y_N)}{\mathcal{E}_q\,(\mathcal{E}_N - 2\mathcal{E}_l + y_N)}\right]}{2\,(\mathcal{E}_N - \mathcal{E}_l)}. \end{aligned}$$

- Fourth integral:

$$
C_{S,t}^{(4)} = \frac{3\,T}{2^6\,\pi^3\,\mathcal{E}_N\,y_N}\,\frac{h_t^2\,M\,\tilde{m}_1}{v^2}\int_z^{\frac{4\mathcal{E}_l^2+z^2}{4\mathcal{E}_l}} d\mathcal{E}_N \int_{\frac{1}{2}(\mathcal{E}_N+y_N)}^{\infty} d\mathcal{E}_q\,\Lambda_t^{(l-\bar{l})}\,I_t^{(4)},
$$

(B.145)

$$
\begin{aligned}
I_t^{(4)} &= \int_{\mathcal{E}_l-y_N}^{\mathcal{E}_l+y_N} d\tilde{k}\,\frac{(\mathcal{E}_N-\mathcal{E}_l)^2-z^2-\tilde{k}^2}{(\mathcal{E}_N-\mathcal{E}_l)^2-\tilde{k}^2}\\
&= \frac{4\,(\mathcal{E}_N-\mathcal{E}_l)\,y_N+z^2\,\log\left[\frac{(\mathcal{E}_N-2\mathcal{E}_l-y_N)\,(\mathcal{E}_N-y_N)}{(\mathcal{E}_N-2\mathcal{E}_l+y_N)\,(\mathcal{E}_N+y_N)}\right]}{2\,(\mathcal{E}_N-\mathcal{E}_l)}.
\end{aligned}
$$

Appendix C

Evolution of the top Yukawa coupling

To determine the gauge and Yukawa couplings at some energy scale $\mu \equiv \log\left(T/m_Z\right)$, we use the renormalisation group equation

$$\frac{dg_i^2}{d\mu} = \frac{c_1}{8\pi^2}\, g_i^4, \tag{C.1}$$

where i denotes the corresponding gauge group of the Standard Model. The constants for the gauge couplings are

$$(c_1, c_2, c_3) = \left(\frac{41}{10} \cdot \frac{5}{3}, \frac{16}{9}, -7\right). \tag{C.2}$$

At one loop the solution of (C.1) for the gauge couplings yields

$$g_i = \sqrt{\frac{g_i^2\left(\mu = 0\right)}{1 - \frac{g_i^2(\mu=0)}{8\pi^2}\,\mu}}. \tag{C.3}$$

Neglecting contributions from the bottom and charm Yukawa couplings, the renormalization group equation for the top Yukawa coupling at one loop is given by [150]

$$\frac{h_t^2}{d\mu} = \frac{c_t}{8\pi^2}\, h_t^2 \left(h_t^2 - \frac{17}{54} \cdot \frac{5}{3}\, g_1^2 - \frac{1}{2}\, g_2^2 - \frac{16}{9}\, g_3^2\right). \tag{C.4}$$

The evolution of h_t from the electroweak scale up to the GUT scale is shown in Figure 4.8.

A detailed study of the evolution of quantities relevant for leptogenesis can be found in [151].

Bibliography

[1] A. H. Guth, Phys. Rev. **D23**, 347 (1981).

[2] E. Kolb and M. Turner, *The Early Universe* (Addison-Wesley, New York, 1990).

[3] A. D. Linde, Phys. Lett. **B129**, 177 (1983).

[4] A. Albrecht and P. J. Steinhardt, Phys. Rev. Lett. **48**, 1220 (1982).

[5] P. J. E. Peebles and B. Ratra, Astrophys. J. **325**, L17 (1988).

[6] C. Wetterich, Nucl. Phys. **B302**, 668 (1988).

[7] G. Steigman, Ann. Rev. Astron. Astrophys. **14**, 339 (1976).

[8] G. Steigman, JCAP **0810**, 001 (2008), 0808.1122.

[9] A. Strumia, (2006), hep-ph/0608347.

[10] B. Fields and S. Sarkar, (2006), astro-ph/0601514.

[11] WMAP, J. Dunkley *et al.*, (2008), 0803.0586.

[12] G. Steigman, Ann. Rev. Nucl. Part. Sci. **57**, 463 (2007), 0712.1100.

[13] Particle Data Group, W. M. Yao *et al.*, J. Phys. **G33**, 1 (2006).

[14] A. Sakharov, JETP Lett. **5**, 24 (1967).

[15] G. 't Hooft, Phys. Rev. Lett. **37**, 8 (1976).

[16] F. R. Klinkhamer and N. S. Manton, Phys. Rev. **D30**, 2212 (1984).

[17] V. A. Rubakov and M. E. Shaposhnikov, Usp. Fiz. Nauk **166**, 493 (1996), hep-ph/9603208.

[18] V. A. Kuzmin, V. A. Rubakov, and M. E. Shaposhnikov, Phys. Lett. **B155**, 36 (1985).

[19] D. Bodeker, G. D. Moore, and K. Rummukainen, Phys. Rev. **D61**, 056003 (2000), hep-ph/9907545.

[20] P. Arnold and L. G. Yaffe, Phys. Rev. **D55**, 7760 (1997), hep-ph/9610447.

[21] P. Arnold, D. T. Son, and L. G. Yaffe, Phys. Rev. **D59**, 105020 (1999), hep-ph/9810216.

[22] D. Bodeker, Phys. Lett. **B426**, 351 (1998), hep-ph/9801430.

[23] P. Arnold and L. G. Yaffe, Phys. Rev. **D62**, 125014 (2000), hep-ph/9912306.

[24] N. Cabibbo, Phys. Rev. Lett. **10**, 531 (1963).

[25] M. Kobayashi and T. Maskawa, Prog. Theor. Phys. **49**, 652 (1973).

[26] M. E. Shaposhnikov, IN *MOSCOW 1987, PROCEEDINGS, QUANTUM GRAVITY* 860-874.

[27] M. Trodden, Rev. Mod. Phys. **71**, 1463 (1999), hep-ph/9803479.

[28] M. B. Gavela, P. Hernandez, J. Orloff, and O. Pene, Mod. Phys. Lett. **A9**, 795 (1994), hep-ph/9312215.

[29] K. Jansen, Nucl. Phys. Proc. Suppl. **47**, 196 (1996), hep-lat/9509018.

[30] M. Losada, Phys. Rev. **D56**, 2893 (1997), hep-ph/9605266.

[31] B. de Carlos and J. R. Espinosa, Nucl. Phys. **B503**, 24 (1997), hep-ph/9703212.

[32] J. R. Espinosa, Nucl. Phys. **B475**, 273 (1996), hep-ph/9604320.

[33] M. Pietroni, Nucl. Phys. **B402**, 27 (1993), hep-ph/9207227.

[34] A. T. Davies, C. D. Froggatt, and R. G. Moorhouse, Phys. Lett. **B372**, 88 (1996), hep-ph/9603388.

[35] A. Menon, D. E. Morrissey, and C. E. M. Wagner, Phys. Rev. **D70**, 035005 (2004), hep-ph/0404184.

[36] I. Affleck and M. Dine, Nucl. Phys. **B249**, 361 (1985).

[37] M. Dine, L. Randall, and S. D. Thomas, Nucl. Phys. **B458**, 291 (1996), hep-ph/9507453.

[38] S. Eidelman *et al.*, Physics Letters B **592**, 1+ (2004).

[39] E. W. Kolb and M. S. Turner, Ann. Rev. Nucl. Part. Sci. **33**, 645 (1983).

[40] L. F. Abbott, E. Farhi, and M. B. Wise, Phys. Lett. **B117**, 29 (1982).

[41] A. D. Dolgov and A. D. Linde, Phys. Lett. **B116**, 329 (1982).

[42] M. Fukugita and T. Yanagida, Phys. Lett. **B174**, 45 (1986).

[43] P. Minkowski, Phys. Lett. **B67**, 421 (1977).

[44] A. Staudt, K. Muto, and H. V. Klapdor-Kleingrothaus, Europhys. Lett. **13**, 31 (1990).

[45] A. Strumia and F. Vissani, (2006), hep-ph/0606054.

[46] R. Davis, Phys. Rev. Lett. **12**, 303 (1964).

[47] J. N. Bahcall, M. H. Pinsonneault, and S. Basu, Astrophys. J. **555**, 990 (2001), astro-ph/0010346.

[48] SAGE, J. N. Abdurashitov *et al.*, J. Exp. Theor. Phys. **95**, 181 (2002), astro-ph/0204245.

[49] GALLEX, W. Hampel *et al.*, Phys. Lett. **B447**, 127 (1999).

[50] GNO, M. Altmann *et al.*, Phys. Lett. **B616**, 174 (2005), hep-ex/0504037.

[51] Super-Kamiokande, S. Fukuda *et al.*, Phys. Rev. Lett. **86**, 5651 (2001), hep-ex/0103032.

[52] Super-Kamkiokande, J. Hosaka *et al.*, Phys. Rev. **D73**, 112001 (2006), hep-ex/0508053.

[53] SNO, Q. R. Ahmad *et al.*, Phys. Rev. Lett. **87**, 071301 (2001), nucl-ex/0106015.

[54] SNO, Q. R. Ahmad *et al.*, Phys. Rev. Lett. **89**, 011302 (2002), nucl-ex/0204009.

[55] Borexino, C. Arpesella *et al.*, Phys. Lett. **B658**, 101 (2008), 0708.2251.

[56] KamLAND, K. Eguchi *et al.*, Phys. Rev. Lett. **90**, 021802 (2003), hep-ex/0212021.

[57] KamLAND, T. Araki *et al.*, Phys. Rev. Lett. **94**, 081801 (2005), hep-ex/0406035.

[58] Super-Kamiokande, Y. Fukuda *et al.*, Phys. Rev. Lett. **81**, 1562 (1998), hep-ex/9807003.

[59] K2K, M. H. Ahn *et al.*, Phys. Rev. **D74**, 072003 (2006), hep-ex/0606032.

[60] MINOS, D. G. Michael *et al.*,   Phys. Rev. Lett. **97**, 191801 (2006), hep-ex/0607088.

[61] CHOOZ, M. Apollonio *et al.*, Eur. Phys. J. **C27**, 331 (2003), hep-ex/0301017.

[62] C. Kraus *et al.*, Eur. Phys. J. **C40**, 447 (2005), hep-ex/0412056.

[63] V. M. Lobashev *et al.*, Nucl. Phys. Proc. Suppl. **91**, 280 (2001).

[64] V. M. Lobashev, Prepared for 11th International Workshop on Neutrino Telescopes, Venice, Italy, 22-25 Feb 2005.

[65] KATRIN, A. Osipowicz *et al.*, (2001), hep-ex/0109033.

[66] H. V. Klapdor-Kleingrothaus *et al.*,   Eur. Phys. J. **A12**, 147 (2001), hep-ph/0103062.

[67] IGEX, C. E. Aalseth *et al.*, Phys. Rev. **C59**, 2108 (1999).

[68] IGEX, C. E. Aalseth *et al.*, Phys. Rev. **D65**, 092007 (2002), hep-ex/0202026.

[69] H. V. Klapdor-Kleingrothaus, I. V. Krivosheina, A. Dietz, and O. Chkvorets, Phys. Lett. **B586**, 198 (2004), hep-ph/0404088.

[70] H. V. Klapdor-Kleingrothaus, A. Dietz, H. L. Harney, and I. V. Krivosheina, Mod. Phys. Lett. **A16**, 2409 (2001), hep-ph/0201231.

[71] I. Abt *et al.*, (2004), hep-ex/0404039.

[72] Majorana, C. E. Aalseth *et al.*,   Phys. Atom. Nucl. **67**, 2002 (2004), hep-ex/0405008.

[73] R. Ardito *et al.*, (2005), hep-ex/0501010.

[74] S. Hannestad and G. G. Raffelt, JCAP **0611**, 016 (2006), astro-ph/0607101.

[75] T. Yanagida, *Workshop on Unified Theories* (KEK report 79-18, 1979), p.95.

[76] M. Gell-Man, P. Ramond, and R. Slansky, *Supergravity* (North Holland, Amsterdam, 1979), eds. P.van Nieuwenhuizen, D.Freedman, p.315.

[77] R. Barbieri, D. V. Nanopoulos, G. Morchio, and F. Strocchi, Phys. Lett. **B90**, 91 (1980).

[78] R. N. Mohapatra and G. Senjanovic, Phys. Rev. **D23**, 165 (1981).

[79] M. Magg and C. Wetterich, Phys. Lett. **B94**, 61 (1980).

[80] G. Lazarides, Q. Shafi, and C. Wetterich, Nucl. Phys. **B181**, 287 (1981).

[81] R. Foot, H. Lew, X. G. He, and G. C. Joshi, Z. Phys. **C44**, 441 (1989).

[82] E. Ma, Phys. Rev. Lett. **81**, 1171 (1998), hep-ph/9805219.

[83] F. Hahn-Woernle, M. Plümacher, and Y. Y. Y. Wong, JCAP **0908**, 028 (2009), 0907.0205.

[84] L. Covi, E. Roulet, and F. Vissani, Phys. Lett. **B384**, 169 (1996), hep-ph/9605319.

[85] W. Buchmüller, P. Di Bari, and M. Plümacher, Nucl. Phys. **B665**, 445 (2003), hep-ph/0302092.

[86] M. Flanz, E. A. Paschos, and U. Sarkar, Phys. Lett. **B345**, 248 (1995), hep-ph/9411366.

[87] K. Hamaguchi, H. Murayama, and T. Yanagida, Phys. Rev. **D65**, 043512 (2002), hep-ph/0109030.

[88] S. Davidson and A. Ibarra, Phys. Lett. **B535**, 25 (2002), hep-ph/0202239.

[89] M. Plümacher, Z. Phys. **C74**, 549 (1997), hep-ph/9604229.

[90] W. Buchmüller and M. Plümacher, Phys. Lett. **B389**, 73 (1996), hep-ph/9608308.

[91] M. Plümacher, Nucl. Phys. **B530**, 207 (1998), hep-ph/9704231.

[92] W. Buchmüller, P. Di Bari, and M. Plümacher, Ann. Phys. **315**, 305 (2005), hep-ph/0401240.

[93] M. Bolz, A. Brandenburg, and W. Buchmüller, Nucl. Phys. **B606**, 518 (2001), hep-ph/0012052.

[94] J. Pradler, (2007), 0708.2786.

[95] M. Kawasaki, K. Kohri, and T. Moroi, Phys. Rev. **D71**, 083502 (2005), astro-ph/0408426.

[96] T. Moroi, H. Murayama, and M. Yamaguchi, Phys. Lett. **B303**, 289 (1993).

[97] J. Pradler and F. D. Steffen, Phys. Rev. **D75**, 023509 (2007), hep-ph/0608344.

[98] A. Pilaftsis, Phys. Rev. **D56**, 5431 (1997), hep-ph/9707235.

[99] A. Pilaftsis, Int. J. Mod. Phys. **A14**, 1811 (1999), hep-ph/9812256.

[100] A. Pilaftsis and T. E. J. Underwood, Nucl. Phys. **B692**, 303 (2004), hep-ph/0309342.

[101] G. Lazarides and Q. Shafi, Phys. Lett. **B258**, 305 (1991).

[102] H. Murayama, H. Suzuki, T. Yanagida, and J. Yokoyama, Phys. Rev. Lett. **70**, 1912 (1993).

[103] T. Asaka, K. Hamaguchi, M. Kawasaki, and T. Yanagida, Phys. Rev. **D61**, 083512 (2000), hep-ph/9907559.

[104] R. Jeannerot, S. Khalil, and G. Lazarides, Phys. Lett. **B506**, 344 (2001), hep-ph/0103229.

[105] G. F. Giudice, A. Notari, M. Raidal, A. Riotto, and A. Strumia, Nucl. Phys. **B685**, 89 (2004), hep-ph/0310123.

[106] F. Hahn-Woernle and M. Plümacher, Nucl. Phys. **B806**, 68 (2009), 0801.3972.

[107] Y. Grossman, T. Kashti, Y. Nir, and E. Roulet, Phys. Rev. Lett. **91**, 251801 (2003), hep-ph/0307081.

[108] Y. Grossman, T. Kashti, Y. Nir, and E. Roulet, JHEP **11**, 080 (2004), hep-ph/0407063.

[109] G. D'Ambrosio, G. F. Giudice, and M. Raidal, Phys. Lett. **B575**, 75 (2003), hep-ph/0308031.

[110] L. Covi, N. Rius, E. Roulet, and F. Vissani, Phys. Rev. **D57**, 93 (1998), hep-ph/9704366.

[111] A. Abada, S. Davidson, F.-X. Josse-Michaux, M. Losada, and A. Riotto, JCAP **0604**, 004 (2006), hep-ph/0601083.

[112] A. Abada *et al.*, JHEP **09**, 010 (2006), hep-ph/0605281.

[113] E. Nardi, Y. Nir, E. Roulet, and J. Racker, JHEP **01**, 164 (2006), hep-ph/0601084.

[114] S. Blanchet and P. Di Bari, JCAP **0703**, 018 (2007), hep-ph/0607330.

[115] A. Anisimov, S. Blanchet, and P. Di Bari, JCAP **0804**, 033 (2008), 0707.3024.

[116] S. Blanchet, P. Di Bari, and G. G. Raffelt, JCAP **0703**, 012 (2007), hep-ph/0611337.

[117] M. Lindner and M. M. Müller, Phys. Rev. **D73**, 125002 (2006), hep-ph/0512147.

[118] M. Lindner and M. M. Müller, Phys. Rev. **D77**, 025027 (2008), 0710.2917.

[119] A. Basbøll and S. Hannestad, JCAP **0701**, 003 (2007), hep-ph/0609025.

[120] E. W. Kolb and S. Wolfram, Nucl. Phys. **B172**, 224 (1980).

[121] J. A. Harvey and M. S. Turner, Phys. Rev. **D42**, 3344 (1990).

[122] J. Garayoa, S. Pastor, T. Pinto, N. Rius, and O. Vives, (2009), 0905.4834.

[123] S. Weinberg, *Gravitation and Cosmology* (Wiley, New York, 1972).

[124] M. Kawasaki, G. Steigman, and H.-S. Kang, Nucl. Phys. **B403**, 671 (1993).

[125] S. Blanchet and P. Di Bari, JCAP **0606**, 023 (2006), hep-ph/0603107.

[126] S. Y. Khlebnikov and M. E. Shaposhnikov, Nucl. Phys. **B308**, 885 (1988).

[127] N. Kaiser, R. A. Malaney, and G. D. Starkman, Phys. Rev. Lett. **71**, 1128 (1993), hep-ph/9302261.

[128] W. Buchmüller, P. Di Bari, and M. Plümacher, Nucl. Phys. **B643**, 367 (2002), hep-ph/0205349.

[129] A. Pilaftsis and T. E. J. Underwood, Phys. Rev. **D72**, 113001 (2005), hep-ph/0506107.

[130] E. Nardi, J. Racker, and E. Roulet, JHEP **09**, 090 (2007), 0707.0378.

[131] M. A. Luty, Phys. Rev. **D45**, 455 (1992).

[132] A. Hohenegger, (2008), 0806.3098.

[133] W. Buchmüller and M. Plümacher, Int. J. Mod. Phys. **A15**, 5047 (2000), hep-ph/0007176.

[134] K. S. Babu, C. N. Leung, and J. T. Pantaleone, Phys. Lett. **B319**, 191 (1993), hep-ph/9309223.

[135] S. Antusch, J. Kersten, M. Lindner, and M. Ratz, Nucl. Phys. **B674**, 401 (2003), hep-ph/0305273.

[136] J. A. Casas and A. Ibarra, Nucl. Phys. **B618**, 171 (2001), hep-ph/0103065.

[137] P. Di Bari, Nucl. Phys. **B727**, 318 (2005), hep-ph/0502082.

[138] S. Davidson, JHEP **03**, 037 (2003), hep-ph/0302075.

[139] G. C. Branco, R. Gonzalez Felipe, F. R. Joaquim, and M. N. Rebelo, Nucl. Phys. **B640**, 202 (2002), hep-ph/0202030.

[140] K. S. Babu, J. C. Pati, and F. Wilczek, Nucl. Phys. **B566**, 33 (2000), hep-ph/9812538.

[141] S. F. King and G. G. Ross, Phys. Lett. **B520**, 243 (2001), hep-ph/0108112.

[142] M. Raidal, A. Strumia, and K. Turzynski, Phys. Lett. **B609**, 351 (2005), hep-ph/0408015.

[143] O. Vives, Phys. Rev. **D73**, 073006 (2006), hep-ph/0512160.

[144] G. Engelhard, Y. Grossman, E. Nardi, and Y. Nir, Phys. Rev. Lett. **99**, 081802 (2007), hep-ph/0612187.

[145] R. Barbieri, P. Creminelli, A. Strumia, and N. Tetradis, Nucl. Phys. **B575**, 61 (2000), hep-ph/9911315.

[146] S. Blanchet, (2008), 0807.1408.

[147] P. Di Bari and A. Riotto, Phys. Lett. **B671**, 462 (2009), 0809.2285.

[148] C. Itzykson and J. B. Zuber, New York, Usa: Mcgraw-hill (1980) 705 P.(International Series In Pure and Applied Physics).

[149] M. Plümacher, Preprint - Plümacher, M. (95,rec.Feb.96) 74 p.

[150] M. Lindner, Zeit. Phys. **C31**, 295 (1986).

[151] S. Antusch, J. Kersten, M. Lindner, M. Ratz, and M. A. Schmidt, JHEP **03**, 024 (2005), hep-ph/0501272.